

## SUPPORTING INFORMATION

# Dinuclear thiolato-bridged arene ruthenium complexes: from reaction conditions and mechanism to synthesis of new complexes

Hedvika Primasová<sup>a,†\*</sup>, Silviya Ninova<sup>a,b,†</sup>, Mario De Capitani<sup>a</sup>, Jana Daepf<sup>a</sup>, Ulrich Aschauer<sup>a\*</sup>, Julien Furrer<sup>a\*</sup>

<sup>a</sup> Departement für Chemie und Biochemie, Universität Bern, Freiestrasse 3, CH-3012 Bern, Switzerland

<sup>b</sup> Department of Chemistry and Physics of Materials, Paris-Lodron Universität Salzburg, Jakob-Haringer-Strasse 2a, A-5020 Salzburg, Austria

### Table of Contents

<b>1. Computational part</b> .....	<b>4</b>
<b>1.1 Density functional theory calculations</b> .....	<b>4</b>
Energy barriers and pathways.....	4
<b>1.2 Reaction rates</b> .....	<b>10</b>
<b>1.3 Ru-dimer Geometry and Functional dependence</b> .....	<b>11</b>
<b>2. Experimental part</b> .....	<b>13</b>
<b>2.1 Synthesis</b> .....	<b>13</b>
<b>2.2 Characterisation</b> .....	<b>16</b>
<b>2.3 Kinetics</b> .....	<b>34</b>
<b>References</b> .....	<b>46</b>

### List of Tables

**Table S1.** Activation barriers (in kcal/mol) for each of the three thiolphenolato-substitutions.

**Table S2.** Activation barriers (in kcal/mol) for the Complex **1** with Chlorine and Iodine.

**Table S3:** Activation barriers (in kcal/mol) for the Complex **1** in implicit solvents.

**Table S4.** Forward reaction rates (min<sup>-1</sup>) for each substitution step.

**Table S5.** Backward reaction rates (min<sup>-1</sup>) for each substitution step.

**Table S6.** Equilibrium constants.

**Table S7.** Theoretical Geometry Parameters for Complex **1**.

**Table S8.** Energy differences (kcal/mol) and functional dependence for the first reaction step.

**Table S9.** Starting materials for kinetics experiments.

### List of Figures

**Figure S1.** NEB reaction pathways for each substitution step of the trithiolato bridged ruthenium complex formation using thiophenol (**1**).

**Figure S2.** NEB reaction pathway for **1**.

**Figure S3.** NEB reaction pathways for each substitutional step of the trithiolato bridged ruthenium complex formation using 4-methoxythiophenol (**2**).

**Figure S4.** NEB reaction pathways for each substitutional step of the trithiolato bridged ruthenium complex formation using 4-nitrothiophenol (**3**).

**Figure S5.** NEB reaction pathways for each substitutional step of the trithiolato bridged ruthenium complex formation using cyclohexylthiol (**4**).

**Figure S6.** NEB reaction pathways for each substitutional step of the trithiolato bridged ruthenium complex formation, where the halogen element is Iodine.

**Figure S7.** The geometry of the initial ruthenium dimer without any thiolate ligands

**Figure S8.** Projected Density of States for the initial Ru complex (0S)

**Figure S9.** 400 MHz  $^1\text{H}$  NMR of **1** in  $\text{CDCl}_3$ .

**Figure S10.** 100 MHz  $^{13}\text{C}$  NMR of **1** in  $\text{CDCl}_3$ .

**Figure S11.** ESI-MS of **1** dissolved in MeOH and recorded in positive mode.

**Figure S12.** 400.1 MHz  $^1\text{H}$  NMR of **2** in  $\text{CD}_2\text{Cl}_2$ .

**Figure S13.** 100 MHz  $^{13}\text{C}$  NMR of **2** in  $\text{CD}_2\text{Cl}_2$ .

**Figure S14.** ESI-MS of **2** dissolved in MeOH and recorded in positive mode.

**Figure S15.** 400.1 MHz  $^1\text{H}$  NMR of **3** in MeOD.

**Figure S16.** 100 MHz  $^{13}\text{C}$  NMR of **3** in MeOD.

**Figure S17.** ESI-MS of **3** dissolved in MeOH and recorded in positive mode.

**Figure S18.** 500.1 MHz  $^1\text{H}$  NMR of **4** in  $\text{CDCl}_3$ .

**Figure S19.** 100 MHz  $^{13}\text{C}$  NMR of crude **4** in  $\text{CDCl}_3$ .

**Figure S20.** 500.1 MHz  $^{13}\text{C}$  HSQC of **4** in  $\text{CDCl}_3$ .

**Figure S21.** ESI-MS of **4** dissolved in acetonitrile and recorded in positive mode.

**Figure S22.** ESI-MS of **5** dissolved in EtOH and recorded in positive mode.

**Figure S23.** 400.1 MHz  $^1\text{H}$  NMR of complex **5** in  $\text{CDCl}_3$ .

**Figure S24.** 100 MHz  $^{13}\text{C}$  NMR of complex **5** in  $\text{CDCl}_3$ .

**Figure S25.** ESI-MS of **6** dissolved in acetonitrile and recorded in positive mode.

**Figure S26.** 500.1 MHz  $^1\text{H}$  NMR of complex **6** in MeOD.

**Figure S27.** 100 MHz  $^1\text{H}$  NMR of complex **6** in MeOD.

**Figure S28.** ESI-MS of **7** dissolved in EtOH and recorded in positive mode.

**Figure S29.** 400.1 MHz  $^1\text{H}$  NMR of complex **7** in  $\text{CDCl}_3$ .

**Figure S30.** 100 MHz  $^1\text{H}$  NMR of complex **7** in  $\text{CDCl}_3$ .

**Figure S31.** ESI-MS of **8** dissolved in EtOH and recorded in positive mode.

**Figure S32.** 400.1 MHz  $^1\text{H}$  NMR of complex **8** in  $\text{CDCl}_3$ .

**Figure S33.** 100 MHz  $^1\text{H}$  NMR of complex **8** in  $\text{CDCl}_3$ .

**Figure S34.** 400.1 MHz  $^{13}\text{C}$  HSQC of complex **8** in  $\text{CDCl}_3$ .

**Figure S35.** ESI-MS of **9** dissolved in MeOH and recorded in positive mode.

**Figure S36.** 400.1 MHz  $^1\text{H}$  NMR of complex **9** in  $\text{CDCl}_3$ .

**Figure S37.** 100 MHz  $^{13}\text{C}$  NMR of complex **9** in  $\text{CDCl}_3$ .

**Figure S38.** Synthesis of **1** in EtOH under reflux.  $^1\text{H}$  NMR in  $\text{CDCl}_3$  recorded at  $t =$ : 0 h, 30 min, 1 h, 2 h, 3 h, 4 h, 5 h, 7.5 h, 9 h. Aromatic region.

**Figure S39.** Synthesis of **1** in EtOH under reflux.  $^1\text{H}$  NMR in  $\text{CDCl}_3$  recorded at  $t =$ : 0 h, 30 min, 1 h, 2 h, 3 h, 4 h, 5 h, 7.5 h, 9 h. Aliphatic region.

**Figure S40.** Kinetics of formation of **2** and intermediates at 45 °C. Aliquots of reaction mixture in DCM transferred to  $\text{CDCl}_3$ . 500.1 MHz  $^1\text{H}$  NMR recorded at  $t =$ : 0 h, 0.5 h, 1 h, 2 h, 3 h, 5 h, 7 h, 9 h. Aromatic region.

- Figure S41.** Kinetics of formation of **2** and intermediates at 45 °C. Aliquots of reaction mixture in DCM transferred to CDCl<sub>3</sub>. 500.1 MHz <sup>1</sup>H NMR recorded at *t* =: 0 h, 0.5 h, 1 h, 2 h, 3 h, 5 h, 7 h, 9 h. Aliphatic region.
- Figure S42.** Kinetics of formation of **3** at 45 °C in DCM. 500.1 MHz <sup>1</sup>H NMR in CDCl<sub>3</sub> recorded at *t* =: 0 h, 0.25 h, 0.5 h, 1 h, 2 h. Aromatic region.
- Figure S43.** Kinetics of formation of **3** at 45 °C in DCM. 500.1 MHz <sup>1</sup>H NMR in CDCl<sub>3</sub> recorded at *t* =: 0 h, 0.25 h, 0.5 h, 1 h, 2 h. Aliphatic region.
- Figure S44.** Reaction between [(η<sup>6</sup>-*p*-MeC<sub>6</sub>H<sub>4</sub>Pr<sup>*i*</sup>)Ru(μ<sub>2</sub>-Cl)Cl]<sub>2</sub> and thiophenol towards **1** in CD<sub>2</sub>Cl<sub>2</sub> at 0 °C followed by <sup>1</sup>H NMR.
- Figure S45.** Reaction between [(η<sup>6</sup>-*p*-MeC<sub>6</sub>H<sub>4</sub>Pr<sup>*i*</sup>)Ru(μ<sub>2</sub>-Cl)Cl]<sub>2</sub> and thiophenol towards **1** in CD<sub>2</sub>Cl<sub>2</sub> at 25 °C followed by <sup>1</sup>H NMR.
- Figure S46.** Reaction between [(η<sup>6</sup>-*p*-MeC<sub>6</sub>H<sub>4</sub>Pr<sup>*i*</sup>)Ru(μ<sub>2</sub>-Cl)Cl]<sub>2</sub> and *p*-methoxythiophenol towards **2** in CD<sub>2</sub>Cl<sub>2</sub> at 0 °C followed by <sup>1</sup>H NMR.
- Figure S47.** Reaction between [(η<sup>6</sup>-*p*-MeC<sub>6</sub>H<sub>4</sub>Pr<sup>*i*</sup>)Ru(μ<sub>2</sub>-Cl)Cl]<sub>2</sub> and *p*-methoxythiophenol towards **2** in CD<sub>2</sub>Cl<sub>2</sub> at 25 °C followed by <sup>1</sup>H NMR.
- Figure S48.** Reaction between [(η<sup>6</sup>-*p*-MeC<sub>6</sub>H<sub>4</sub>Pr<sup>*i*</sup>)Ru(μ<sub>2</sub>-Cl)Cl]<sub>2</sub> and *p*-nitrothiophenol towards **3** in CD<sub>2</sub>Cl<sub>2</sub> at 0 °C followed by <sup>1</sup>H NMR.
- Figure S49.** Reaction between [(η<sup>6</sup>-*p*-MeC<sub>6</sub>H<sub>4</sub>Pr<sup>*i*</sup>)Ru(μ<sub>2</sub>-Cl)Cl]<sub>2</sub> and *p*-nitrothiophenol towards **3** in CD<sub>2</sub>Cl<sub>2</sub> at 25 °C followed by <sup>1</sup>H NMR.
- Figure S50.** Kinetics of formation of **4** and intermediates. 400.1 MHz <sup>1</sup>H NMR in CD<sub>2</sub>Cl<sub>2</sub> recorded at *t* =: 0 h, 2 h, 5 h, 11 h, 15 h, 30 h, 35 h, 50 h, 70 h, 409 h. Aromatic region.
- Figure S51.** Kinetics of formation of **4** and intermediates. 400.1 MHz <sup>1</sup>H NMR in CD<sub>2</sub>Cl<sub>2</sub> recorded at *t* =: 0 h, 2 h, 5 h, 11 h, 15 h, 30 h, 35 h, 50 h, 70 h, 409 h. Aliphatic region.
- Figure S52.** Stability test, 400.1 MHz <sup>1</sup>H NMR of crude **7** in CD<sub>2</sub>Cl<sub>2</sub> at 25°C.
- Figure S53.** Stability test, 400.1 MHz <sup>1</sup>H NMR of crude **7** in MeOD at 25°C.
- Figure S54.** Stability test, 400.1 MHz <sup>1</sup>H NMR of crude **8** in CD<sub>2</sub>Cl<sub>2</sub> at 25°C.
- Figure S55.** Stability test, 400.1 MHz <sup>1</sup>H NMR of crude **8** in MeOD at 25°C.

# 1. Computational part

## 1.1 Density functional theory calculations

### Energy barriers and pathways

The theoretically derived reaction barriers are schematically presented in Figures 3 and 4 in the main text. The corresponding values for the two transition states at each substitution step are presented in Table S1 and Table S2. The NEB pathways for each substitutional step are summarised in Figure S1 for the  $[(\eta^6\text{-}p\text{-MeC}_6\text{H}_4\text{Pr}^i)_2\text{Ru}_2(\mu\text{-SC}_6\text{H}_4\text{-R})_3]^+$  complexes **1** (R=H), Figure S3 for **2** (R=OCH<sub>3</sub>), Figure S4 for **3** (R=NO<sub>2</sub>), Figure S5 for complex **4**, Figure S6 for **1** with Iodine; where (a) is the 1<sup>st</sup> step, (b) the 2<sup>nd</sup> step and (c) the 3<sup>rd</sup> step, respectively.

**Table S1.** Activation barriers (in kcal/mol) for each of the three thiophenolato-substitutions. Each substitution step has two transition states (TS), while the third number is the energy of the products with respect to the reactants in each step.

	<i>1<sup>st</sup> step</i>			<i>2<sup>nd</sup> step</i>			<i>3<sup>rd</sup> step</i>		
	1 TS	2 TS	<b>1S</b>	1 TS	2 TS	<b>2S</b>	1 TS	2 TS	<b>3S</b>
<b>1</b> R=H	12.8	19.9	-18.4	24.0	10.9	-16.7	17.5	31.4	-4.1
<b>2</b> R=OCH <sub>3</sub>	19.8	22.0	-13.9	21.8	9.5	-16.7	24.7	41.0	2.4
<b>3</b> R=NO <sub>2</sub>	15.7	16.1	-17.7	23.5	21.2	-13.7	27.9	43.9	7.6
<b>4</b>	21.1	-	-11.6	42.0	-	-10.4	25.2	40.3	5.2

**Table S2.** Activation barriers (in kcal/mol) for the trithiolato bridged ruthenium complex reaction pathway, where different halogen atoms are used. Each substitution step has two transition states (TS), while the third number is the energy of the products with respect to the reactants in each step.

<b>Halogen</b>	<i>1<sup>st</sup> step</i>			<i>2<sup>nd</sup> step</i>			<i>3<sup>rd</sup> step</i>		
	1 TS	2 TS	<b>1S</b>	1 TS	2 TS	<b>2S</b>	1 TS	2 TS	<b>3S</b>
<b>Chlorine</b>	12.8	19.9	-18.4	24.0	10.9	-16.7	17.5	31.4	-4.1
<b>Iodine</b>	22.7	19.6	-6.5	22.6	11.4	-4.2	17.9	34.0	3.0

**Table S3:** Activation barriers (in kcal/mol) for the Complex **1** reaction pathway calculated in vacuum and in DCM or Ethanol as implicit solvents without further optimization of the geometries. Each substitution step has two transition states (TS), while the third number is the energy of the products with respect to the reactants in each step.

	<i>1<sup>st</sup> step</i>			<i>2<sup>nd</sup> step</i>			<i>3<sup>rd</sup> step</i>		
	1 TS	2 TS	<b>1S</b>	1 TS	2 TS	<b>2S</b>	1 TS	2 TS	<b>3S</b>
<b>Vacuum</b>	12.8	19.9	-18.4	24.0	10.9	-16.7	17.5	31.4	-4.1
<b>DCM</b>	11.8	19.0	-18.3	37.4	10.6	-16.0	59.5	30.8	-7.8
<b>Ethanol</b>	5.6	12.8	-24.4	74.7	10.5	-16.0	177.2	36.9	-8.5

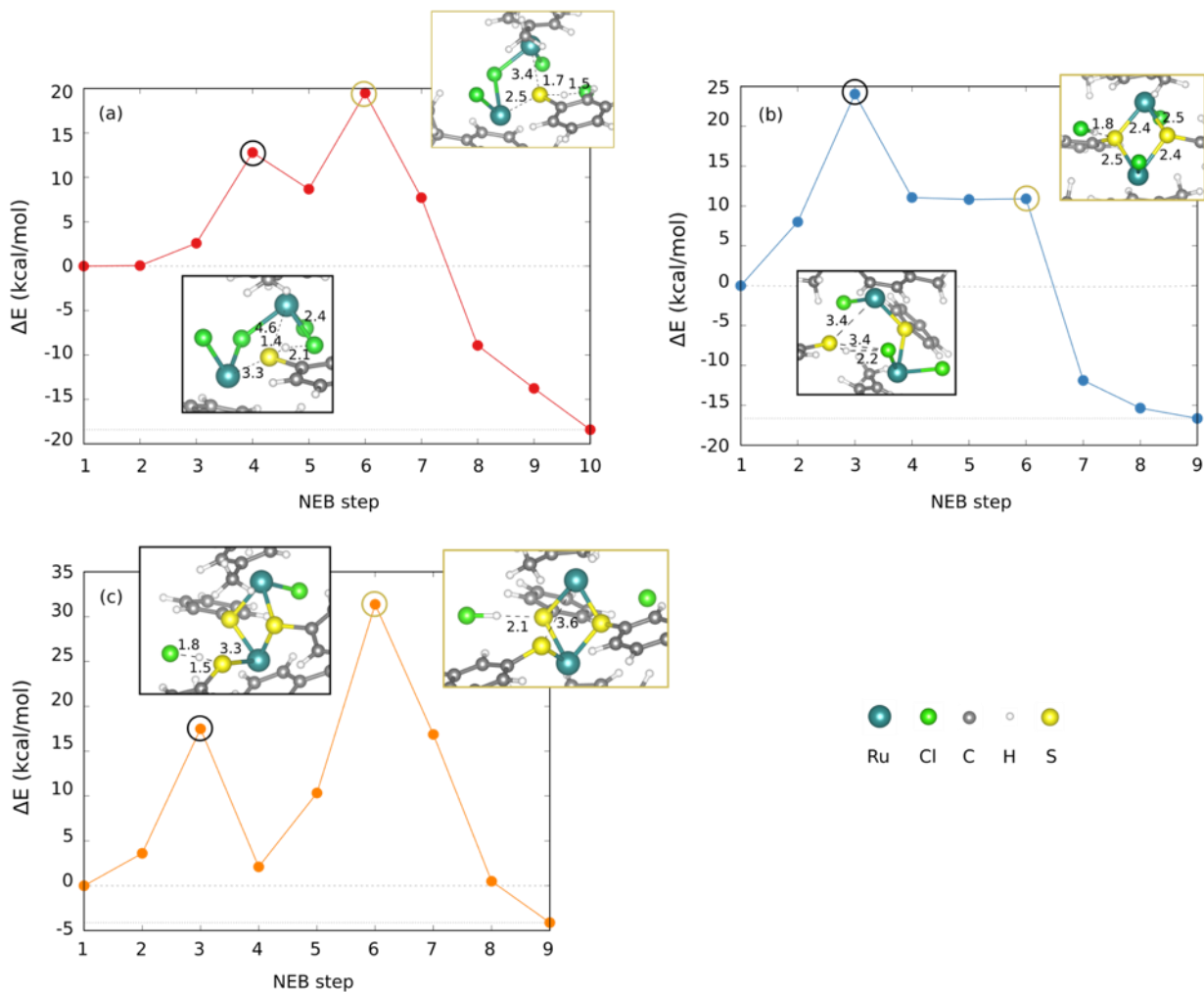


**Figure S1.** NEB reaction pathways for each substitution step of the trithiolato bridged ruthenium complex formation using thiophenol (1).

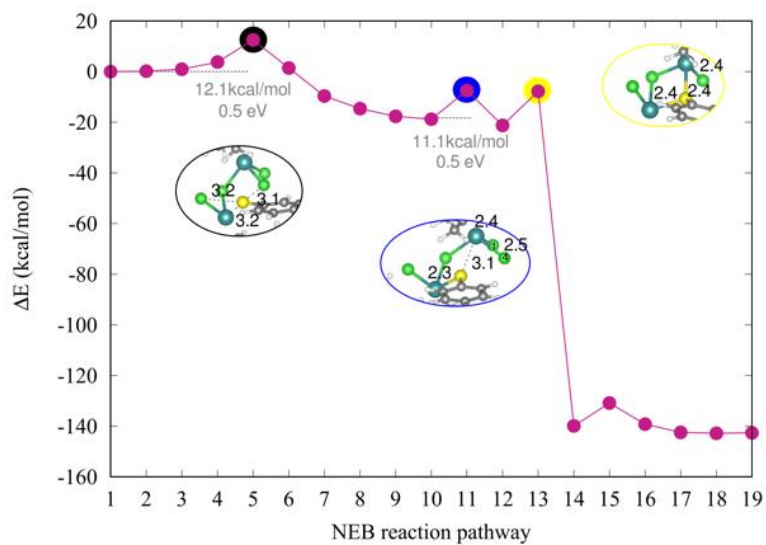


**Figure S2.** NEB reaction pathway for 1, where a deprotonated thiophenol was used for the reaction. The first transition state corresponds to the insertion of the thiophenol anion, the second transition state would normally correspond to the deprotonation and formation of H-Cl bond; in this case and together with the third transition state it corresponds to the adjustments of the structure when the Cl anion leaves.

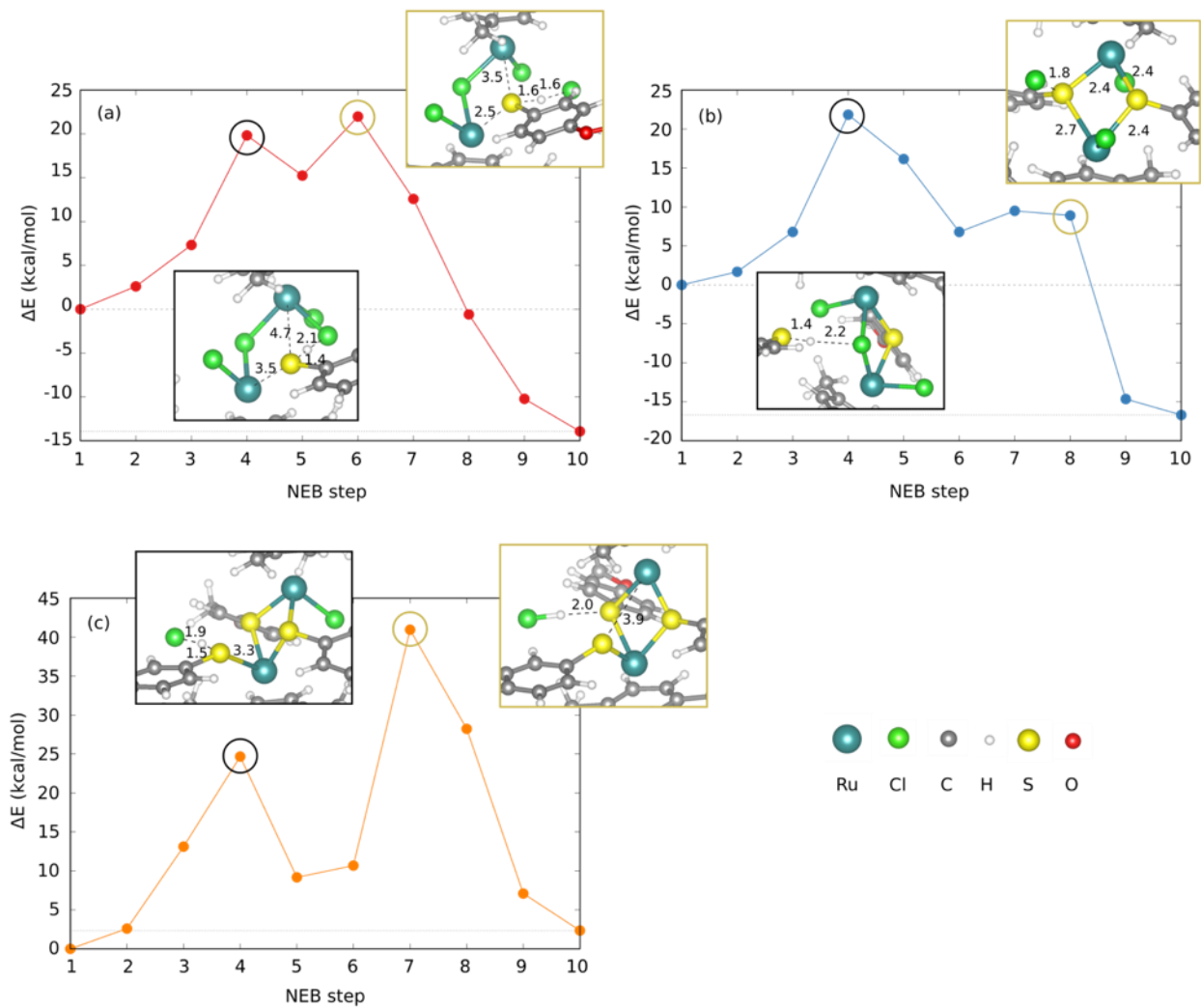


**Figure S3.** NEB reaction pathways for each substitutional step of the trithiolato bridged ruthenium complex formation using 4-methoxythiophenol (**2**).

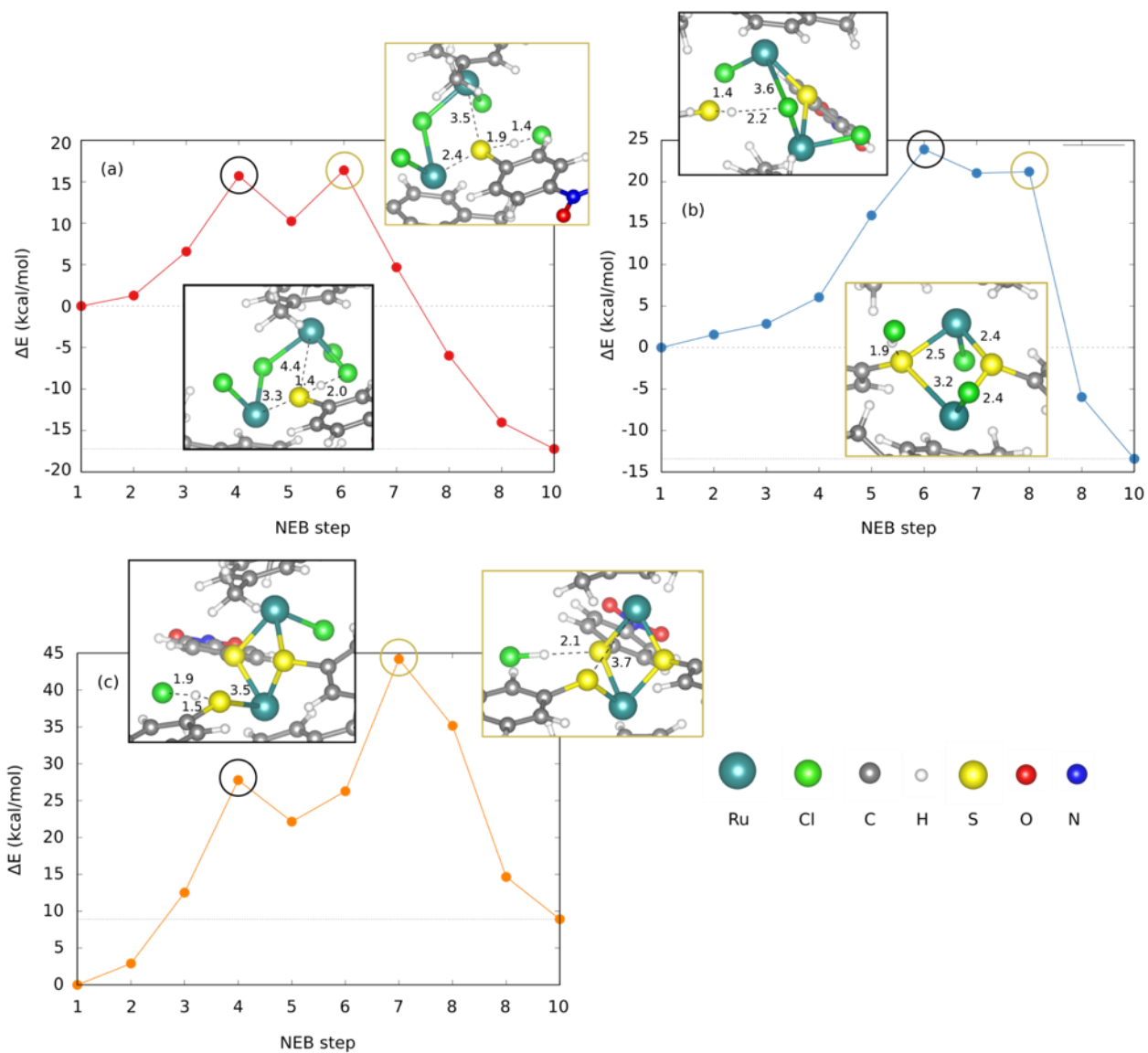


**Figure S4.** NEB reaction pathways for each substitutional step of the trithiolato bridged ruthenium complex formation using 4-nitrothiophenol (**3**).

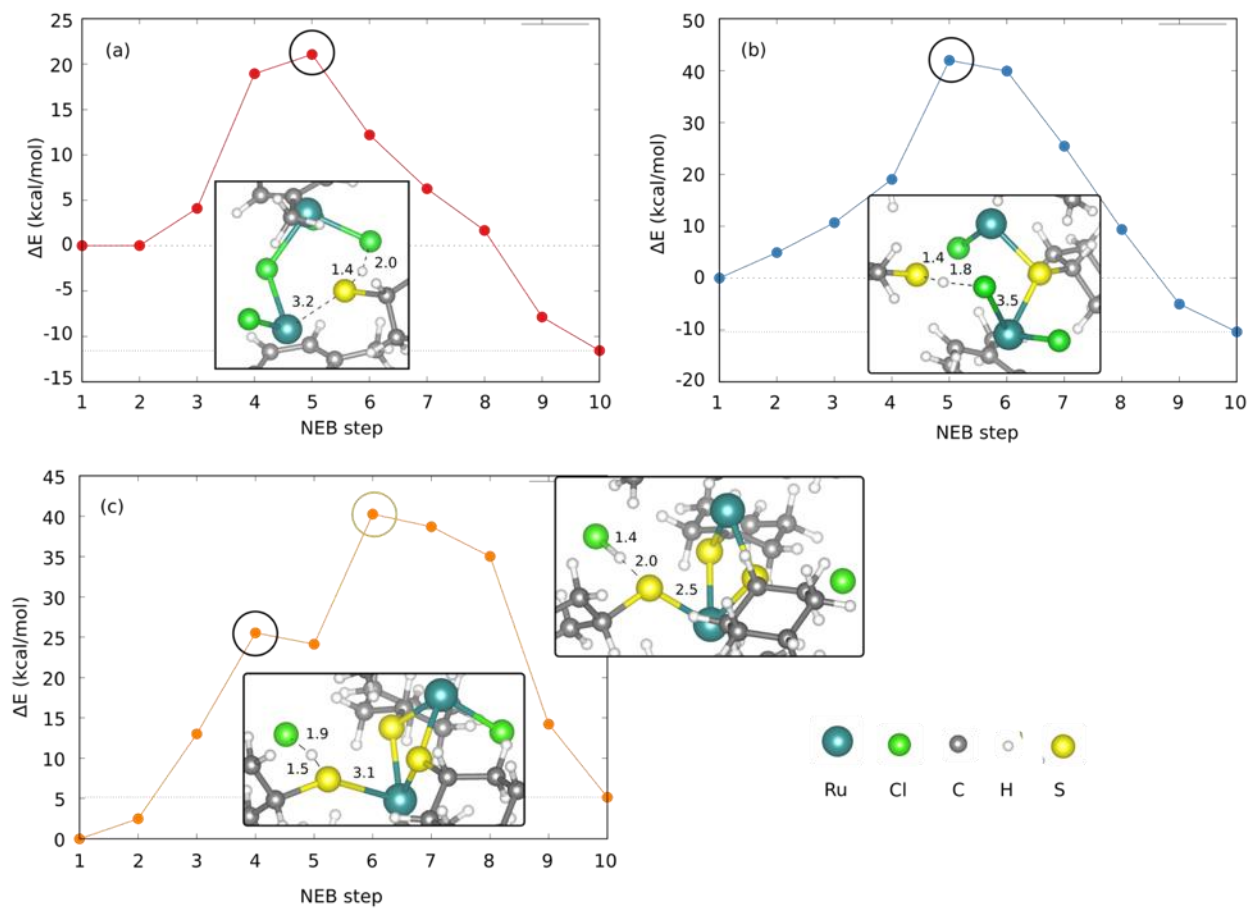


**Figure S5.** NEB reaction pathways for each substitutional step of the trithiolato bridged ruthenium complex formation using cyclohexylthiol (**4**).

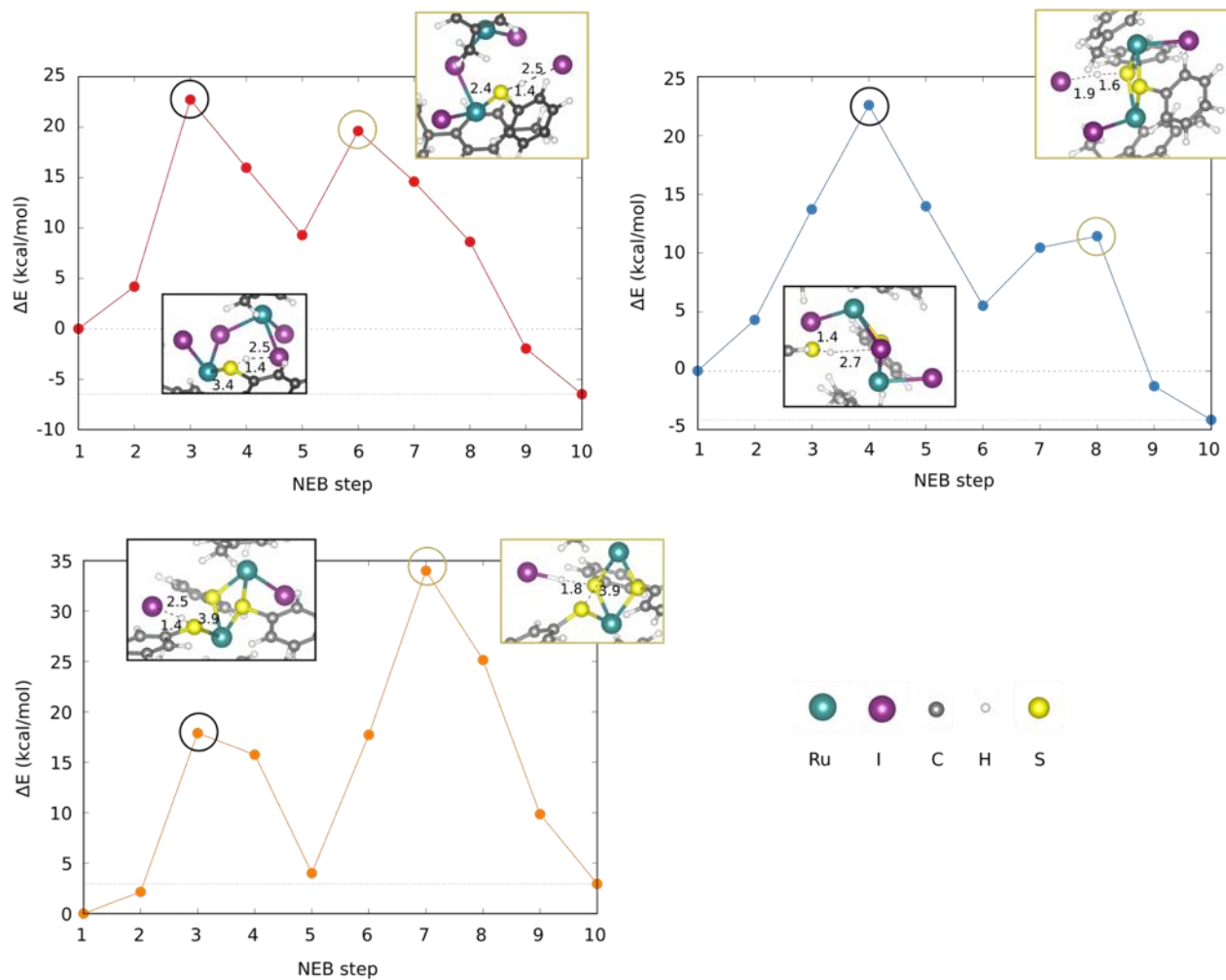


**Figure S6.** NEB reaction pathways for each substitutional step of the trithiolato bridged ruthenium complex formation, where the halogen element is Iodine.

## 1.2 Reaction rates

**Table S4.** Forward reaction rates ( $\text{min}^{-1}$ ) for each substitution step where only the highest barrier per step is considered (see Table S1) at four temperatures.

	1 <sup>st</sup> step	2 <sup>nd</sup> step	3 <sup>rd</sup> step
k ( $\text{min}^{-1}$ ) at 0°C			
1 R=H	$4.1 \cdot 10^{-2}$	$2.1 \cdot 10^{-5}$	$2.6 \cdot 10^{-11}$
2 R=OCH <sub>3</sub>	$8.9 \cdot 10^{-4}$	$1.2 \cdot 10^{-3}$	$5.9 \cdot 10^{-19}$
3 R=NO <sub>2</sub>	$4.6 \cdot 10^1$	$5.3 \cdot 10^{-5}$	$2.8 \cdot 10^{-21}$
4	$4.8 \cdot 10^{-3}$	$8.7 \cdot 10^{-20}$	$2.1 \cdot 10^{-18}$
k ( $\text{min}^{-1}$ ) at 25°C			
1 R=H	$9.7 \cdot 10^{-1}$	$9.5 \cdot 10^{-4}$	$3.6 \cdot 10^{-9}$
2 R=OCH <sub>3</sub>	$2.9 \cdot 10^{-2}$	$3.7 \cdot 10^{-2}$	$3.6 \cdot 10^{-16}$
3 R=NO <sub>2</sub>	$6.0 \cdot 10^2$	$2.2 \cdot 10^{-3}$	$2.6 \cdot 10^{-18}$
4	$1.4 \cdot 10^{-1}$	$6.2 \cdot 10^{-17}$	$1.2 \cdot 10^{-15}$
k ( $\text{min}^{-1}$ ) at 40°C			
1 R=H	$5.1 \cdot 10^0$	$7.0 \cdot 10^{-3}$	$4.8 \cdot 10^{-8}$
2 R=OCH <sub>3</sub>	$1.8 \cdot 10^{-1}$	$2.3 \cdot 10^{-1}$	$1.0 \cdot 10^{-14}$
3 R=NO <sub>2</sub>	$2.3 \cdot 10^3$	$1.5 \cdot 10^{-2}$	$9.6 \cdot 10^{-17}$
4	$7.9 \cdot 10^{-1}$	$1.9 \cdot 10^{-15}$	$3.2 \cdot 10^{-14}$
k ( $\text{min}^{-1}$ ) at 45°C			
1 R=H	$8.5 \cdot 10^0$	$1.3 \cdot 10^{-2}$	$1.1 \cdot 10^{-7}$
2 R=OCH <sub>3</sub>	$3.2 \cdot 10^{-1}$	$4.0 \cdot 10^{-1}$	$3.0 \cdot 10^{-14}$
3 R=NO <sub>2</sub>	$3.5 \cdot 10^3$	$2.8 \cdot 10^{-2}$	$3.0 \cdot 10^{-16}$
4	$1.4 \cdot 10^0$	$5.7 \cdot 10^{-15}$	$8.9 \cdot 10^{-14}$
k ( $\text{min}^{-1}$ ) at 80°C			
1 R=H	$2.1 \cdot 10^2$	$6.2 \cdot 10^{-1}$	$1.6 \cdot 10^{-5}$
2 R=OCH <sub>3</sub>	$1.1 \cdot 10^1$	$1.4 \cdot 10^1$	$2.0 \cdot 10^{-11}$
3 R=NO <sub>2</sub>	$4.9 \cdot 10^4$	$1.2 \cdot 10^0$	$3.2 \cdot 10^{-13}$
4	$4.1 \cdot 10^1$	$4.6 \cdot 10^{-12}$	$5.5 \cdot 10^{-11}$

**Table S5.** Backward reaction rates ( $\text{min}^{-1}$ ) for each substitution step where only the highest barrier per step is considered (see Table S1) at two temperatures.

	1 <sup>st</sup> step	2 <sup>nd</sup> step	3 <sup>rd</sup> step
k ( $\text{min}^{-1}$ ) at 0°C			
1 R=H	$7.8 \cdot 10^{-17}$	$9.3 \cdot 10^{-19}$	$1.4 \cdot 10^{-14}$
2 R=OCH <sub>3</sub>	$6.3 \cdot 10^{-15}$	$5.1 \cdot 10^{-17}$	$4.5 \cdot 10^{-17}$
3 R=NO <sub>2</sub>	$3.3 \cdot 10^{-13}$	$5.7 \cdot 10^{-16}$	$3.1 \cdot 10^{-15}$
4	$2.7 \cdot 10^{-12}$	$4.4 \cdot 10^{-28}$	$2.9 \cdot 10^{-14}$
k ( $\text{min}^{-1}$ ) at 25°C			
1 R=H	$3.1 \cdot 10^{-14}$	$5.5 \cdot 10^{-16}$	$3.6 \cdot 10^{-12}$
2 R=OCH <sub>3</sub>	$1.8 \cdot 10^{-12}$	$2.1 \cdot 10^{-14}$	$1.9 \cdot 10^{-14}$
3 R=NO <sub>2</sub>	$6.7 \cdot 10^{-11}$	$1.9 \cdot 10^{-13}$	$9.2 \cdot 10^{-13}$
4	$4.6 \cdot 10^{-10}$	$1.6 \cdot 10^{-24}$	$7.1 \cdot 10^{-12}$

**Table S6.** Equilibrium constant calculated as the ratio between the forward (see Table S4) and backward (see Table S5) reactions for each step at two temperatures.

	1 <sup>st</sup> step	2 <sup>nd</sup> step	3 <sup>rd</sup> step
K at 0°C			
1 R=H	$5.3 \cdot 10^{14}$	$2.3 \cdot 10^{13}$	$1.9 \cdot 10^3$
2 R=OCH <sub>3</sub>	$1.4 \cdot 10^{11}$	$2.3 \cdot 10^{13}$	$1.3 \cdot 10^{-2}$
3 R=NO <sub>2</sub>	$1.4 \cdot 10^{14}$	$9.3 \cdot 10^{10}$	$8.9 \cdot 10^{-7}$
4	$1.8 \cdot 10^9$	$2.0 \cdot 10^8$	$7.4 \cdot 10^{-5}$
K at 25°C			
1 R=H	$3.1 \cdot 10^{13}$	$1.7 \cdot 10^{12}$	$1.0 \cdot 10^3$
2 R=OCH <sub>3</sub>	$1.6 \cdot 10^{10}$	$1.7 \cdot 10^{12}$	$1.9 \cdot 10^{-2}$
3 R=NO <sub>2</sub>	$9.0 \cdot 10^{12}$	$1.1 \cdot 10^{10}$	$2.9 \cdot 10^{-6}$
4	$3.0 \cdot 10^8$	$4.0 \cdot 10^7$	$1.7 \cdot 10^{-4}$
K(0°C) / K (25°C)			
1 R=H	17.2	13.2	1.9
2 R=OCH <sub>3</sub>	8.6	13.2	0.7
3 R=NO <sub>2</sub>	15.3	8.3	0.3
4	6.0	5.0	0.5

### 1.3 Geometry and Functional dependence of the ruthenium dimer

The starting ruthenium dimer consists of a core with two Ruthenium atoms coordinated with three Chlorine atoms each and a *p*-cymene. Our gas phase calculation with BLYP agrees well with the experimental structure (see **Chyba! N enalezen zdroj odkazů.**). In comparison, other GGA (PBE) or hybrid (B3LYP, PBE0) functionals deviate more from the experimental geometry. We note that the experimental structure is crystallised, so even bigger deviations could be expected with respect to the calculated gas phase geometry.

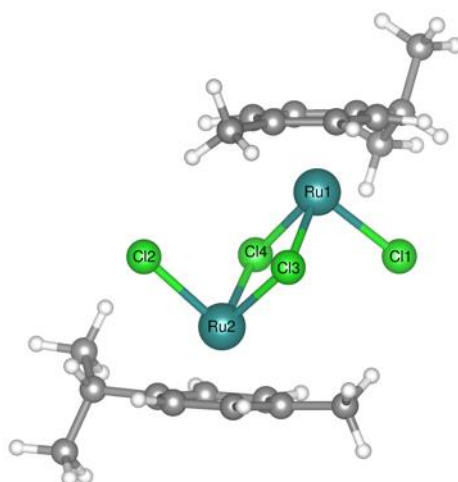


**Figure S7.** The geometry of the initial ruthenium dimer without any thiolate ligands is presented with the labels on the atoms in the core of the complex, to be related to the structural parameters in Table S7.

**Table S7.** Change in the bond lengths and angles with respect to the experimental values as obtained after a geometry relaxation of **0S** using different exchange-correlation functionals.

Bonds (Å)/Angles (°)	Experiment <sup>1</sup>	<b>0S</b>			
		BLYP	B3LYP	PBE	PBE0
Ru1-Ru2	3.693	3.708	3.658	3.681	3.615
Ru1-C11	2.435	2.411	2.399	2.384	2.374
Ru1-C13(S)	2.488	2.484	2.461	2.453	2.430
Ru1-C14	2.461	2.479	2.459	2.449	2.427
Ru2-C12	2.420	2.416	2.403	2.387	2.377
Ru2-C13(S)	2.450	2.482	2.461	2.451	2.428
Ru2-C14	2.437	2.476	2.455	2.446	2.425
Ru1-C13(S)-Ru2	96.8	96.6	96.0	97.3	96.2
Ru1-C14-Ru2	97.9	96.9	96.2	97.5	96.3
C11-Ru1-C13(S)	88.4	87.4	87.7	87.0	87.2
C12-Ru2-C13(S)	87.2	87.5	87.7	86.9	87.3
C11-Ru1-C14	87.1	87.0	87.2	86.8	86.8
C12-Ru2-C14	85.2	87.2	87.4	86.9	86.9
Average error (%)		0.81	0.92	0.87	1.34

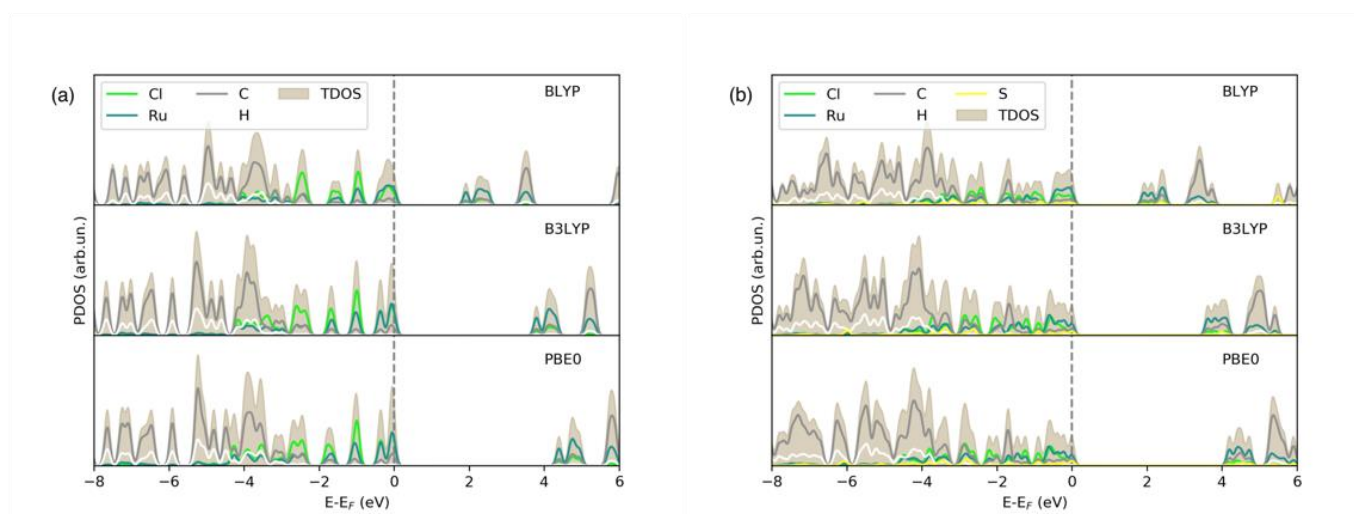


**Figure S8.** Projected Density of States for the initial ruthenium dimer (**0S**) (a) and the thiophenolato-substituted one (**1S**) (b) calculated with BLYP (above) and B3LYP (below). A Gaussian broadening of 0.1 eV was used.

In terms of electronic structure, there are no pronounced differences when the GGA (BLYP) or the two hybrid (B3LYP, PBE0) exchange-correlation functionals are used (see Figure S8) neither for the initial ruthenium dimer (**0S**) nor for the monosubstituted one (**1S**). Indeed, the characters of HOMO/LUMO states are similar with all three functionals, giving us the reason to assume that our results with BLYP would be qualitatively confirmed by the other two functionals. Moreover, the energetics of the first reaction step - the monothiolato complex (**1S**) formation - agrees well with the BLYP results. Quantitatively, the hybrid functionals predict a higher barrier for the transition states. The PBE approximation stabilises to a great extent the product, as opposed to the BLYP/B3LYP.

**Table S8:** Energy differences (kcal/mol) for the first reaction step as calculated with different functionals on the BLYP geometry.

	BLYP	B3LYP	PBE	PBE0
<b>0S</b>	0.0	0.0	0.0	0.0
<b>1 TS</b>	12.8	15.5	11.9	15.7
<b>2 TS</b>	19.5	22.8	16.5	21.3
<b>1S</b>	-18.4	-19.5	-25.3	-25.1

## 2. Experimental part

### 2.1 Synthesis

#### Synthesis of 1

**Synthesis in EtOH**  $[(\eta^6\text{-}p\text{-MeC}_6\text{H}_4\text{Pr}^i)\text{Ru}(\mu_2\text{-Cl})\text{Cl}]_2$  (101.6 mg, 0.166 mmol) was dissolved in EtOH abs. (45 mL) under reflux. Thiophenol (75.6 mg, 0.686 mmol, 4.1 eq) in EtOH abs. (5 mL) was slowly dropped into the refluxing solution and the mixture was left to react for 23 h. After purification on silica column **1** was obtained as an orange solid (105.7 mg, 0.114 mmol, 69%).

**Synthesis in DCM**  $[(\eta^6\text{-}p\text{-MeC}_6\text{H}_4\text{Pr}^i)\text{Ru}(\mu_2\text{-Cl})\text{Cl}]_2$  (106.3 mg, 0.174 mmol) was dissolved in dry DCM (45 mL) and thereafter left to reflux. Thiophenol (80.2 mg, 0.728 mmol, 4.2 eq) in dry DCM (5 mL) was added dropwise into the refluxing solution and left to react for 7 h. After purification **1** was obtained as an orange solid (127.4 mg, 0.138 mmol, 62%).

**Synthesis in DCM with DIPEA**  $[(\eta^6\text{-}p\text{-MeC}_6\text{H}_4\text{Pr}^i)\text{Ru}(\mu_2\text{-Cl})\text{Cl}]_2$  (106.6 mg, 0.174 mmol) was dissolved in dry DCM (45 mL) and left to reflux thereafter. Thiophenol (81.4 mg, 0.739 mmol, 4.2 eq) in dry DCM (5 mL) was added dropwise and the reaction mixture was left to react for 1 h. Next, the reaction mixture was cooled down in ice/water bath. DIPEA (69.6 mg, 0.539 mmol, 3.1 eq) in dry DCM (1 mL) was added dropwise into cooled and stirred reaction mixture dropwise during 10 min. Afterwards, the reaction mixture was heated again and left to react for further 1 h and 50 min under reflux. Purification allowed **1** to be obtained as an orange solid (127.4 mg, 0.138 mmol, 79%).

**Synthesis in EtOH with DIPEA**  $[(\eta^6\text{-}p\text{-MeC}_6\text{H}_4\text{Pr}^i)\text{Ru}(\mu_2\text{-Cl})\text{Cl}]_2$  (101.4 mg, 0.166 mmol) was dissolved in EtOH abs. (45 mL) under reflux. Thiophenol (76.2 mg, 0.692 mmol, 4.2 eq) in EtOH abs. (5 mL) was added dropwise into refluxing solution and the reaction was left stirred. After 1 h, DIPEA (66.6 mg, 0.515 mmol, 3.1 eq) in EtOH abs. (1 mL) was added slowly dropwise into refluxing mixture during 10 min. The reaction was left to react for 1 h and 50 min. Purification allowed to obtain **1** as an orange solid (123.0 mg, 0.132 mmol, 80%).

For purification of **1** column chromatography with DCM/EtOH 10:1 was used. As needed in case of reaction performed in EtOH employing DIPEA, the product was further loaded on silica column with hexane/chloroform 100:1 and washed with gradient of hexane/chloroform, pure chloroform and finally released with DCM/EtOH 5:1.

**Analytical data** (Figures S9-11):  $^1\text{H NMR}$  (400.1 MHz,  $\text{CDCl}_3$ ):  $\delta_{\text{H}} = 7.89$  (d,  $J_{\text{H,H}} = 6.0$  Hz, 6H; Ar H2, H6), 7.39 (m, 9H; Ar H3, H4, H5), 5.41 (d,  $J_{\text{H,H}} = 5.6$  Hz, 2H; H-Ar *p*-cymene), 5.24 (d,  $J_{\text{H,H}} = 5.6$  Hz, 2H; H-Ar *p*-cymene), 5.12 (m, 4H; H-Ar *p*-cymene), 1.92 (sept,  $J_{\text{H,H}} = 6.8$  Hz, 2H;  $\text{CH}(\text{CH}_3)_2$ ), 1.62 (s, 6H;  $\text{CH}_3$ ), 0.89 (d,  $J_{\text{H,H}} = 6.8$  Hz, 6H;  $\text{CH}(\text{CH}_3)_2$ ), 0.77 ppm (d,  $J_{\text{H,H}} = 6.8$  Hz, 6H;  $\text{CH}(\text{CH}_3)_2$ );  $^{13}\text{C NMR}$  (100 MHz,  $\text{CDCl}_3$ ):  $\delta_{\text{C}} = 137.8$  (thiol C1), 132.6 (thiol C2/C6), 129.2 (thiol C3/C4/C5), 128.5 (thiol C3/C4/C5), 107.4 (C1 *p*-cymene), 100.0 (C4 *p*-cymene), 85.4 (Ar CH *p*-cymene), 85.0 (Ar CH *p*-cymene), 84.7 (Ar CH *p*-cymene), 83.6 (Ar CH *p*-cymene), 30.6 ( $\underline{\text{C}}\text{H}(\text{CH}_3)_2$ ), 22.5 ( $\underline{\text{C}}\text{H}(\underline{\text{C}}\text{H}_3)_2$ ), 22.0 ( $\text{CH}(\underline{\text{C}}\text{H}_3)_2$ ), 17.7 ppm ( $\underline{\text{C}}\text{H}_3$ ); ESI-MS (positive mode, MeOH)  $m/z = 799.1$ ; elemental analysis calcd (%) for  $\text{C}_{38}\text{H}_{43}\text{S}_3\text{Ru}_2\text{Cl}_2 \cdot 2\text{CH}_3\text{CH}_2\text{OH}$ : C 54.50, H 5.99; found: C 54.22, H 6.26; Mw = 925.67 g/mol.

#### Synthesis of 2

$[(\eta^6\text{-}p\text{-MeC}_6\text{H}_4\text{Pr}^i)\text{Ru}(\mu_2\text{-Cl})\text{Cl}]_2$  (100.6 mg, 0.164 mmol) was dissolved in dry DCM (45 mL) under  $\text{N}_2$  atmosphere and heated to reflux at 38-45 °C. *p*-methoxythiophenol (92.4 mg, 0.659 mmol, 4.0 eq) in dry DCM (5 mL) was added dropwise into refluxing solution and it was left to react for 9 h. Purification on silica column employing DCM/EtOH 5:1 as mobile phase allowed to obtain **2** as an orange solid (115.7 mg, 0.121 mmol, 73%).

**Analytical data** (Figures S12-14):  $^1\text{H NMR}$  (400.1 MHz,  $\text{CD}_2\text{Cl}_2$ ):  $\delta_{\text{H}} = 7.79$  (d,  $J_{\text{H,H}} = 8.8$  Hz, 6H; H-Ar thiol), 6.91 (d,  $J_{\text{H,H}} = 8.8$  Hz, 6H; H-Ar thiol), 5.31 (d,  $J_{\text{H,H}} = 5.8$  Hz, 2H; H-Ar *p*-cymene), 5.18 (d,  $J_{\text{H,H}} = 5.8$  Hz, 2H;

H-Ar *p*-cymene), 5.08 (m, 4H; H-Ar *p*-cymene), 3.86 (s, 9H; OCH<sub>3</sub>), 1.96 (sept, J<sub>H,H</sub> = 6.9 Hz, 2H; CH(CH<sub>3</sub>)<sub>2</sub>), 1.61 (s, 6H; CH<sub>3</sub> *p*-cymene), 0.91 (d, J<sub>H,H</sub> = 6.9 Hz, 6H; CH(CH<sub>3</sub>)<sub>2</sub>), 0.81 ppm (d, J<sub>H,H</sub> = 6.9 Hz, 6H; CH(CH<sub>3</sub>)<sub>2</sub>); <sup>13</sup>C NMR (100 MHz, CD<sub>2</sub>Cl<sub>2</sub>): δ<sub>C</sub> = 160.1 (C=OCH<sub>3</sub>), 133.7, 128.6, 114.5, 107.3, 99.5, 85.3, 84.7, 84.4, 83.5, 55.5, 30.6, 22.2, 21.8, 17.5 (CH<sub>3</sub>); ESI-MS (positive mode, MeOH): *m/z* 889.1; elemental analysis calcd (%) for C<sub>41</sub>H<sub>49</sub>O<sub>3</sub>Ru<sub>2</sub>S<sub>3</sub>Cl·2H<sub>2</sub>O: C 51.32, H 5.57; found: C 51.58, H 5.70; Mw = 959.64 g/mol; Figure S24-26.

### Synthesis of 3

[(η<sup>6</sup>-*p*-MeC<sub>6</sub>H<sub>4</sub>Pr<sup>i</sup>)Ru(μ<sub>2</sub>-Cl)Cl]<sub>2</sub> (101.6 mg, 0.166 mmol) was dissolved in dry DCM (40 mL) under N<sub>2</sub> atmosphere and heated to reflux at 40–45 °C. 80% technical grade *p*-nitrothiophenol (128.7 mg, 0.664 mmol, 4.0 eq) in dry DCM (10 mL) was added dropwise into the refluxing solution. After 30–60 min after addition of the thiol the mixture turned slowly dark red. The reaction was left to react for 2 h in total. Purification on silica column using DCM/EtOH 5:1 as an eluent allowed **3** to be isolated as a red solid (125.8 mg, 0.121 mmol, 73%).

An alternative approach employing an organic base was tested: [(η<sup>6</sup>-*p*-MeC<sub>6</sub>H<sub>4</sub>Pr<sup>i</sup>)Ru(μ<sub>2</sub>-Cl)Cl]<sub>2</sub> (99.1 mg, 0.161 mmol) was dissolved in dry DCM (40 mL) under N<sub>2</sub> and heated to reflux. *p*-nitrothiophenol (150.1 mg, 0.967 mmol, 6.0 eq) was added dropwise into refluxing solution. After 1 h, heating was stopped and DIPEA (69.1 mg, 0.535 mmol, 3.3 eq) has been added dropwise into temperature-regulated stirred reaction mixture. Afterwards, the mixture was left to react for further 1 h under reflux, but progressively turned black indicating starting material decomposition. This approach has been abandoned.

**Analytical data** (Figures S15-17): <sup>1</sup>H NMR (400.1 MHz, MeOD): δ<sub>H</sub> = 8.25 (ABq, J<sub>H,H</sub> = 8.9 Hz, 12H; H-Ar thiol), 5.76 (d, J<sub>H,H</sub> = 5.7 Hz, 2H; H-Ar *p*-cymene), 5.63 (d, J<sub>H,H</sub> = 5.7 Hz, 2H; H-Ar *p*-cymene), 5.43 (m, 4H; H-Ar *p*-cymene), 1.99 (sept, J<sub>H,H</sub> = 6.9 Hz, 2H; CH(CH<sub>3</sub>)<sub>2</sub>), 1.67 (s, 6H; CH<sub>3</sub> *p*-cymene), 0.92 (d, J<sub>H,H</sub> = 6.9 Hz, 6H; CH(CH<sub>3</sub>)<sub>2</sub>), 0.80 ppm (d, J<sub>H,H</sub> = 6.9 Hz, 6H; CH(CH<sub>3</sub>)<sub>2</sub>); <sup>13</sup>C NMR (100 MHz, MeOD): δ<sub>C</sub> = 147.8 (thiol C1/C4), 146.8 (thiol C1/C4), 133.7 (thiol CH), 123.6 (thiol CH), 108.3 (C1 *p*-cymene), 101.1 (C4 *p*-cymene), 85.8 (Ar CH *p*-cymene), 85.8 (Ar CH *p*-cymene), 85.5 (Ar CH *p*-cymene), 85.0 (Ar CH *p*-cymene), 30.9 (CH(CH<sub>3</sub>)<sub>2</sub>), 21.4 (CH(CH<sub>3</sub>)<sub>2</sub>), 20.7 (CH(CH<sub>3</sub>)<sub>2</sub>), 16.5 ppm (CH<sub>3</sub>); ESI-MS (positive mode, MeOH): *m/z* 934.0; elemental analysis calcd (%) for C<sub>38</sub>H<sub>40</sub>N<sub>3</sub>O<sub>6</sub>S<sub>3</sub>Ru<sub>2</sub>Cl·6/7 DCM: C 44.82, H 4.04; found: C 45.03, H 3.74; Mw = 1041.32 g/mol.

### Synthesis of 4

[(η<sup>6</sup>-*p*-MeC<sub>6</sub>H<sub>4</sub>Pr<sup>i</sup>)Ru(μ<sub>2</sub>-Cl)Cl]<sub>2</sub> (100 mg, 0.163 mmol) was dissolved in dry DCM (40 mL) under Ar and heated to reflux at 40–45 °C. Cyclohexanethiol (166.5 mg, 1.433 mmol, 8.8 eq) in dry DCM (10 mL) was added dropwise into refluxing solution and the reaction mixture was left to react for 18 h. As a next step, DIPEA (86.0 mg, 0.665 mmol, 4.1 eq) in dry DCM (5 mL) was added slowly into the solution during 5–10 min. The mixture was left to react for further 6 days. Three-step purification on silica column was applied. First, the product was pre-purified on silica column using DCM/EtOH 5:1 as a mobile phase. The orange fraction has been concentrated and further purified on silica column using CHCl<sub>3</sub>/acetone 3:2 as an eluent. Finally, a concentrate of fractions containing the product was purified on silica column using gradient elution system of acetone with increasing amount of 10% acetic acid up to 1:1 ratio to obtain **4** as viscous orange brown matter (30 mg). The product contained impurities. Due to the nature and amount of the product no thermal analysis could be done.

### Synthesis of 5

[(η<sup>6</sup>-*p*-MeC<sub>6</sub>H<sub>4</sub>Pr<sup>i</sup>)Ru(μ<sub>2</sub>-Cl)Cl]<sub>2</sub> (101.3 mg, 0.165 mmol) was dissolved in DCM (40 mL) under Ar atmosphere, heated to reflux at 40–45 °C and 1-hexanethiol (77.9 mg, 0.659 mmol, 4.0 eq) was slowly dropped into refluxing solution. It was left to react for 1 h. Next, DIPEA (62 mg, 0.480 mmol, 2.9 eq) was added dropwise into solution and this was then left to react for further 67 h. The crude product was concentrated under reduced pressure and subsequently purified on silica column using acetone/DCM 9:1 to yield orange-brown solid giving a yield of 62% (88.3 mg, 0.103 mmol). For comparison, performing the reaction in EtOH under reflux with use of DIPEA analogously, **5** was obtained in 42% yield (59.3 mg, 0.068 mmol).

### Synthesis of 6

[(η<sup>6</sup>-*p*-MeC<sub>6</sub>H<sub>4</sub>Pr<sup>i</sup>)Ru(μ<sub>2</sub>-Cl)Cl]<sub>2</sub> (100.0 mg, 0.163 mmol) was dissolved in DCM (40 mL) under Ar atmosphere and heated to reflux at 40–45 °C. *p*-fluorothiophenol (122.5 mg, 0.956 mmol, 5.9 eq) was added slowly and the reaction mixture was left stirred for 2 h. Next, DIPEA (69.3 mg, 0.536 mmol, 3.3 eq) was added dropwise and the mixture was left stirred for further 1.5 h. Afterwards the crude product was concentrated under reduced pressure and purified on silica column using DCM/EtOH 5:1 as an eluent. **6** was obtained as an orange solid in 80% yield (121.1 mg, 0.131 mmol).

**Analytical data** (Figures S25-27):  $^1\text{H}$  NMR (500.1 MHz, MeOD):  $\delta_{\text{H}} = 7.97$  (m, 6H; H-Ar thiol), 7.17 (m, 6H; H-Ar thiol), 5.56 (d,  $J_{\text{H,H}} = 5.6$  Hz, 2H; H-Ar *p*-cymene), 5.45 (d,  $J_{\text{H,H}} = 5.6$  Hz, 2H; H-Ar *p*-cymene), 5.30 (m, 4H; H-Ar *p*-cymene), 1.96 (sept,  $J_{\text{H,H}} = 5.6$  Hz, 2H;  $\text{CH}(\text{CH}_3)_2$ ), 1.64 (s, 6H;  $\text{CH}_3$ ), 0.93 (d,  $J_{\text{H,H}} = 6.8$  Hz, 6H;  $\text{CH}(\text{CH}_3)_2$ ), 0.83 ppm (d,  $J_{\text{H,H}} = 6.8$  Hz, 6H;  $\text{CH}(\text{CH}_3)_2$ ).  $^{13}\text{C}$  NMR (100.1 MHz, MeOD):  $\delta_{\text{C}} = 164.3$  (CF), 161.8 (CF), 134.5 and 134.4 (CH thiol), 133.23 and 133.21 (Ar C thiol), 115.8 and 115.5 (Ar C thiol), 107.3 (Ar C thiol), 100.2 (Ar C thiol), 85.4 (Ar CH *p*-cymene), 85.2 (Ar CH *p*-cymene), 84.8 (Ar CH *p*-cymene), 83.9 (Ar CH *p*-cymene), 30.7 ( $\underline{\text{C}}\text{H}(\text{CH}_3)_2$ ), 21.3 and 20.9 ( $\text{CH}(\underline{\text{C}}\text{H}_3)_2$ ), 16.4 ppm ( $\text{CH}_3$ ); ESI-MS (positive mode, acetonitrile):  $m/z$  853.0; Mw = 926.88 g/mol.

### Synthesis of 7

*p*-*t*-butylthiophenol (53.6 mg, 0.322 mmol, 2.0 eq) was dropwise added into stirred and cooled solution of  $[(\eta^6\text{-}p\text{-MeC}_6\text{H}_4\text{Pr}^i)\text{Ru}(\mu_2\text{-Cl})\text{Cl}]_2$  (99.0 mg, 0.162 mmol) in DCM and the mixture was left to react for 4 h at 0 °C. Subsequently, the crude product was concentrated and purified on silica column using DCM/EtOH 6:1 to give orange solid **7** in 98% yield (144.4 mg, 0.158 mmol).

### Synthesis of 8

$[(\eta^6\text{-}p\text{-MeC}_6\text{H}_4\text{Pr}^i)\text{Ru}(\mu_2\text{-Cl})\text{Cl}]_2$  (105.5 mg, 0.172 mmol) was dissolved in DCM (50 mL) and *p*-methoxythiophenol (50.8 mg, 0.362 mmol, 2.1 eq) was added dropwise into stirred solution. The mixture was left to react stirred at room temperature for 4 h. Subsequently, it was concentrated and purified on silica column using DCM/EtOH 5:1 as an eluent. The product was obtained as dark orange solid (119.7 mg) in 85% purity. The yield accounting for the degree of purity was 72%.

### Synthesis of 9

**8** (80 mg, 0.083 mmol, 85% pure) was dissolved in DCM (50 mL) and *p*-*t*-butylthiophenol (17.9 mg, 0.108 mmol, 1.3 eq) was dropwise added into stirred solution. The mixture was left to react stirred at room temperature for 48 h. Next, the product was concentrated and purified on silica column using DCM/EtOH 9:1 as an eluent. **9** was obtained as orange solid (24.4 mg) in 29% yield.

## 2.2 Characterisation

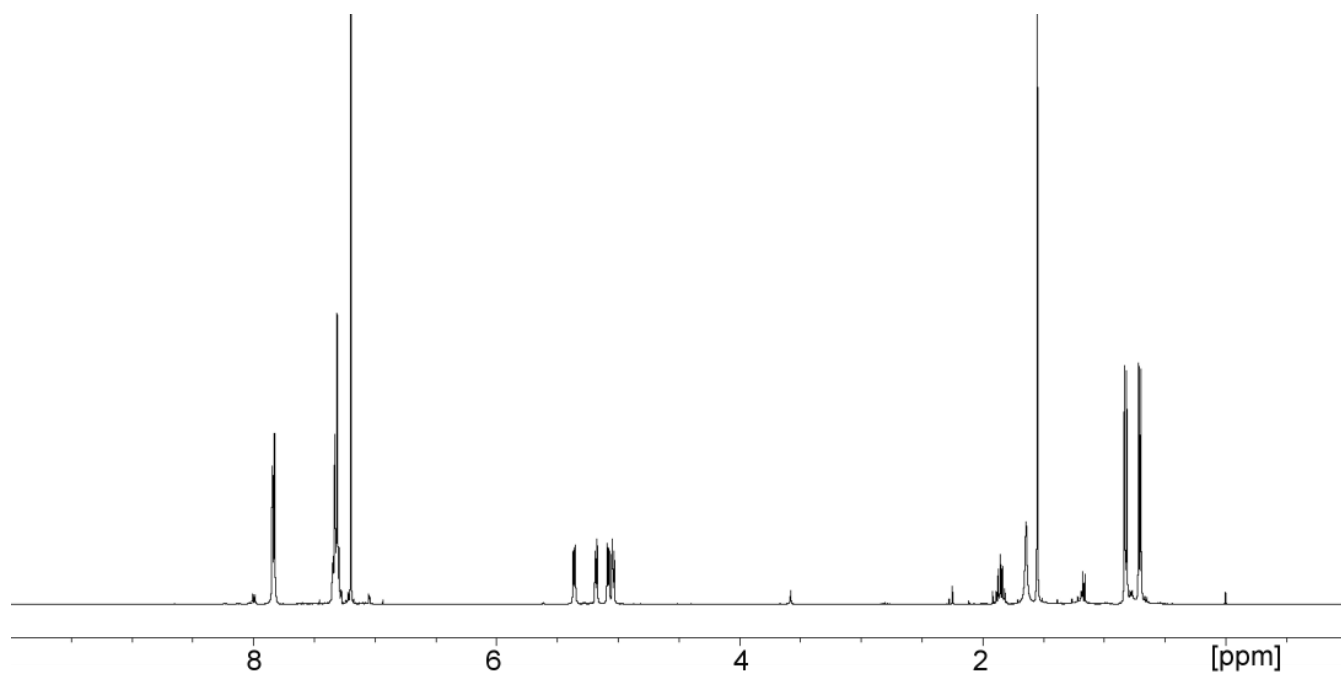


Figure S9. 400.1 MHz <sup>1</sup>H NMR of **1** in CDCl<sub>3</sub>, 32 scans.

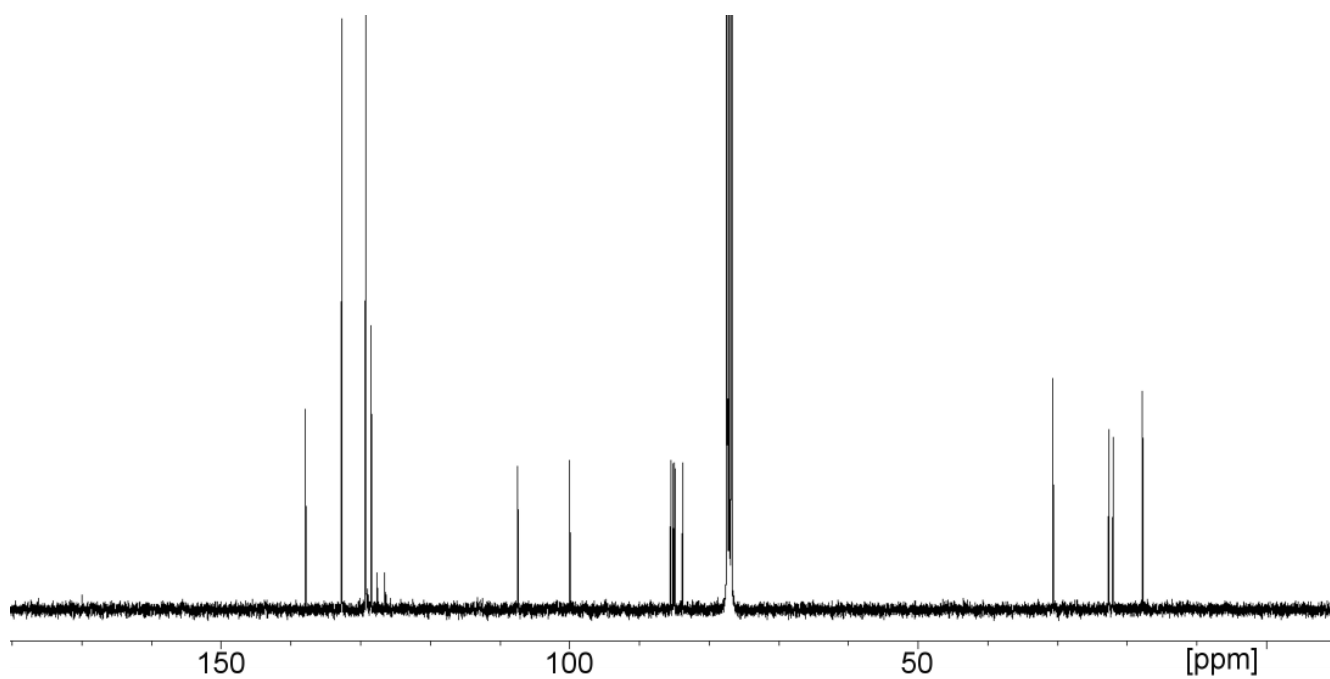


Figure S10. 100 MHz <sup>13</sup>C NMR of **1** in CDCl<sub>3</sub>, 10240 scans.

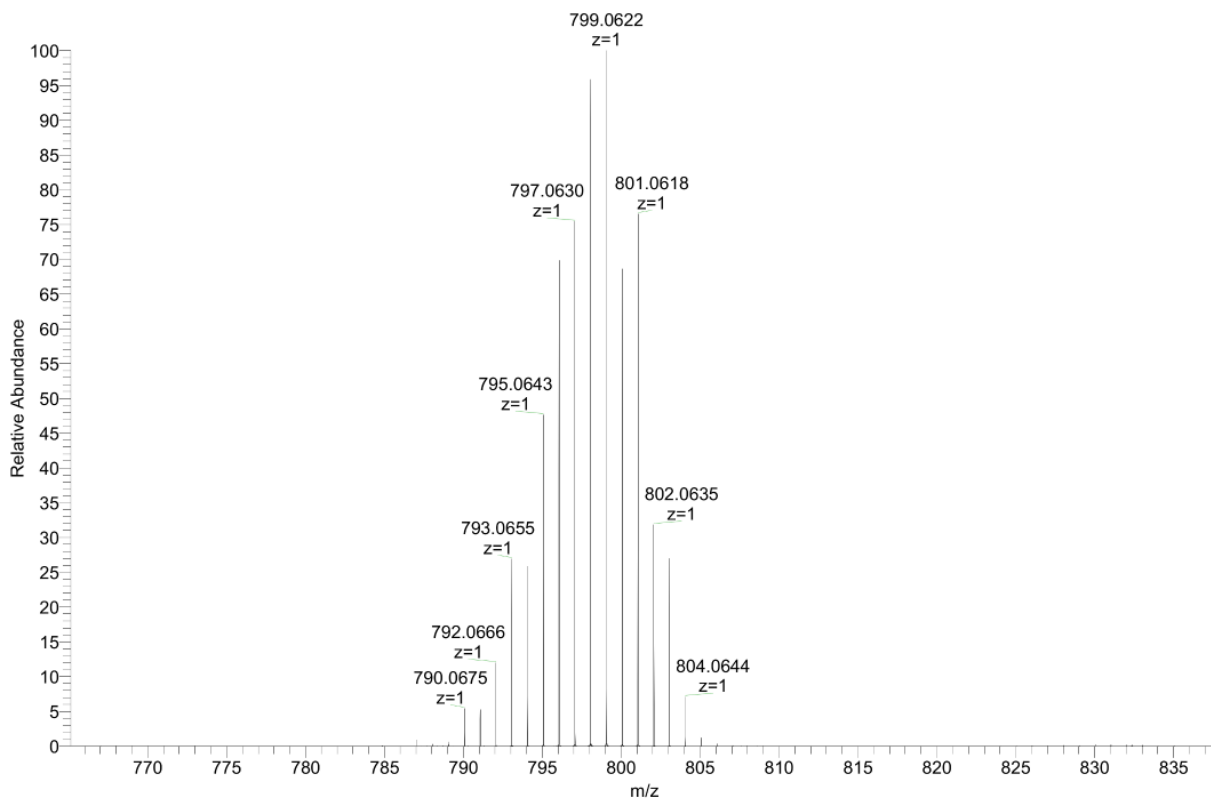


Figure S11. ESI-MS of **1** dissolved in MeOH and recorded in positive mode.

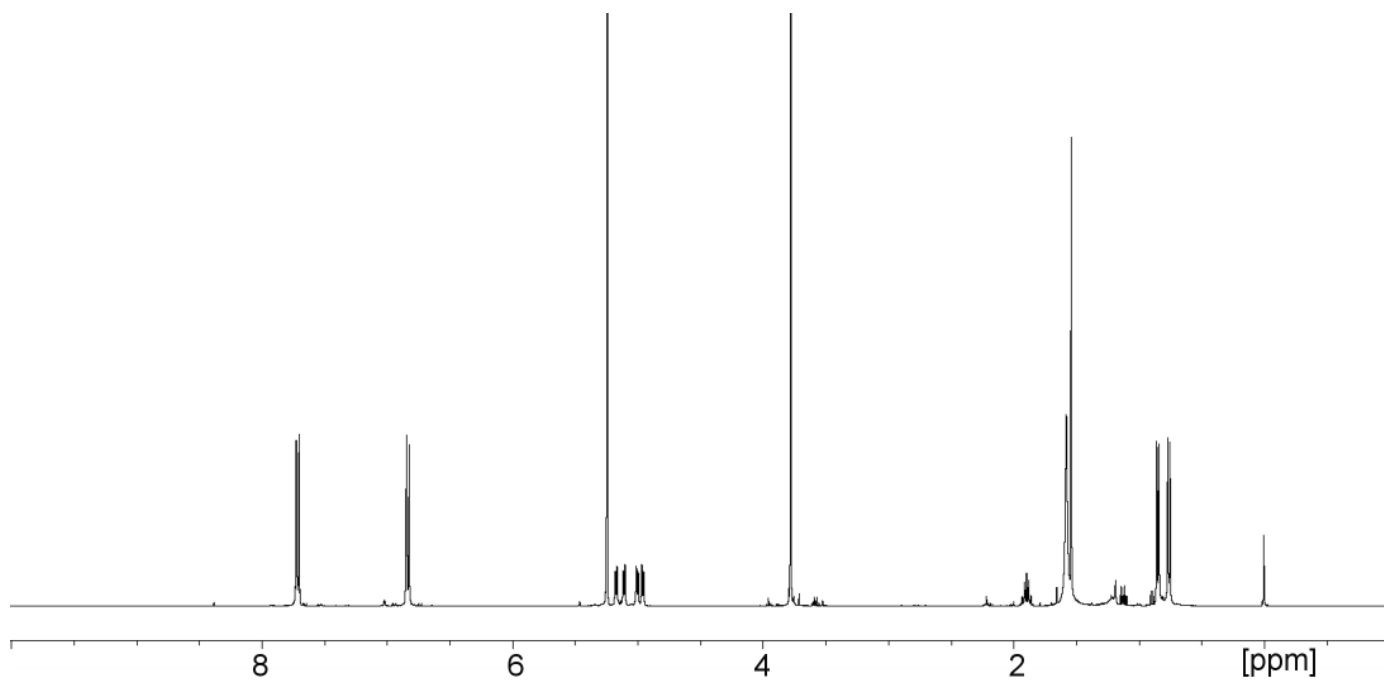


Figure S12. 400.1 MHz  $^1\text{H}$  NMR of **2** in  $\text{CD}_2\text{Cl}_2$ , 32 scans.

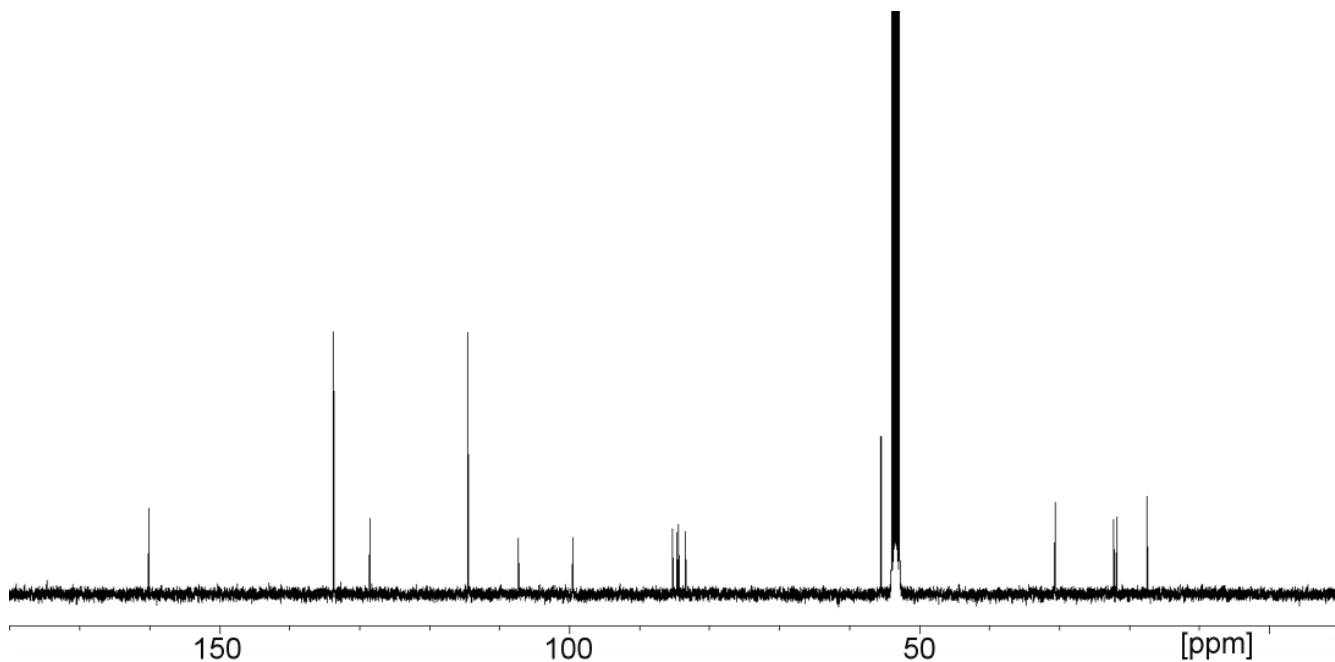


Figure S13. 100 MHz  $^{13}\text{C}$  NMR of **2** in  $\text{CD}_2\text{Cl}_2$ , 8192 scans.

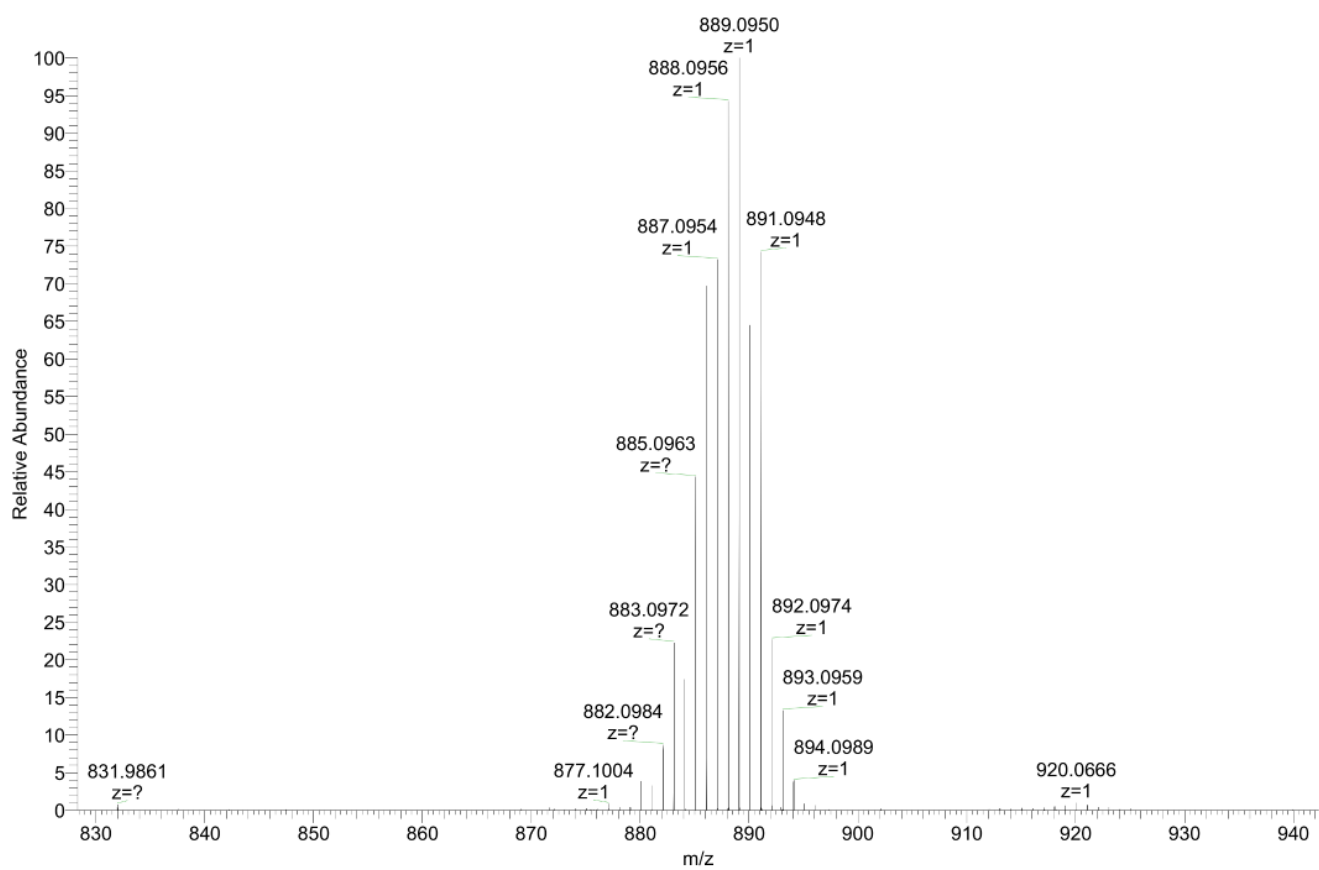
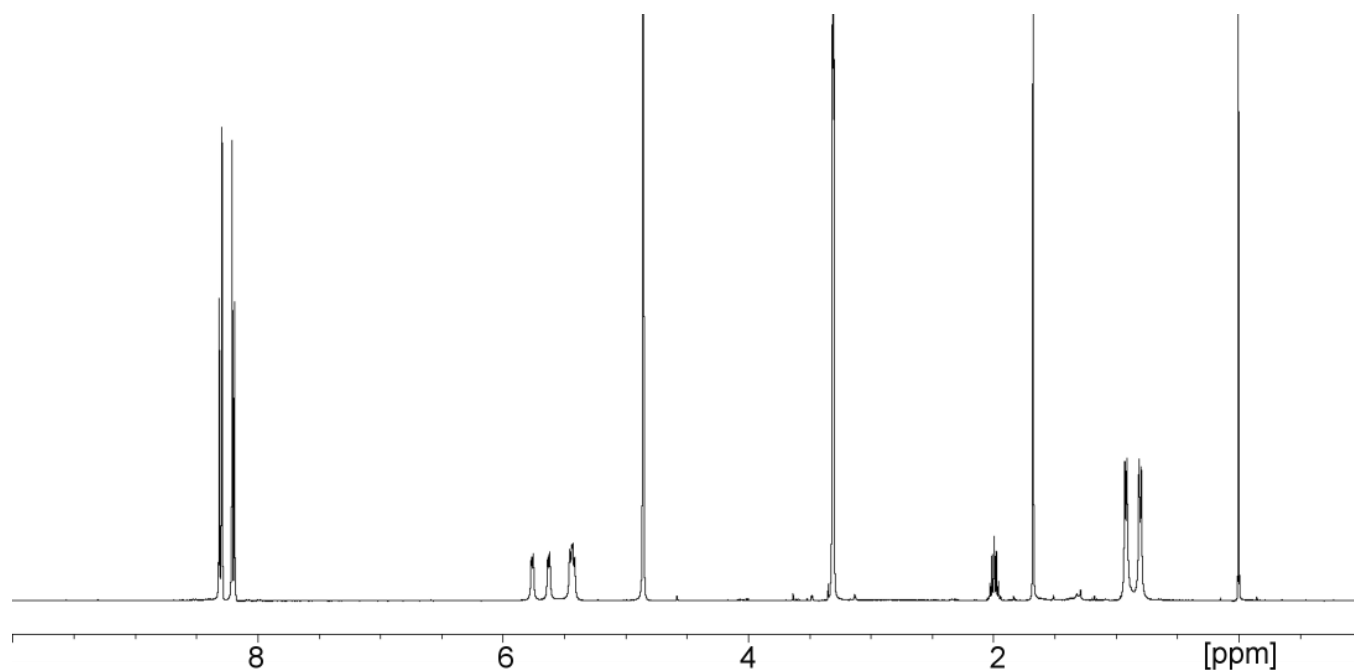
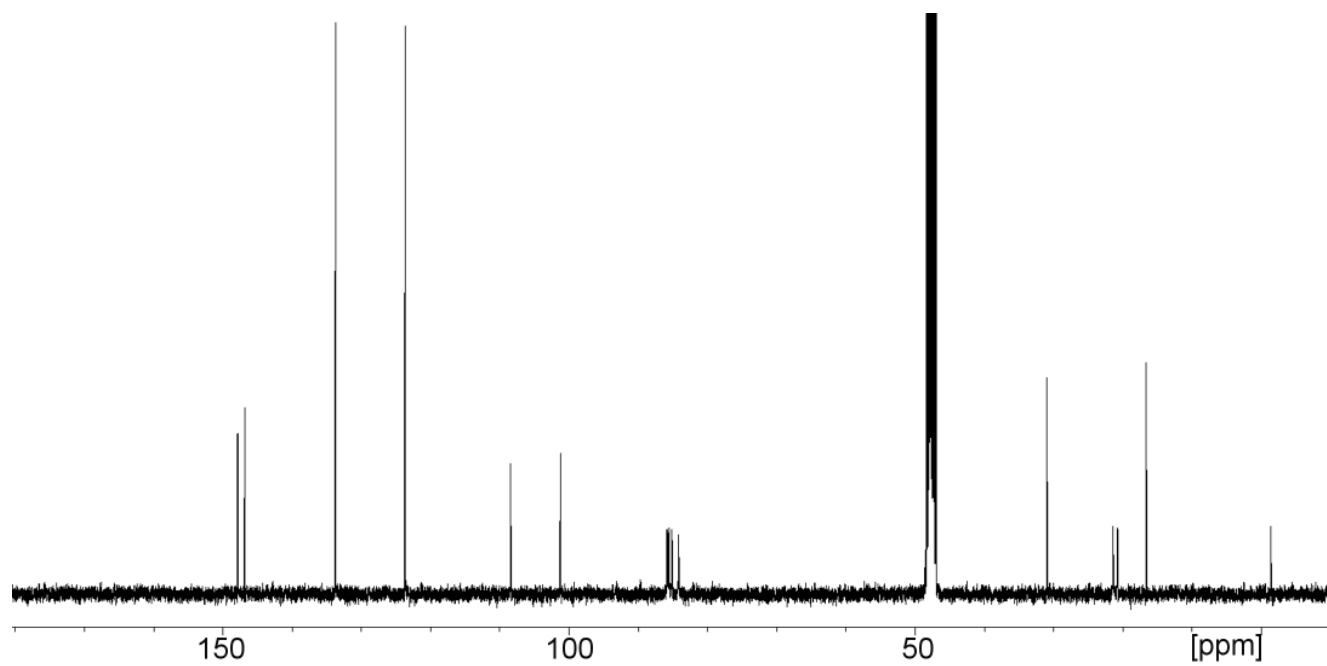


Figure S14. ESI-MS of **2** dissolved in MeOH and recorded in positive mode.



**Figure S15.** 400.1 MHz <sup>1</sup>H NMR of **3** in MeOD, 32 scans.



**Figure S16.** 100 MHz <sup>13</sup>C NMR of **3** in MeOD, 8192 scans.

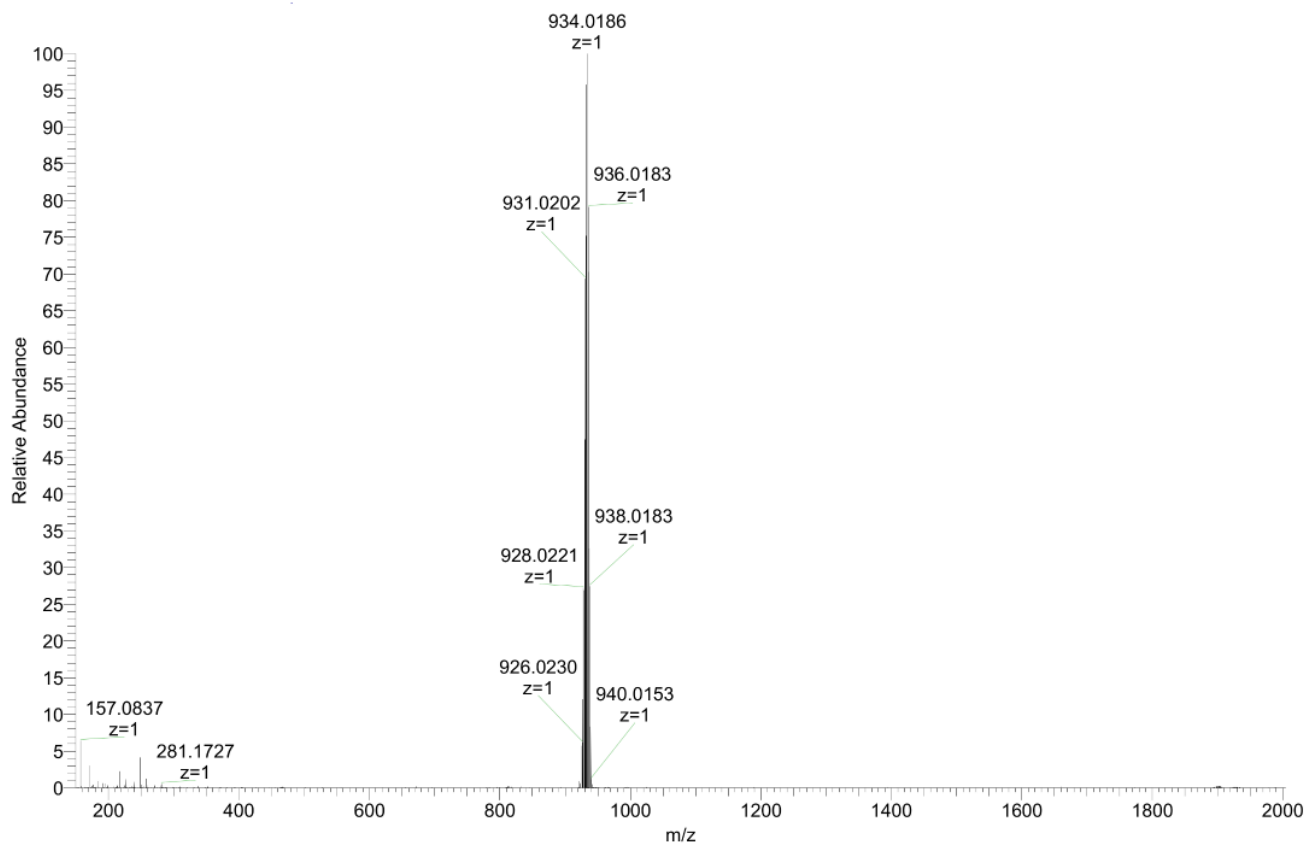


**Figure S17.** ESI-MS of **3** dissolved in MeOH and recorded in positive mode.

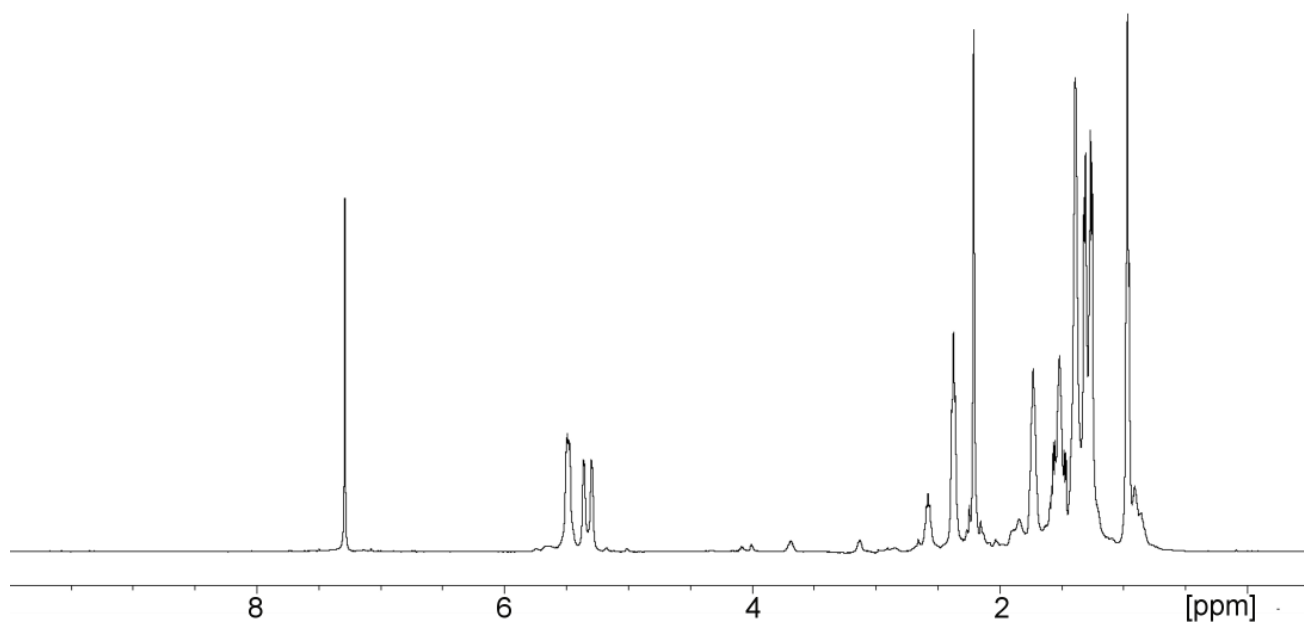


**Figure S18.** 500.1 MHz  $^1\text{H}$  NMR of **4** in  $\text{CDCl}_3$ , 128 scans.

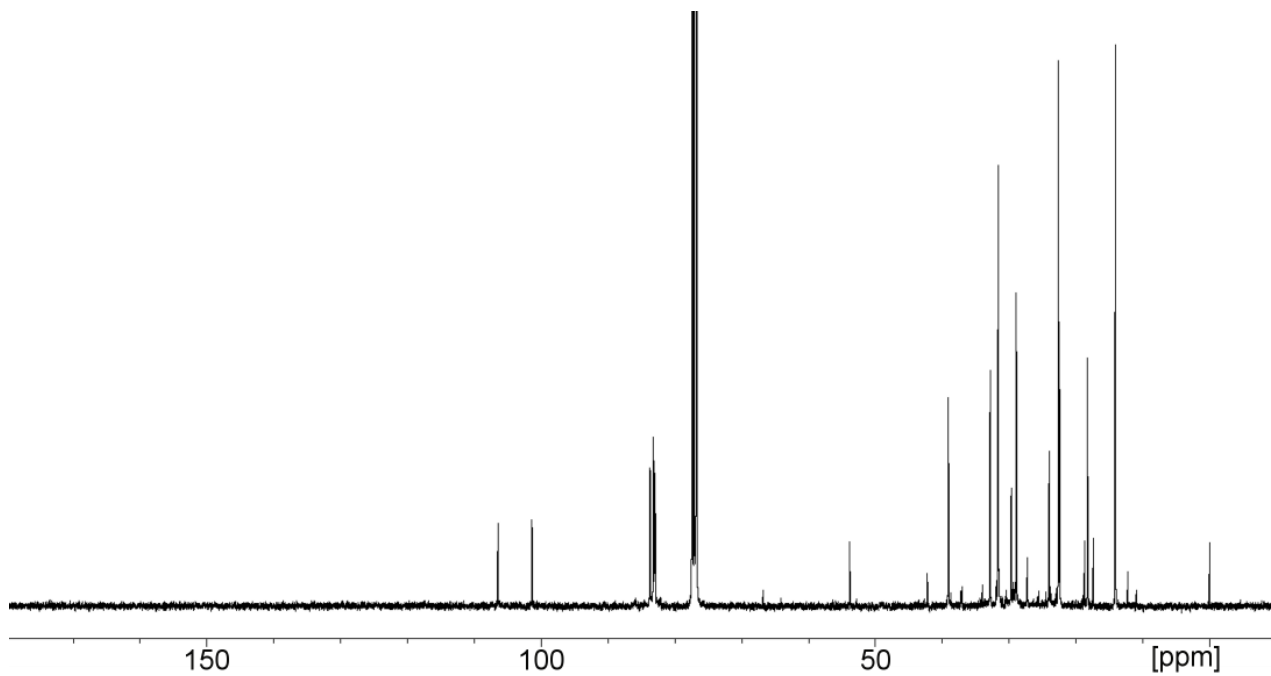


**Figure S19.** 100 MHz <sup>13</sup>C NMR of crude **4** in CDCl<sub>3</sub>, 10240 scans.

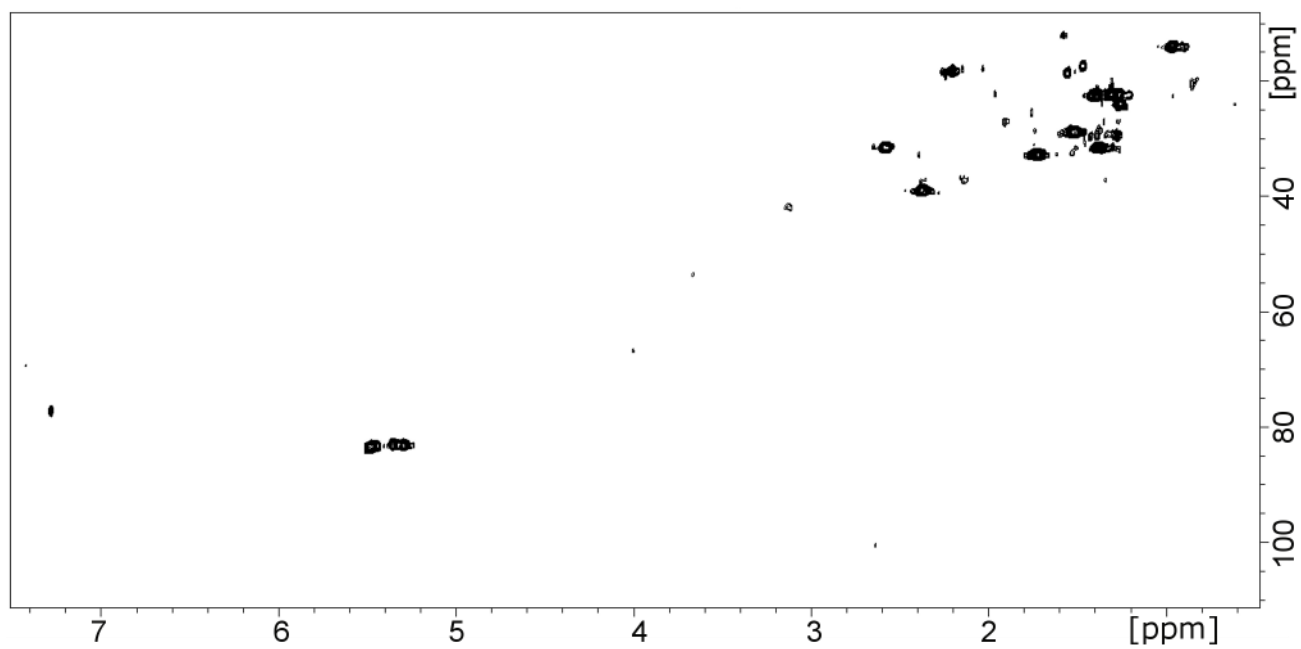


**Figure S20.** 500.1 MHz <sup>13</sup>C HSQC of **4** in CDCl<sub>3</sub>, 128 scans.

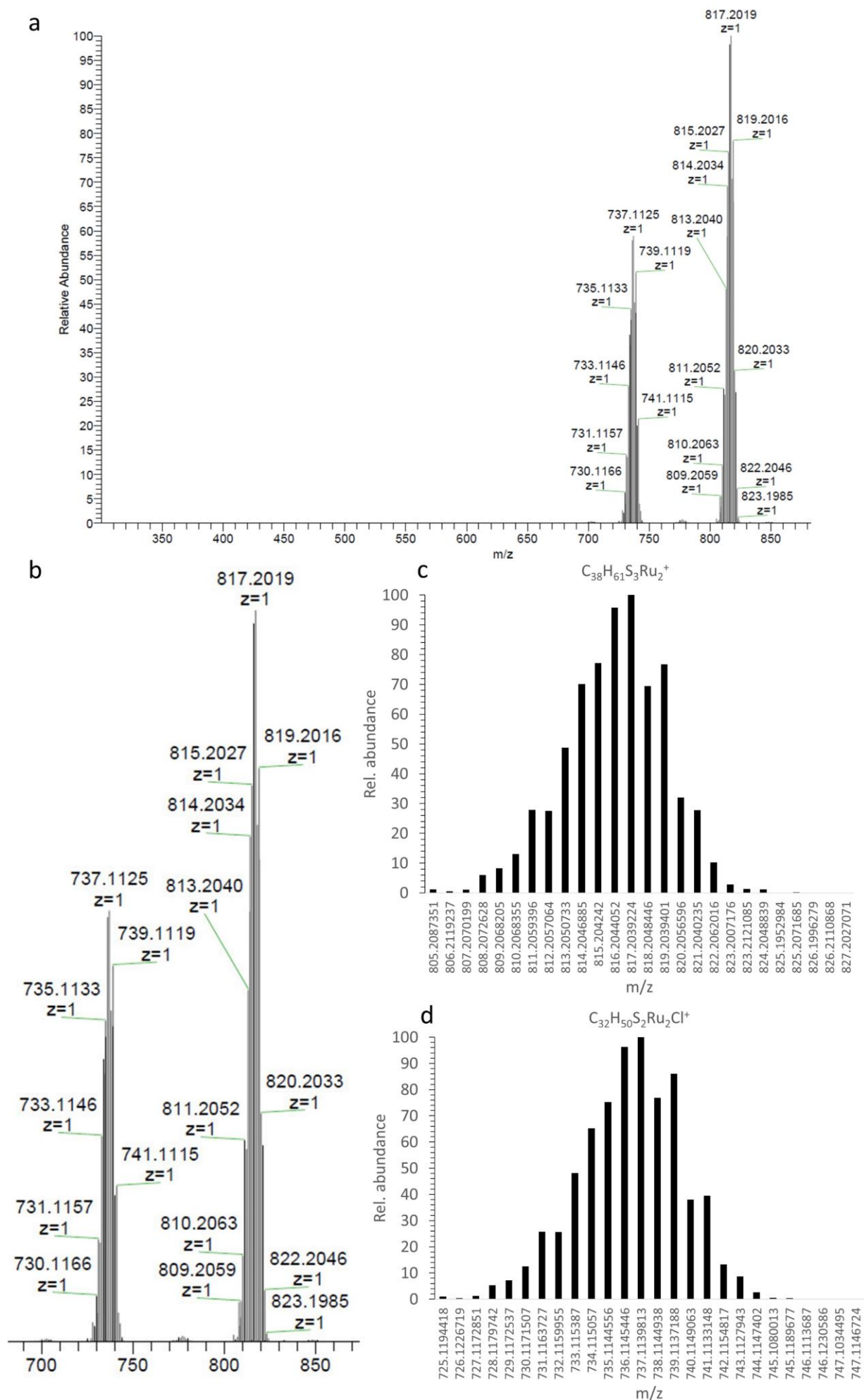


**Figure S21.** ESI-MS of **4** dissolved in ACN and recorded in positive mode (a, b) and theoretical distributions (obtained using an on-line tool of Eawag enviPat Web 2.4) for **4** (c) and dithiolato byproduct (d).

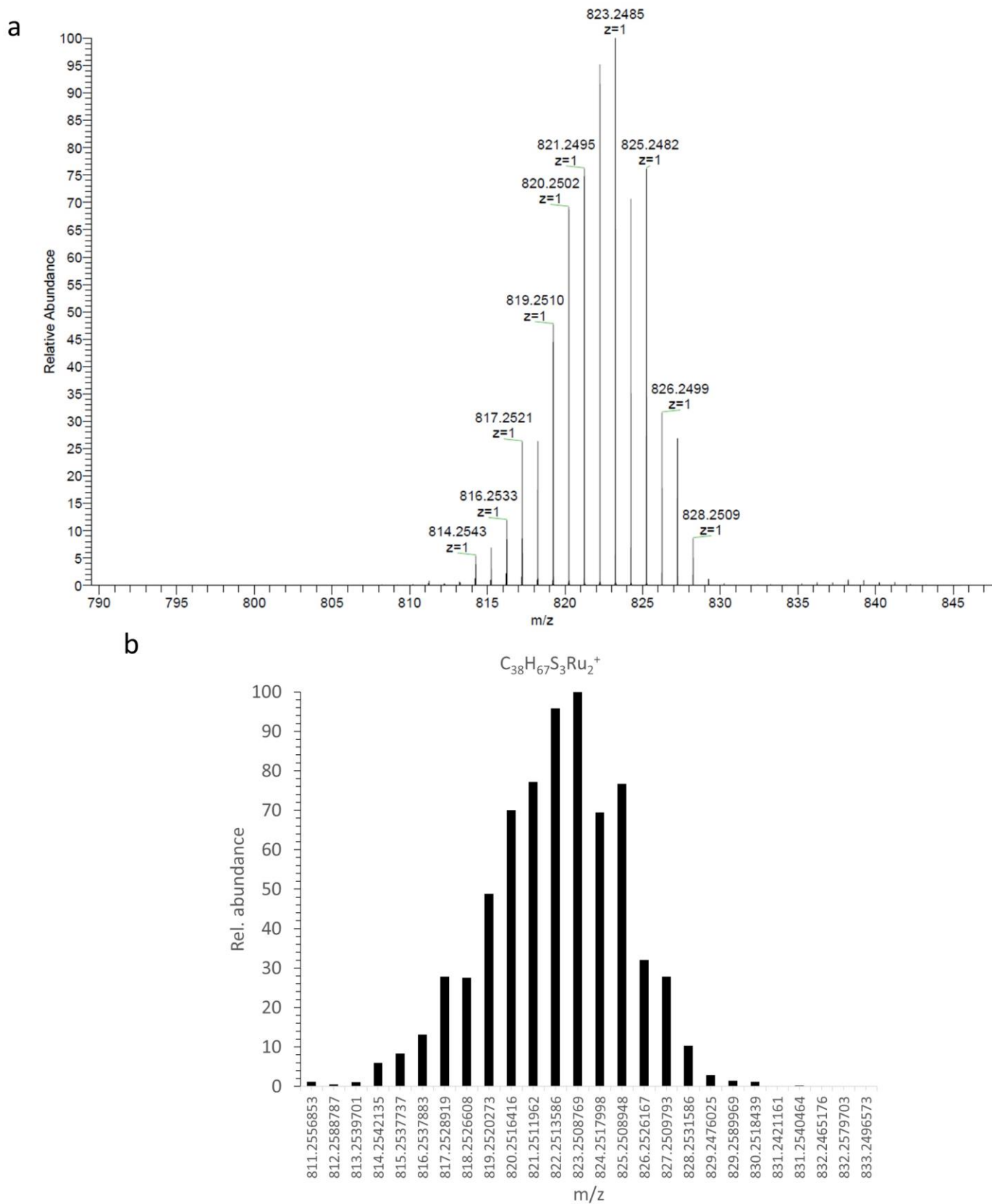


**Figure S22.** ESI-MS of **5** dissolved in EtOH and recorded in positive mode (a) and theoretical distribution (obtained using an on-line tool of Eawag enviPat Web 2.4) (b).

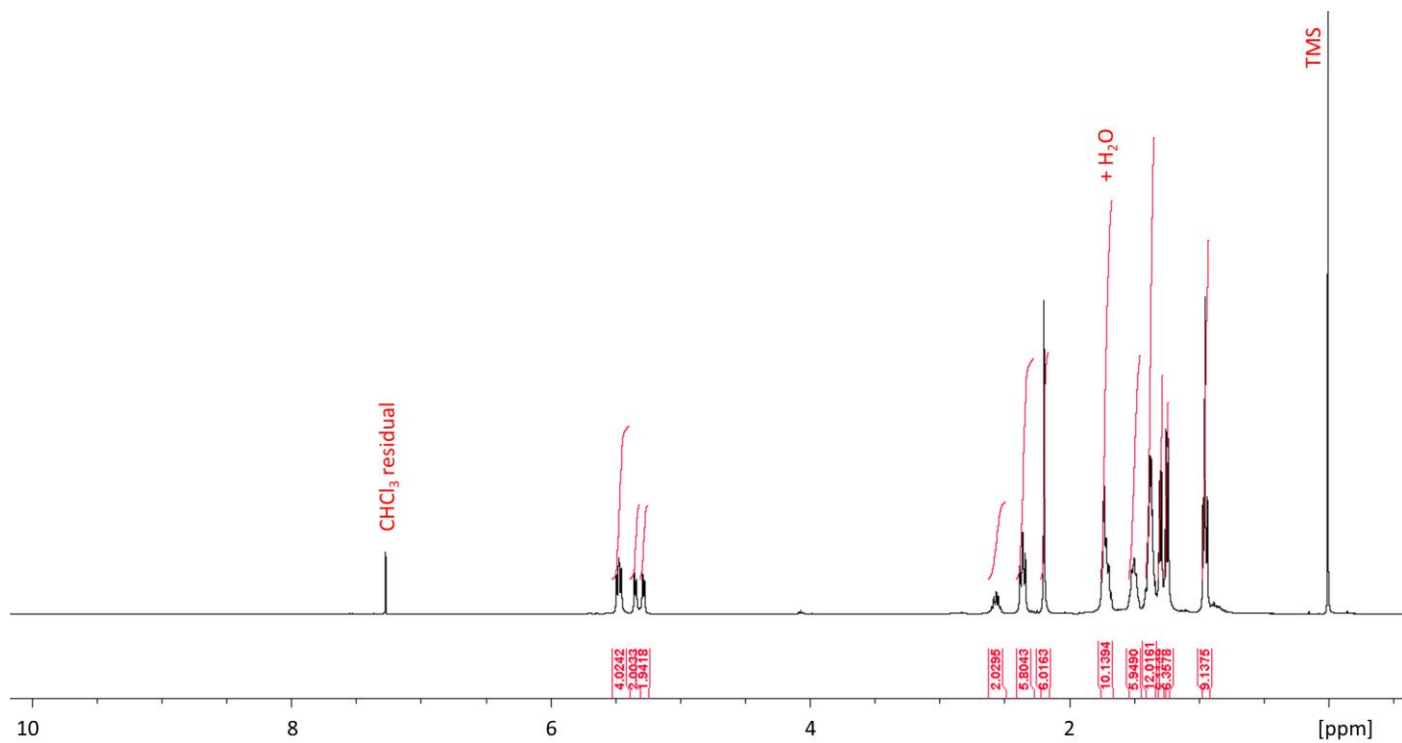


Figure S23. 400.1 MHz  $^1\text{H}$  NMR of complex **5** in  $\text{CDCl}_3$ , 128 scans.

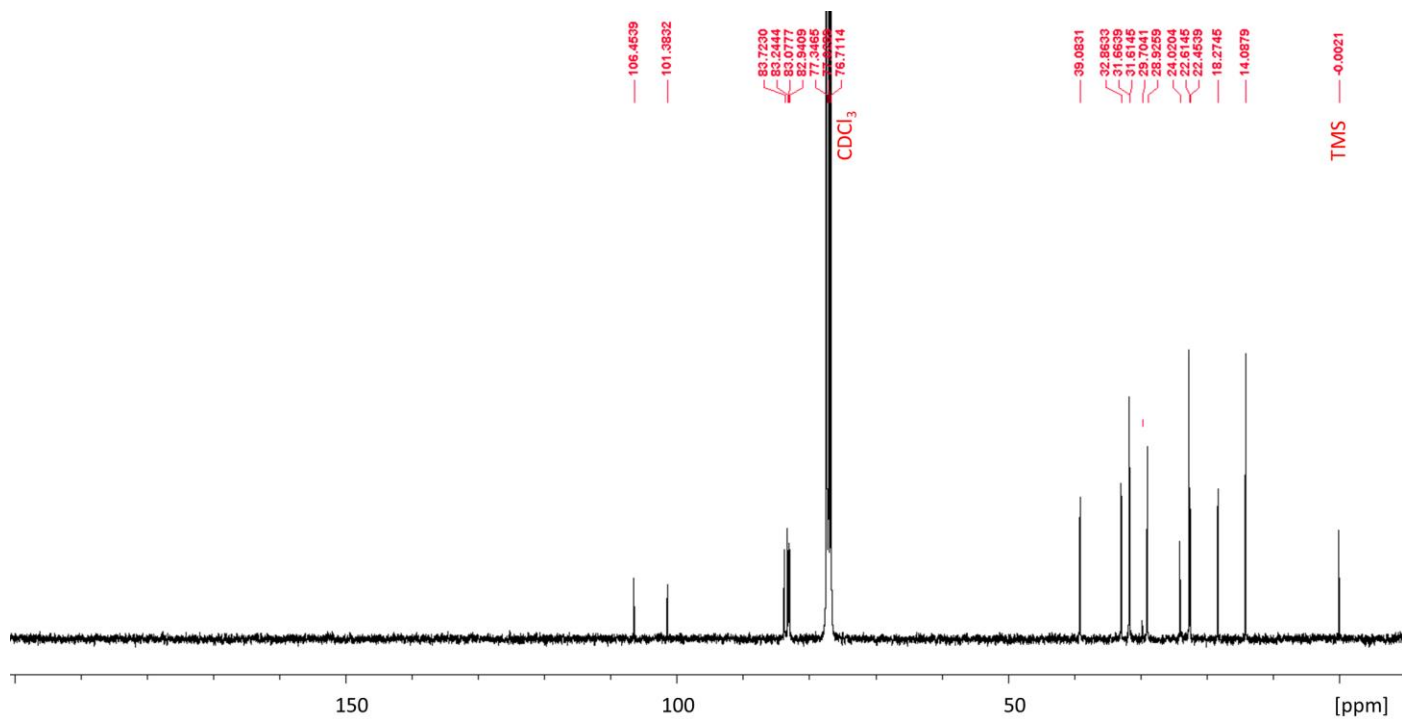


Figure S24. 100 MHz  $^{13}\text{C}$  NMR of complex **5** in  $\text{CDCl}_3$ , 12288 scans.

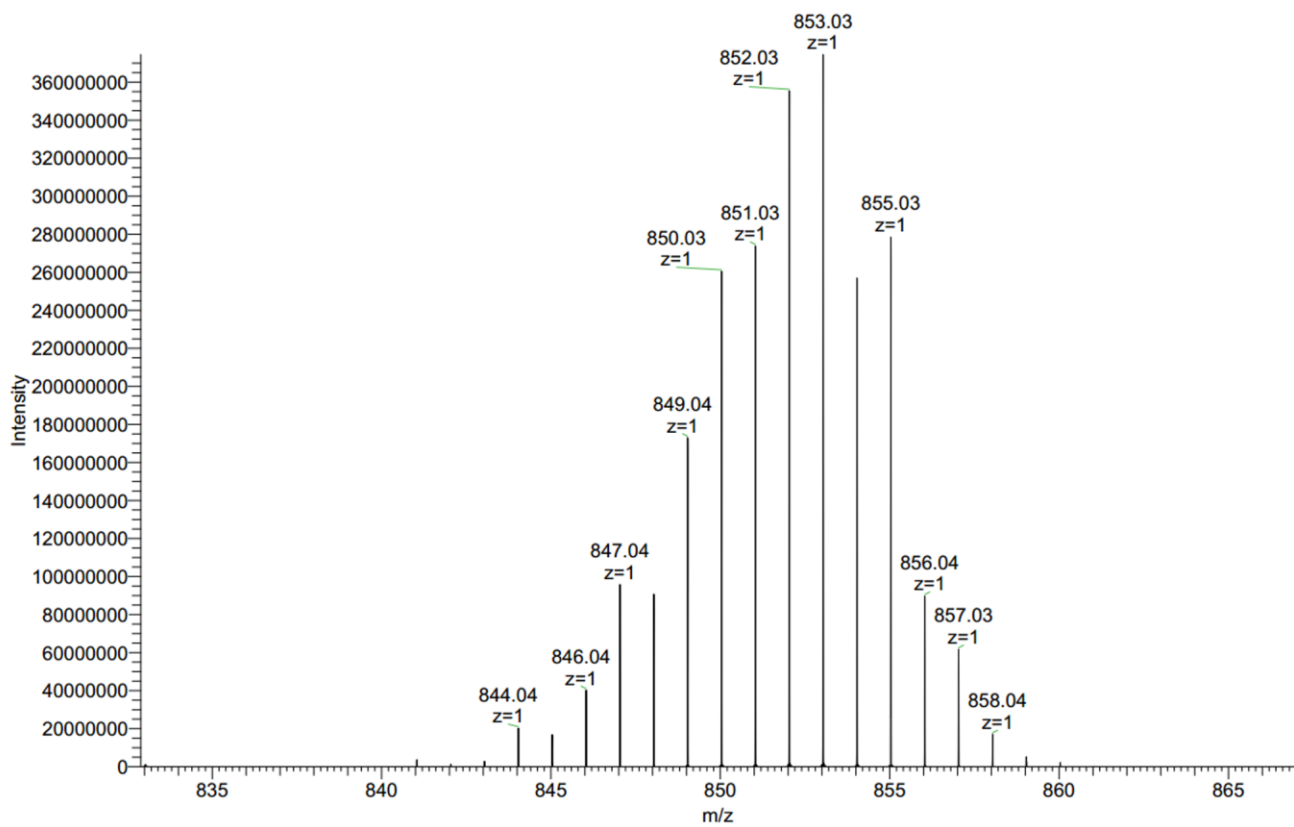


Figure S25. ESI-MS of **6** dissolved in acetonitrile and recorded in positive mode.

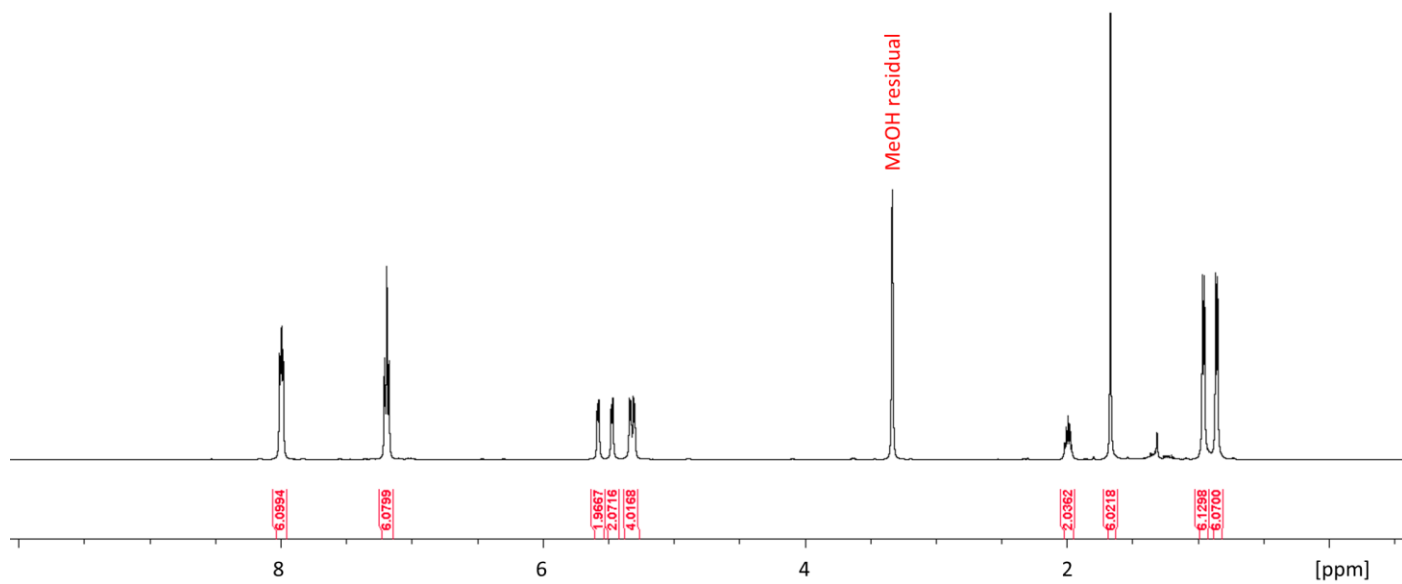


Figure S26. 500.1 MHz  $^1\text{H}$  NMR of complex **6** in MeOD, 16 scans.

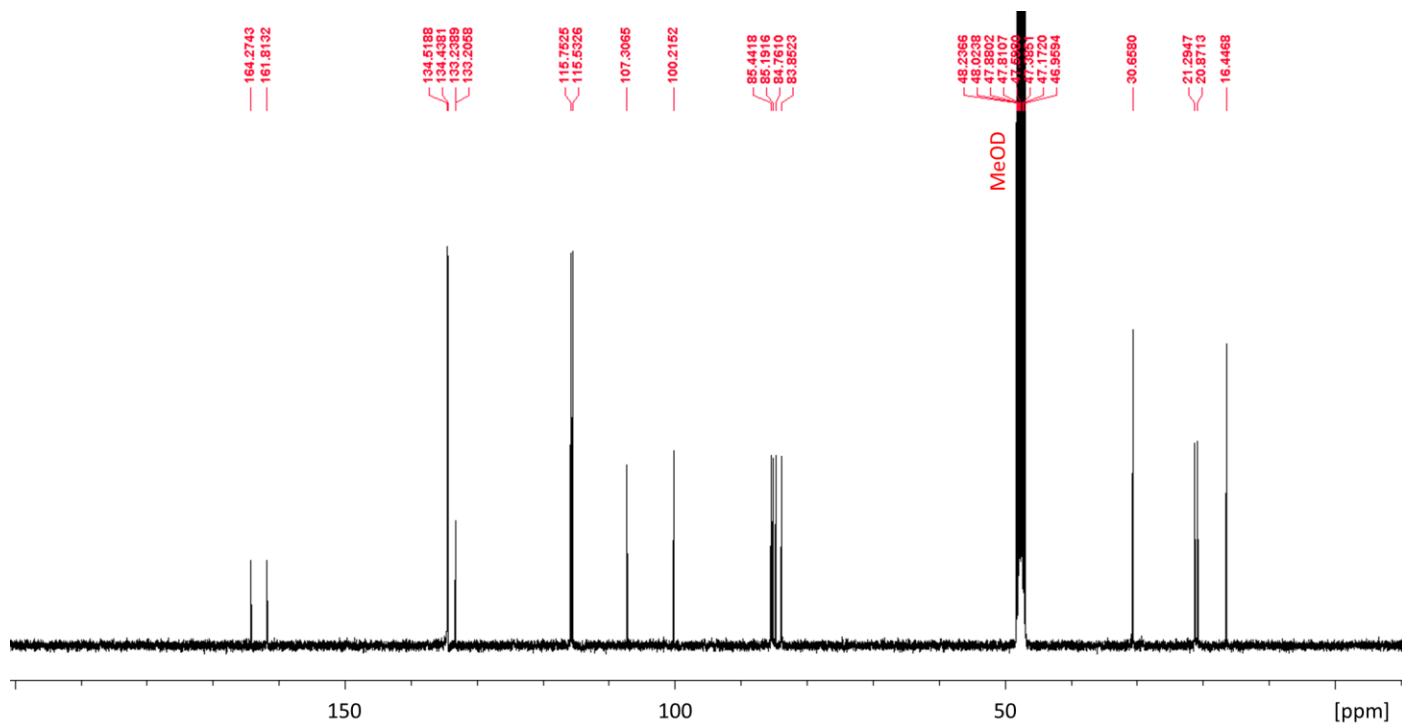
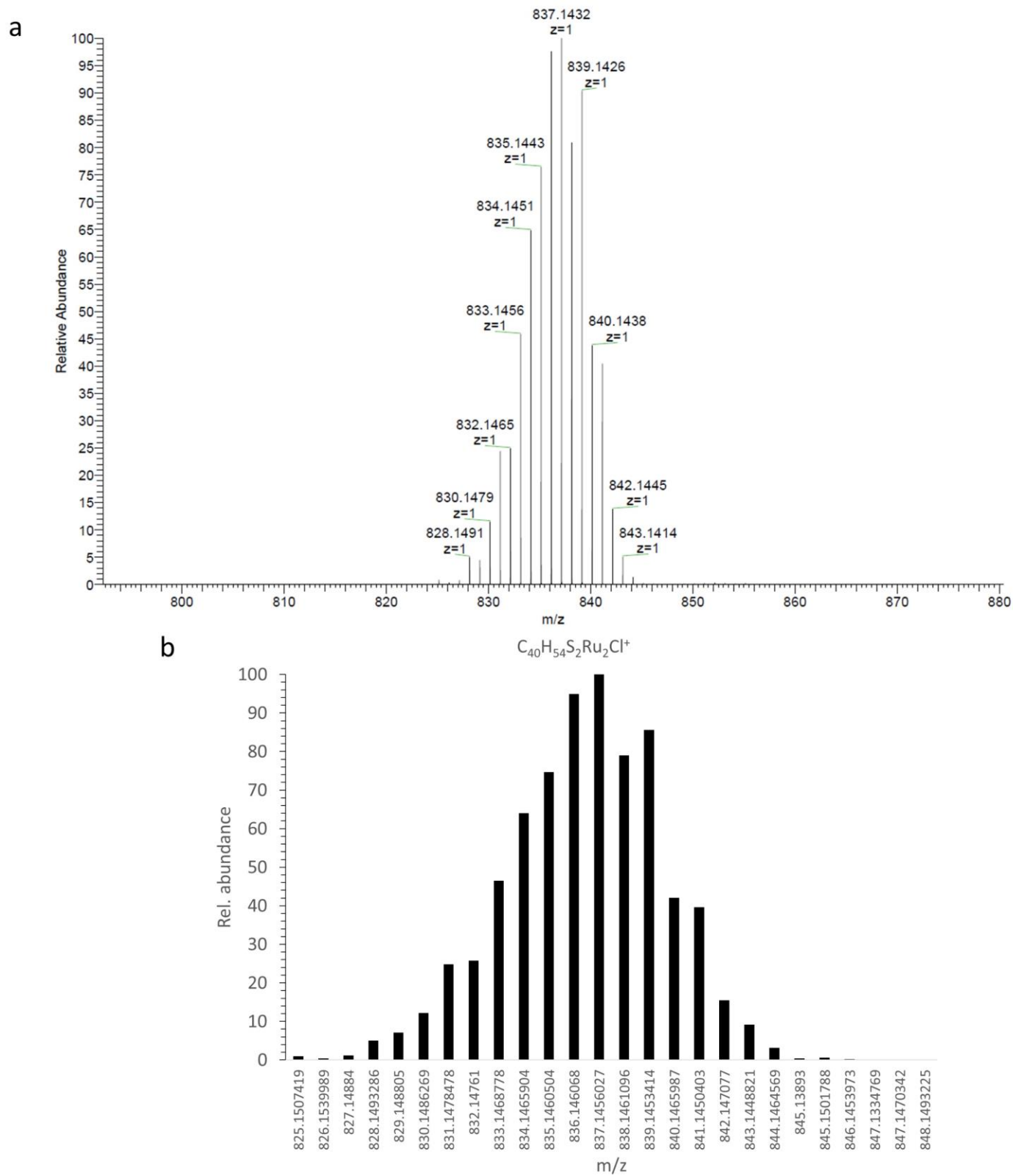
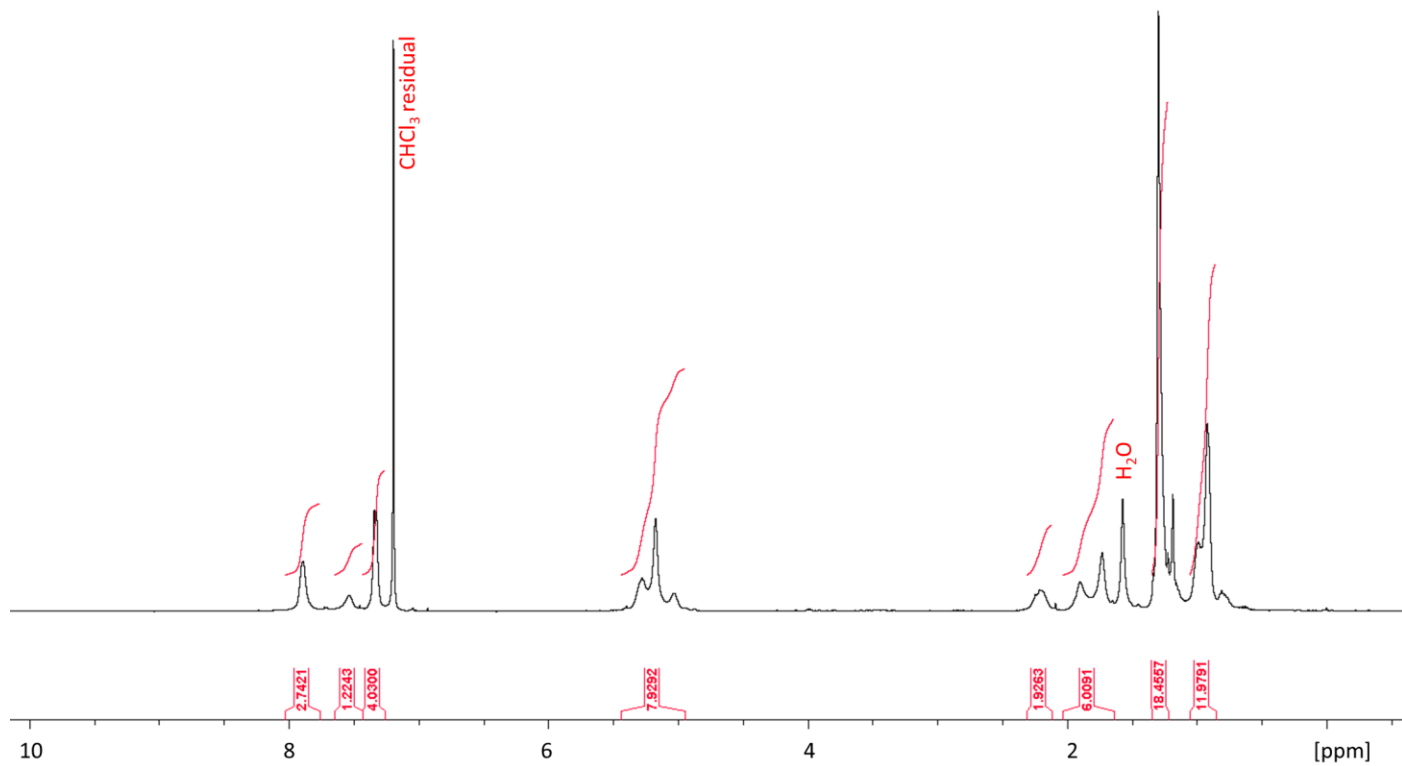


Figure S27. 100 MHz  $^1\text{H}$  NMR of complex **6** in MeOD, 8192 scans.



**Figure S28.** ESI-MS of **7** dissolved in EtOH and recorded in positive mode (a) and theoretical distribution (obtained using an on-line tool of Eawag enviPat Web 2.4) (b).



**Figure S29.** 400.1 MHz  $^1\text{H}$  NMR of complex **7** in  $\text{CDCl}_3$ , 16 scans.

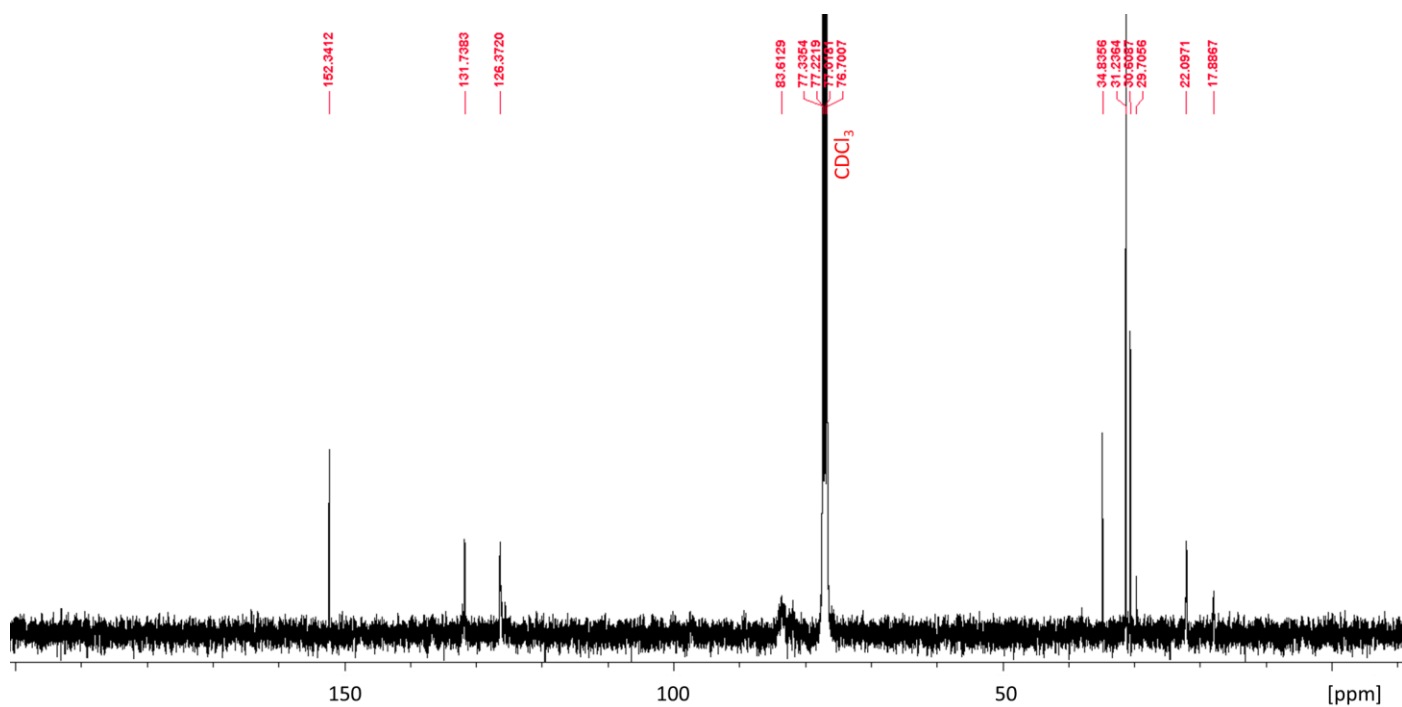


**Figure S30.** 100 MHz  $^{13}\text{C}$  NMR of complex **7** in  $\text{CDCl}_3$ , 8192 scans.

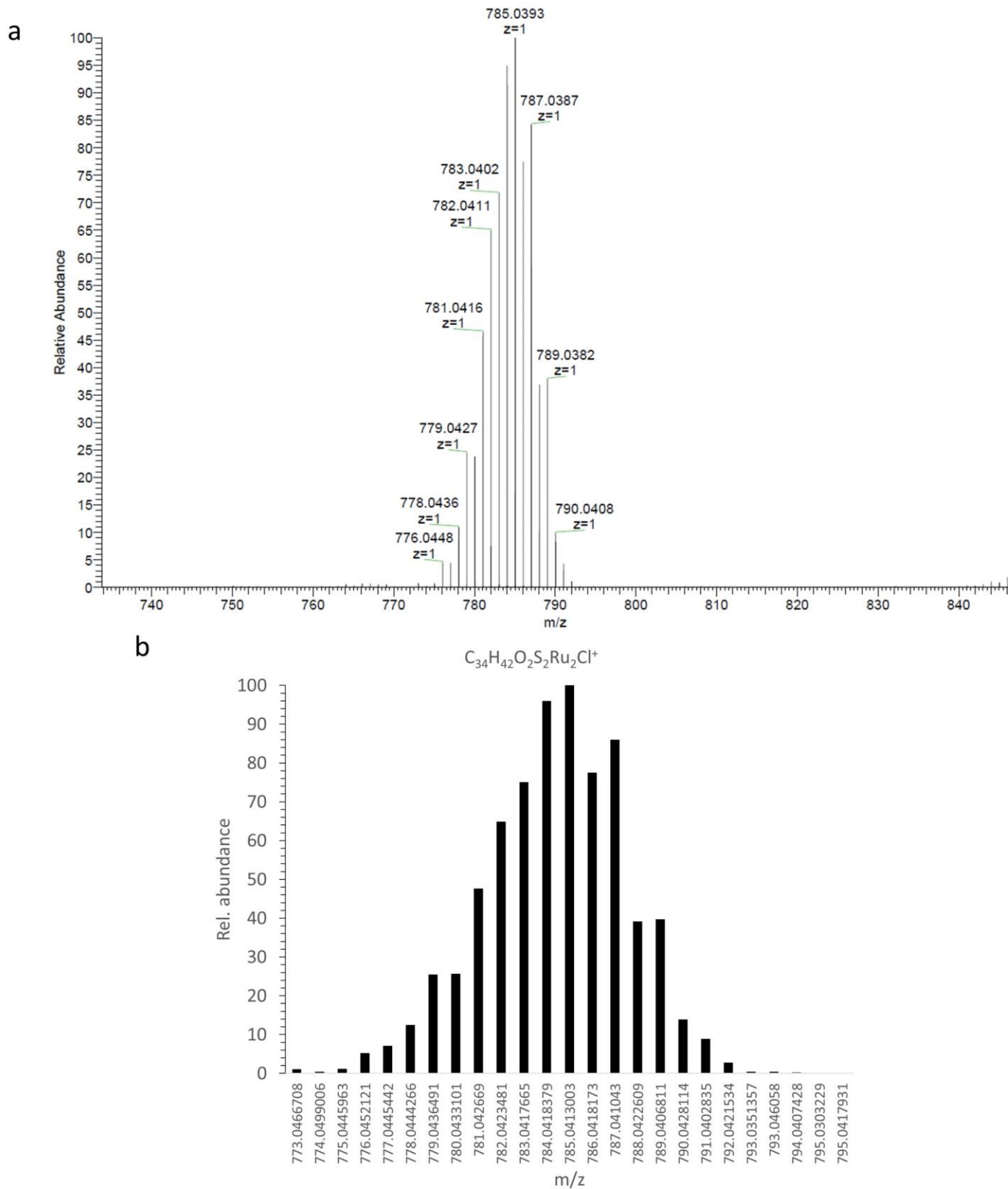


**Figure S31.** ESI-MS of **8** dissolved in MeOH and recorded in positive mode (a) and theoretical distribution (obtained using an on-line tool of Eawag enviPat Web 2.4) (b).

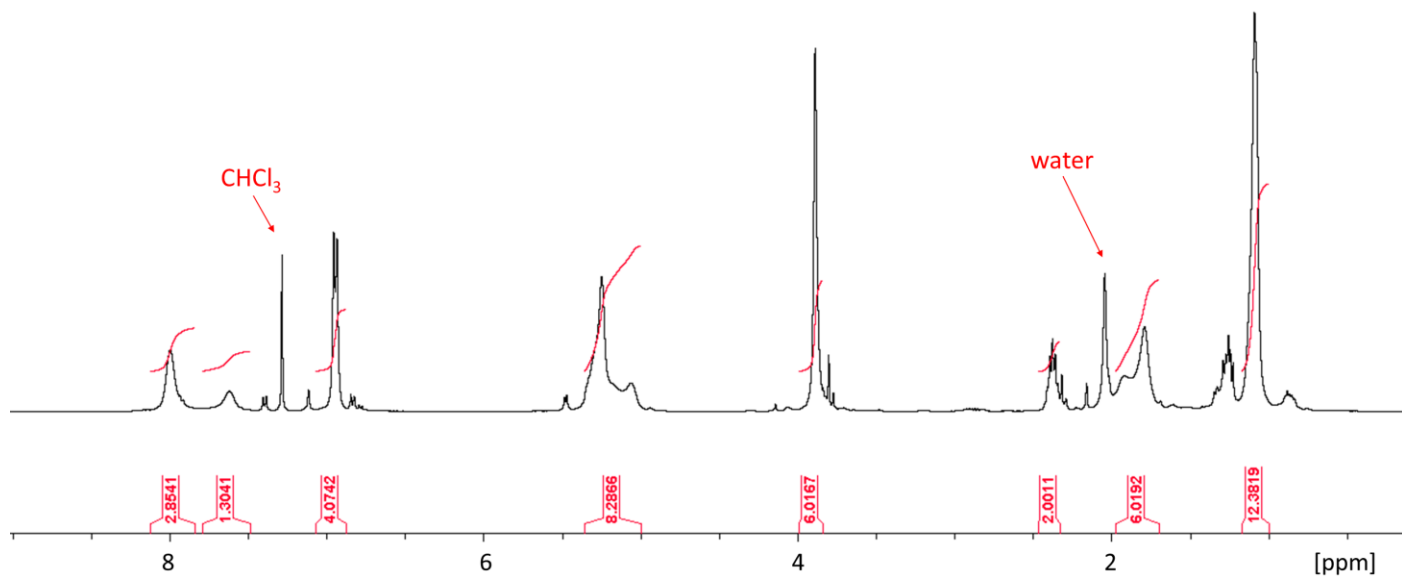


Figure S32. 400.1 MHz  $^1\text{H}$  NMR of complex **8** in  $\text{CDCl}_3$ , 32 scans.

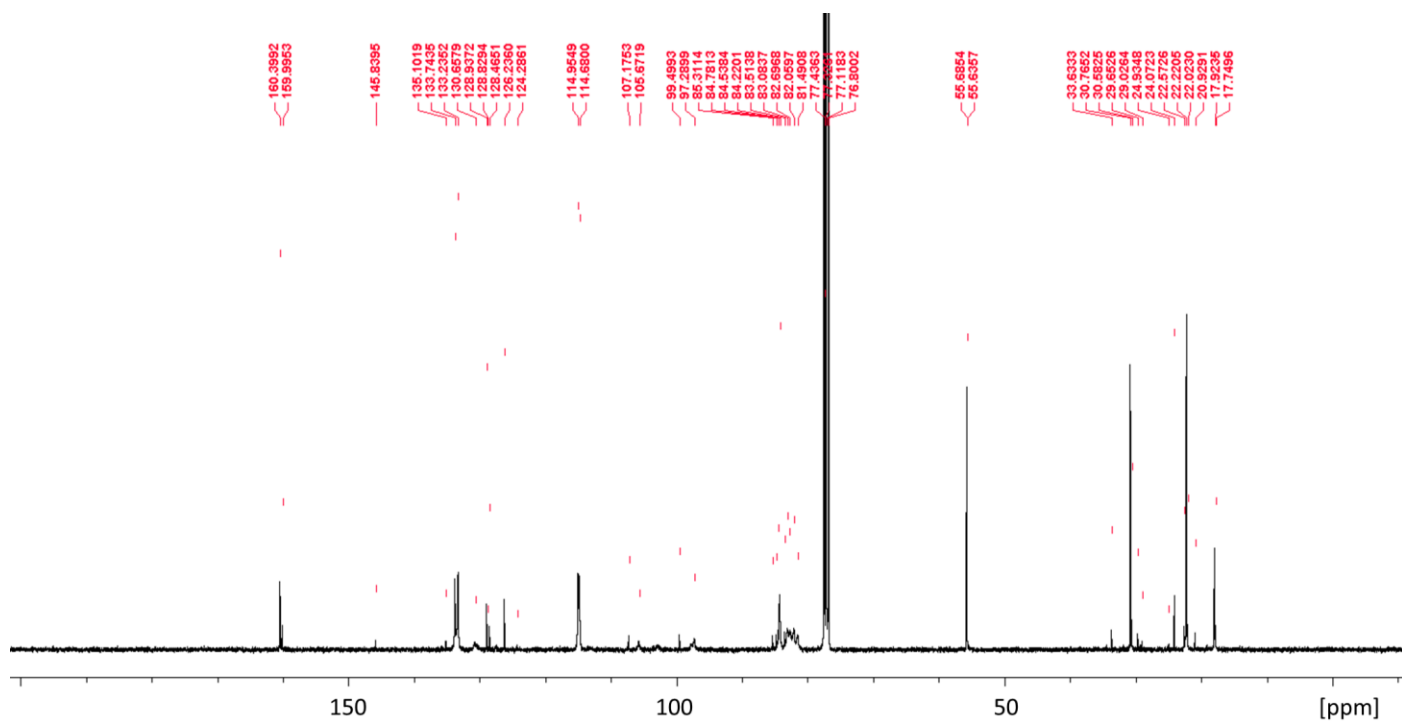
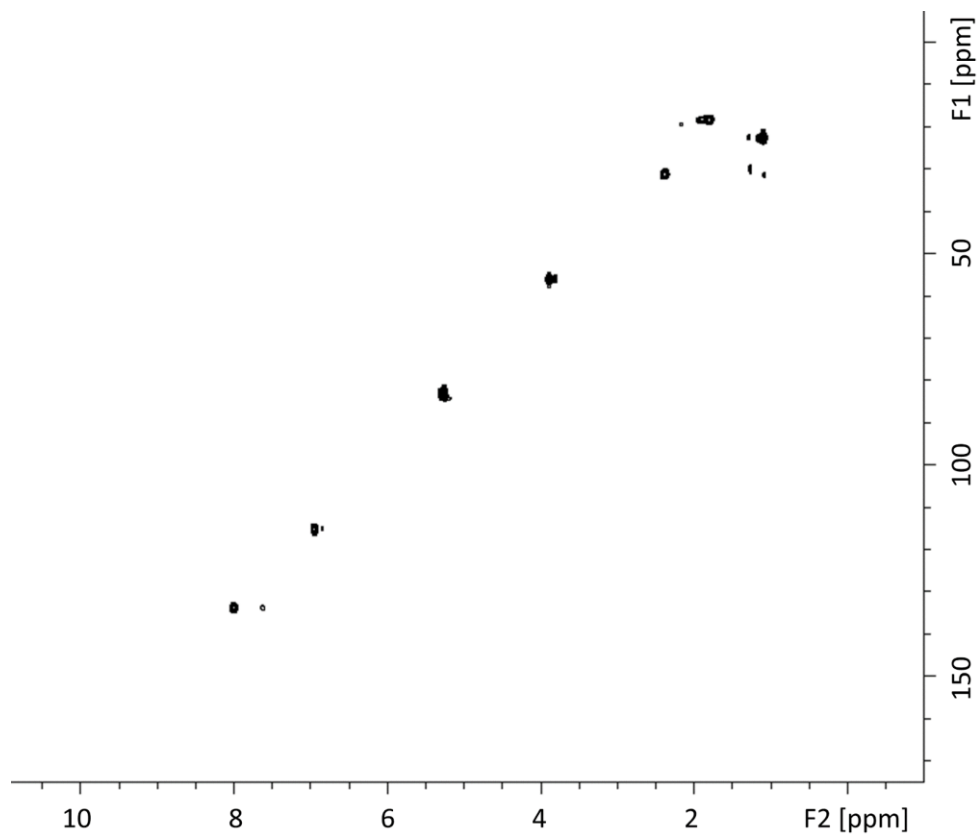
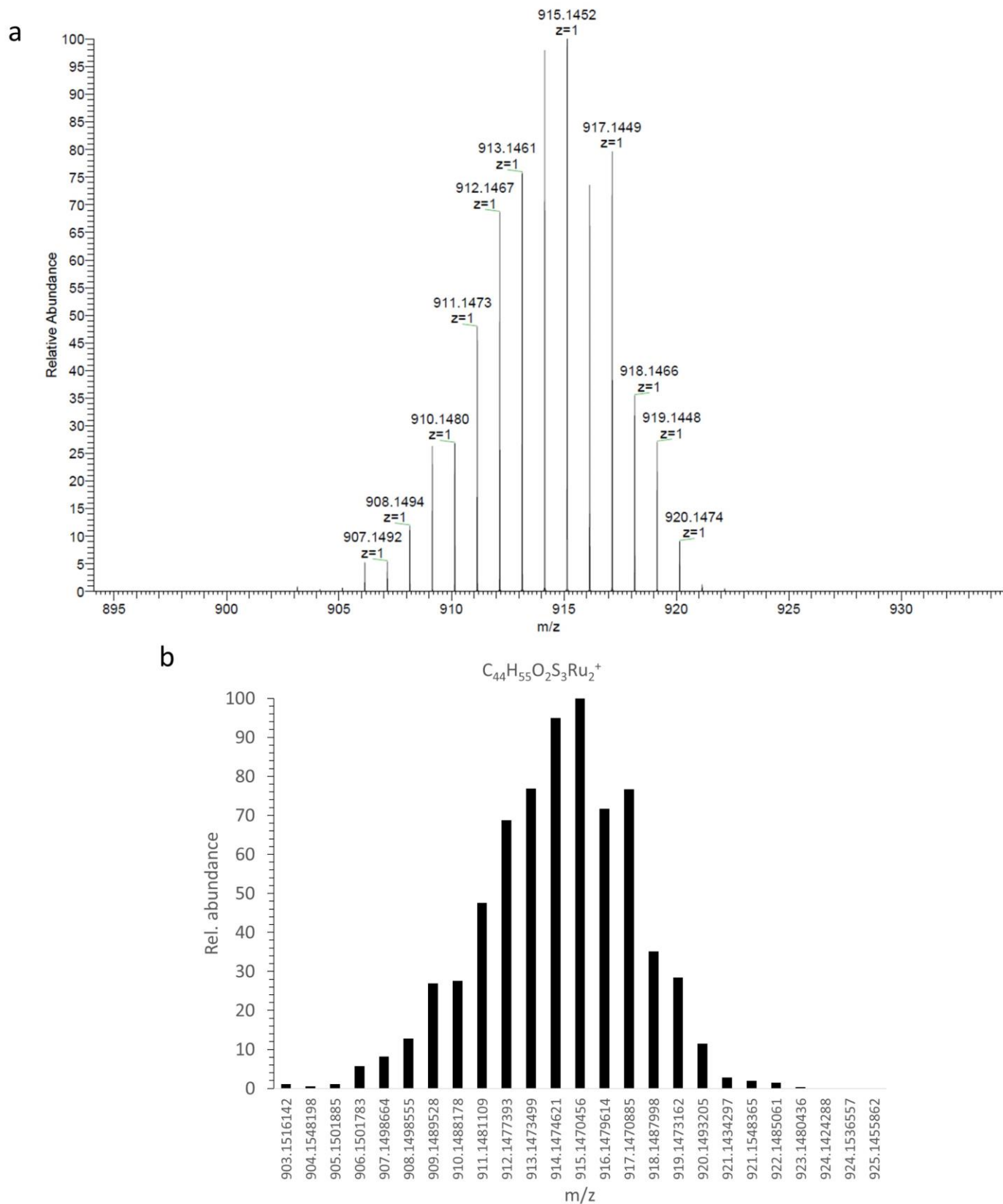


Figure S33. 100 MHz  $^{13}\text{C}$  NMR of complex **8** in  $\text{CDCl}_3$ , 8192 scans.



**Figure S34.** 400 MHz  $^{13}\text{C}$  HSQC of complex **8** in  $\text{CDCl}_3$ , 32 scans.



**Figure S35.** ESI-MS of **9** dissolved in MeOH and recorded in positive mode (a) and theoretical distribution (obtained using an on-line tool of Eawag enviPat Web 2.4) (b).

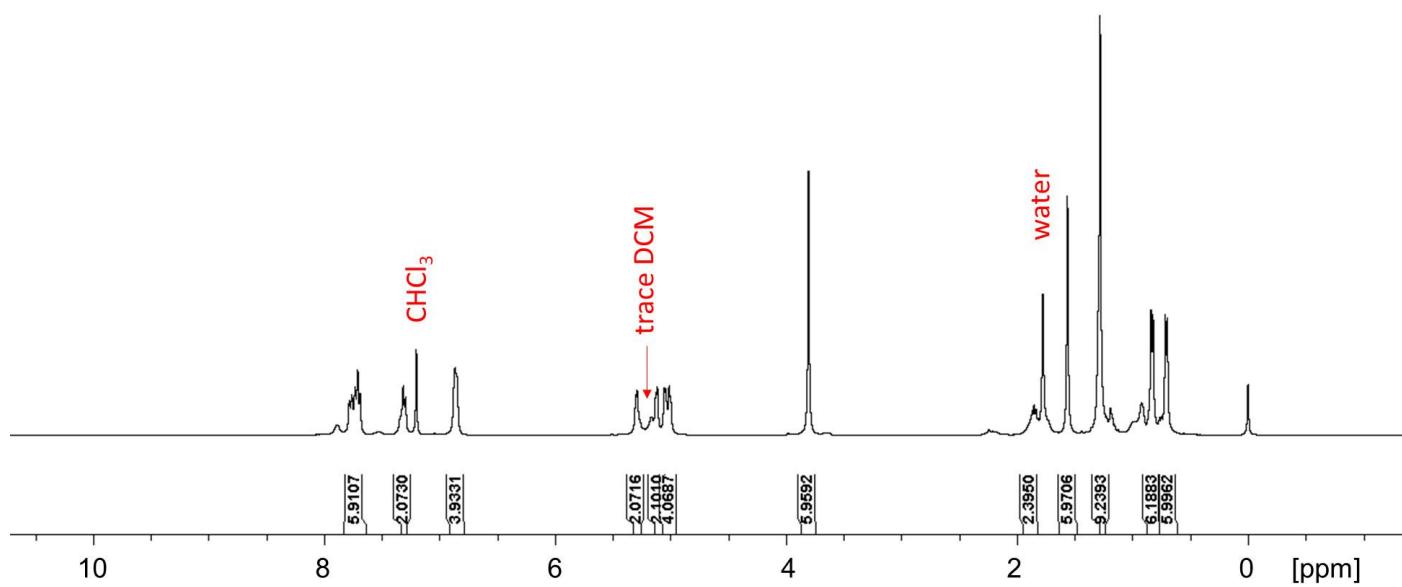


Figure S36. 400.1 MHz  $^1\text{H}$  NMR of complex **9** in  $\text{CDCl}_3$ , 64 scans.

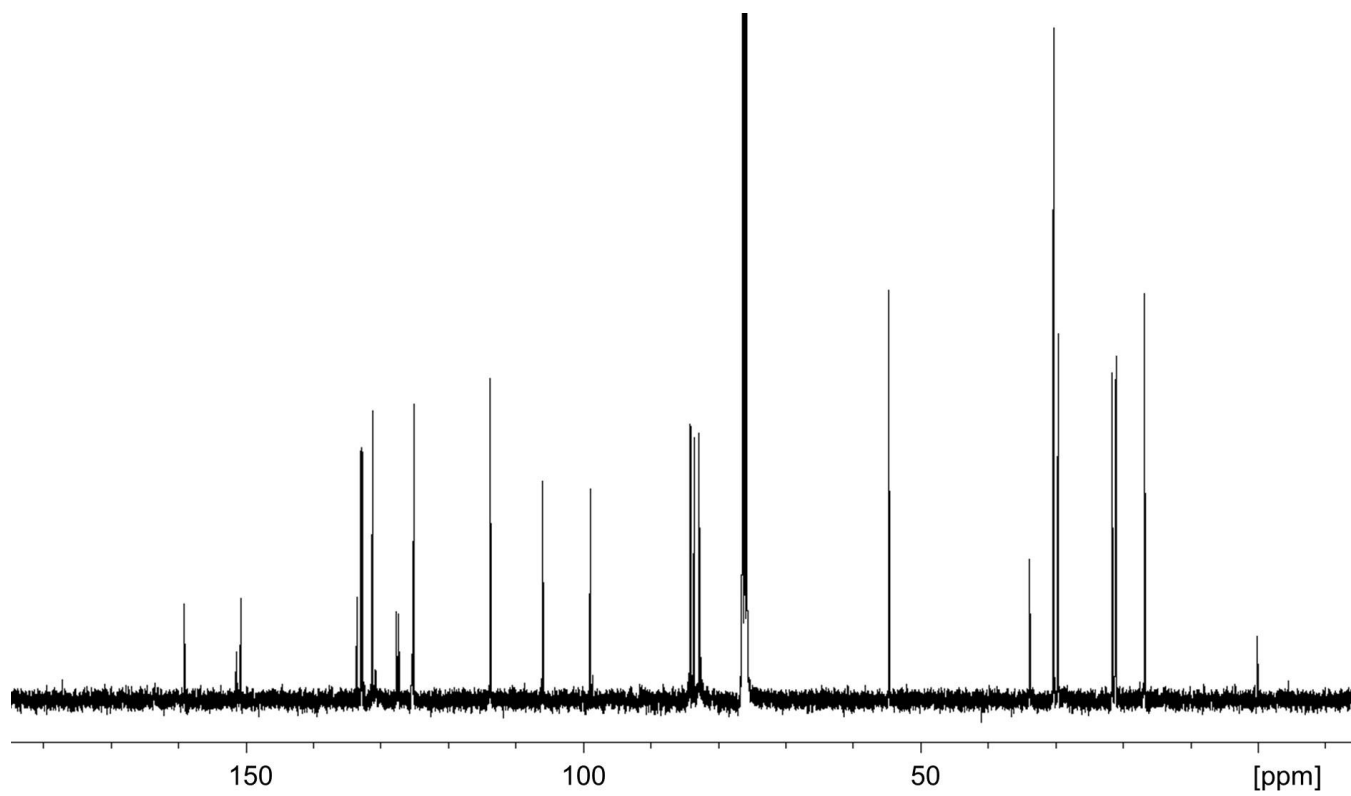
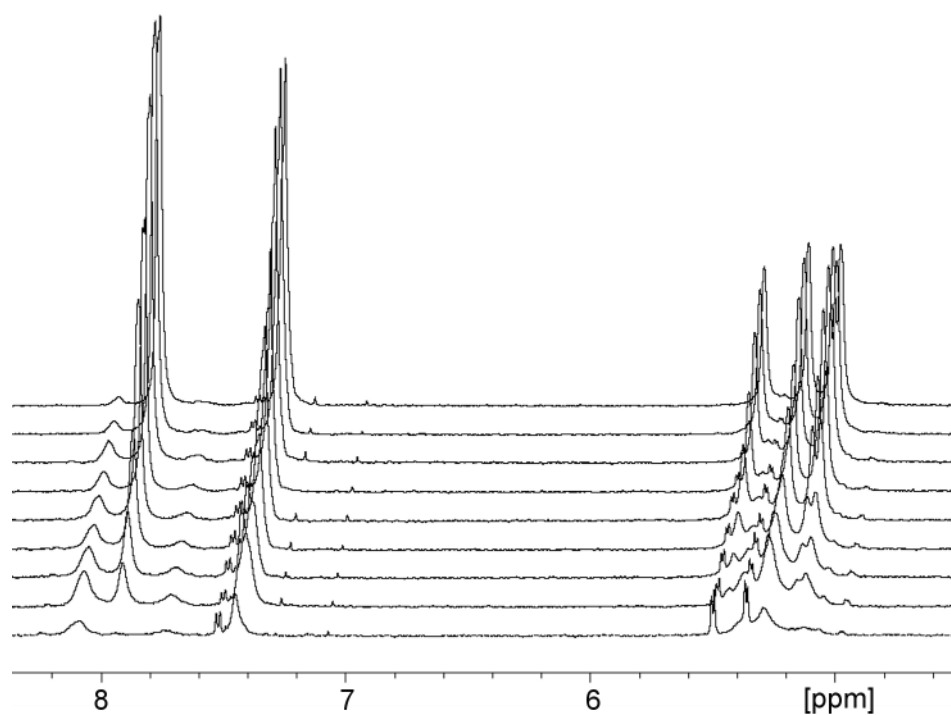


Figure S37. 100 MHz  $^{13}\text{C}$  NMR of complex **9** in  $\text{CDCl}_3$ , 8192 scans.

## 2.3 Kinetics

**Table S9.** Starting materials for kinetics experiments.

R	Ru dimer		Thiol	
	mg	$\mu\text{mol}$	mg	$\mu\text{mol}$
$\text{C}_6\text{H}_5$ ( $0^\circ\text{C}$ )	2.1	3.4	1.5	13.6
$\text{C}_6\text{H}_5$ ( $25^\circ\text{C}$ )	2.0	3.3	1.5	13.6
$\text{C}_6\text{H}_4\text{NO}_2$ ( $0^\circ\text{C}$ )	2.0	3.3	2.6	13.4
$\text{C}_6\text{H}_4\text{NO}_2$ ( $25^\circ\text{C}$ )	2.1	3.4	2.7	13.9
$\text{C}_6\text{H}_4\text{OMe}$	2.0	3.3	1.9	13.6
$\text{C}_6\text{H}_{11}$	2.0	3.3	1.6	13.8



**Figure S38.** Synthesis of **1** in EtOH under reflux at  $78\text{--}83^\circ\text{C}$ .  $^1\text{H}$  NMR in  $\text{CDCl}_3$  recorded at  $t =$ : (from bottom to top): 0h, 30min, 1h, 2h, 3h, 4h, 5h, 7.5h, 9h. Aromatic region.

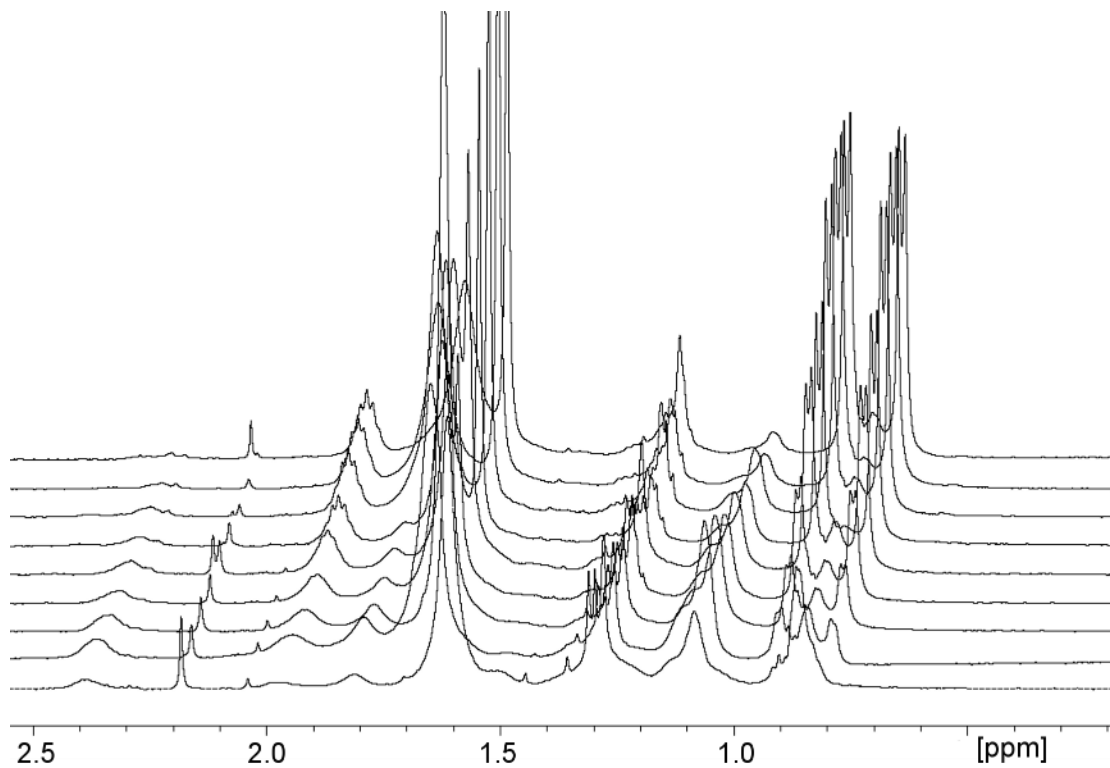


**Figure S39.** Synthesis of **1** in EtOH under reflux at 78-83 °C. <sup>1</sup>H NMR in CDCl<sub>3</sub> recorded at *t* =: (from bottom to top): 0h, 30min, 1h, 2h, 3h, 4h, 5h, 7.5h, 9h. Aliphatic region.

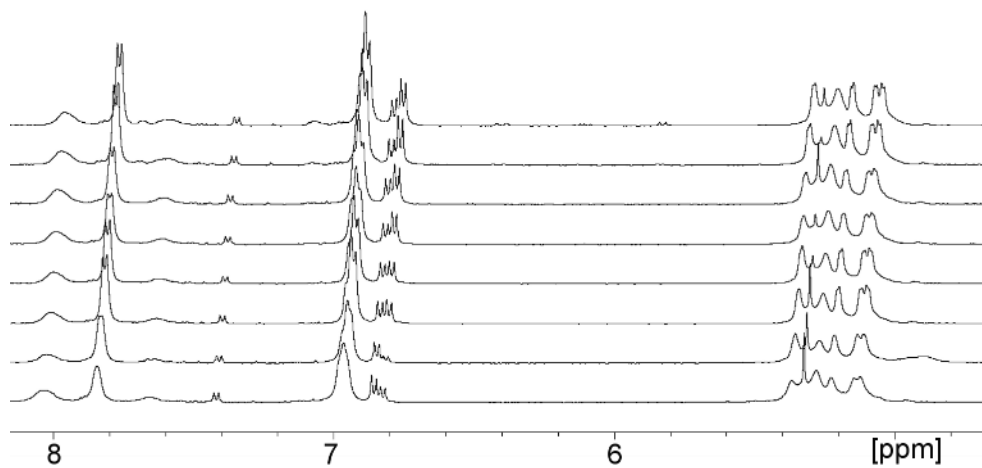


**Figure S40.** Kinetics of formation of **2** and intermediates at 45°C. Aliquots of reaction mixture in DCM transferred to CDCl<sub>3</sub>. 500.1 MHz <sup>1</sup>H NMR recorded at *t* =: (from bottom to top): 0h, 0.5h, 1h, 2h, 3h, 5h, 7h, 9h. Aromatic region.

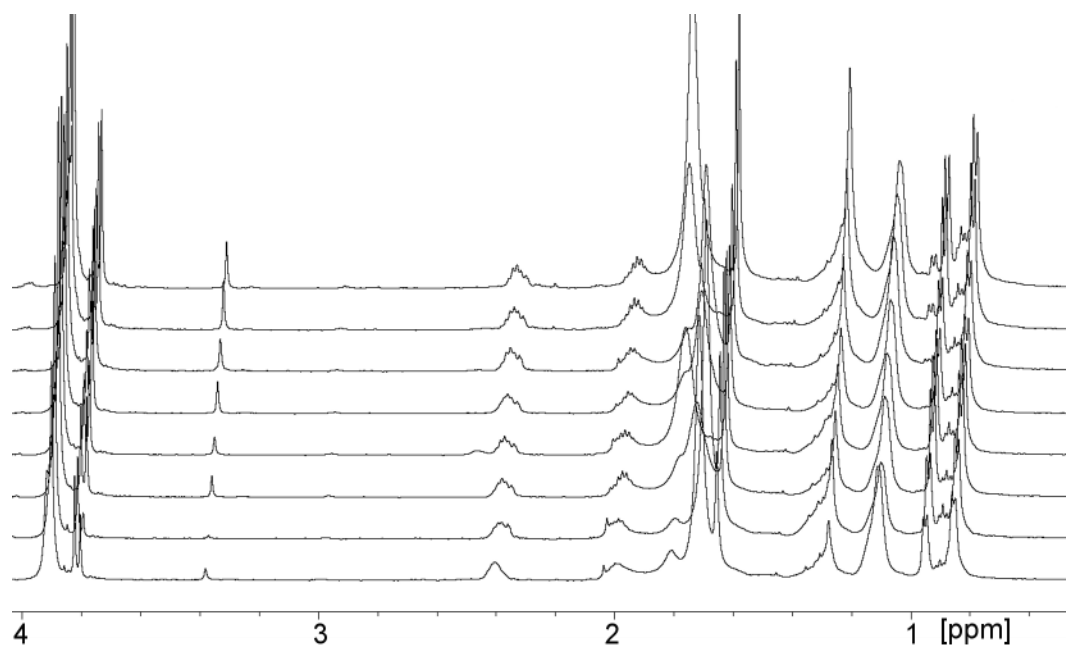


**Figure S41.** Kinetics of formation of **2** and intermediates at 45°C. Aliquots of reaction mixture in DCM transferred to CDCl<sub>3</sub>. 500.1 MHz <sup>1</sup>H NMR recorded at *t* =: (from bottom to top): 0h, 0.5h, 1h, 2h, 3h, 5h, 7h, 9h. Aliphatic region.

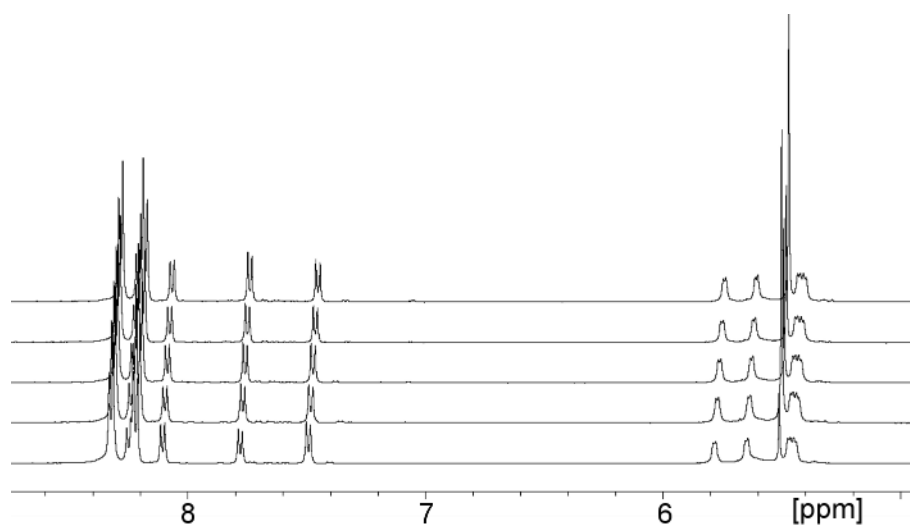


**Figure S42.** Kinetics of formation of **3** at 45°C in DCM. 500.1 MHz <sup>1</sup>H NMR in CDCl<sub>3</sub> recorded at *t* =: (from bottom to top): 0h, 0.25h, 0.5h, 1h, 2h. Aromatic region.

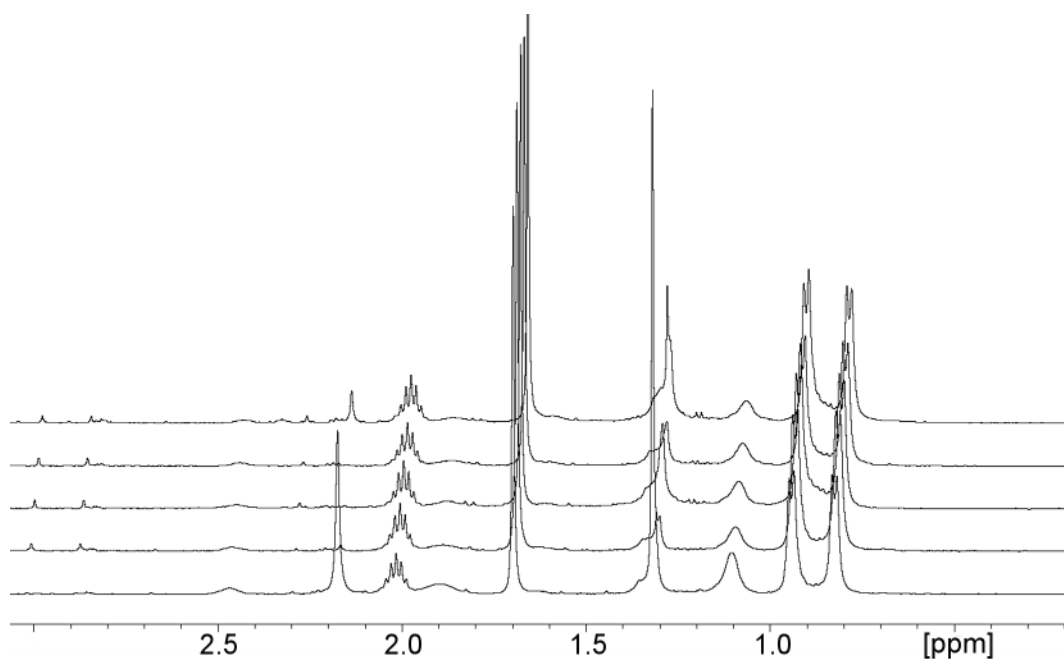


**Figure S43.** Kinetics of formation of **3** at 45°C in DCM. 500.1 MHz  $^1\text{H}$  NMR in  $\text{CDCl}_3$  recorded at  $t =$ : (from bottom to top): 0h, 0.25h, 0.5h, 1h, 2h. Aliphatic region.

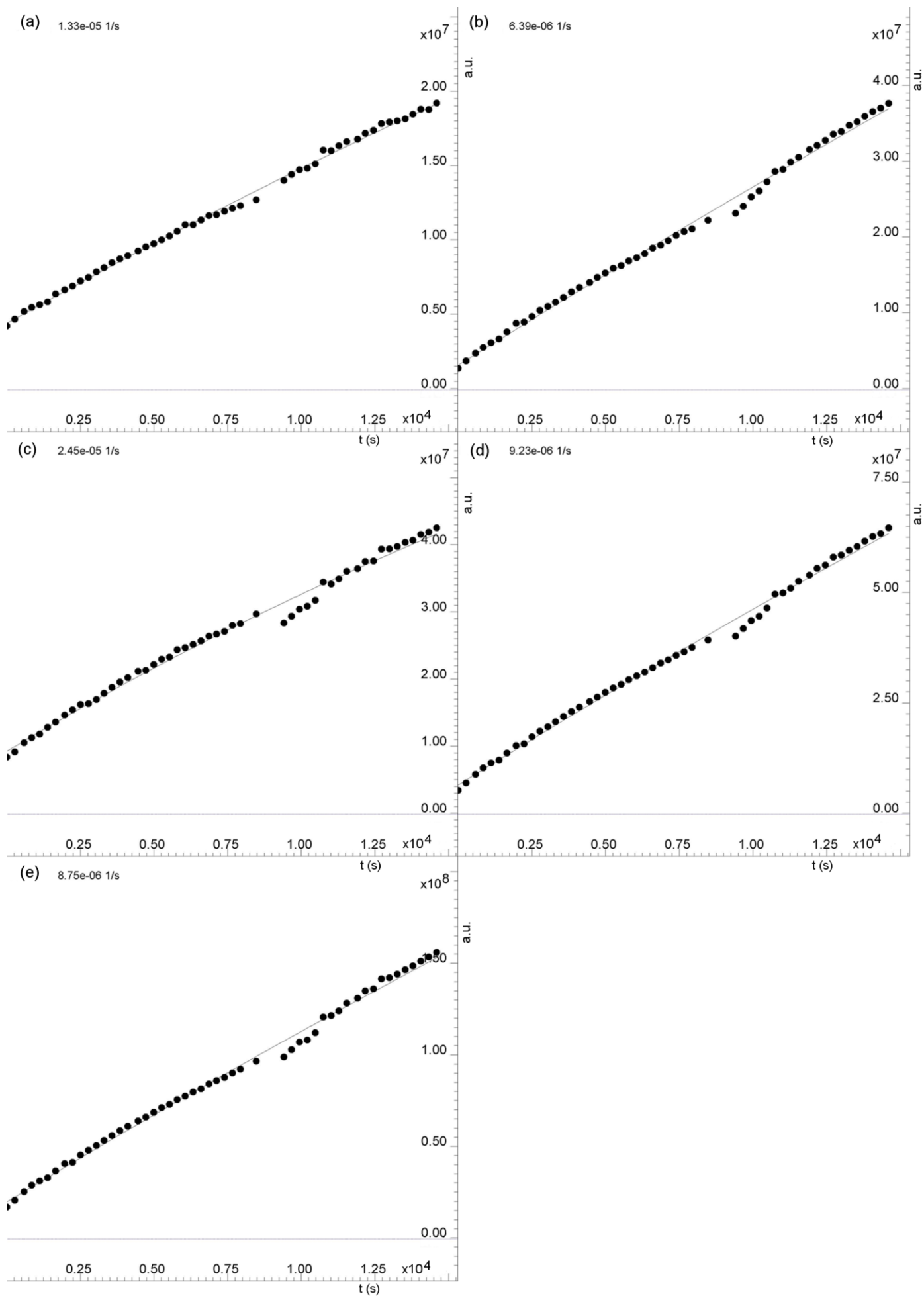


**Figure S44.** Reaction between  $[(\eta^6\text{-}p\text{-MeC}_6\text{H}_4\text{Pr}^i)\text{Ru}(\mu_2\text{-Cl})\text{Cl}]_2$  and thiophenol towards **1** in  $\text{CD}_2\text{Cl}_2$  at  $0^\circ\text{C}$  followed by  $^1\text{H}$  NMR. (a) resonance at 4.92 ppm; (b) 2.28 ppm; (c) 1.84 ppm; (d) 1.68 ppm; (e) 0.94 ppm.

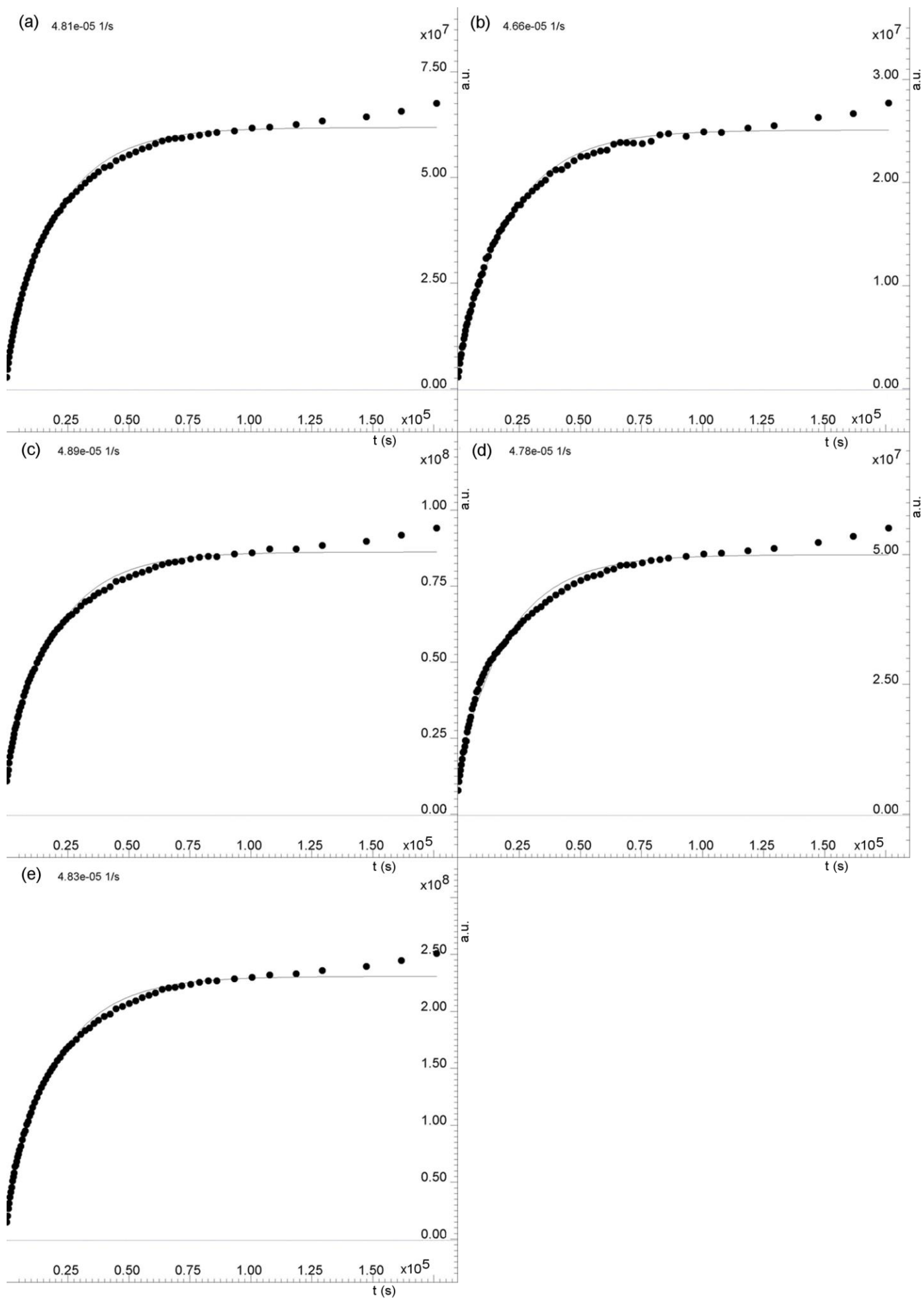


**Figure S45.** Reaction between  $[(\eta^6\text{-p-MeC}_6\text{H}_4\text{Pr}^i)\text{Ru}(\mu_2\text{-Cl})\text{Cl}]_2$  and thiophenol towards **1** in  $\text{CD}_2\text{Cl}_2$  at  $25^\circ\text{C}$  followed by  $^1\text{H}$  NMR. (a) resonance at 7.97 ppm; (b) 7.61 ppm; (c) 5.15 ppm; (d) 2.28 ppm; (e) 0.97 ppm.

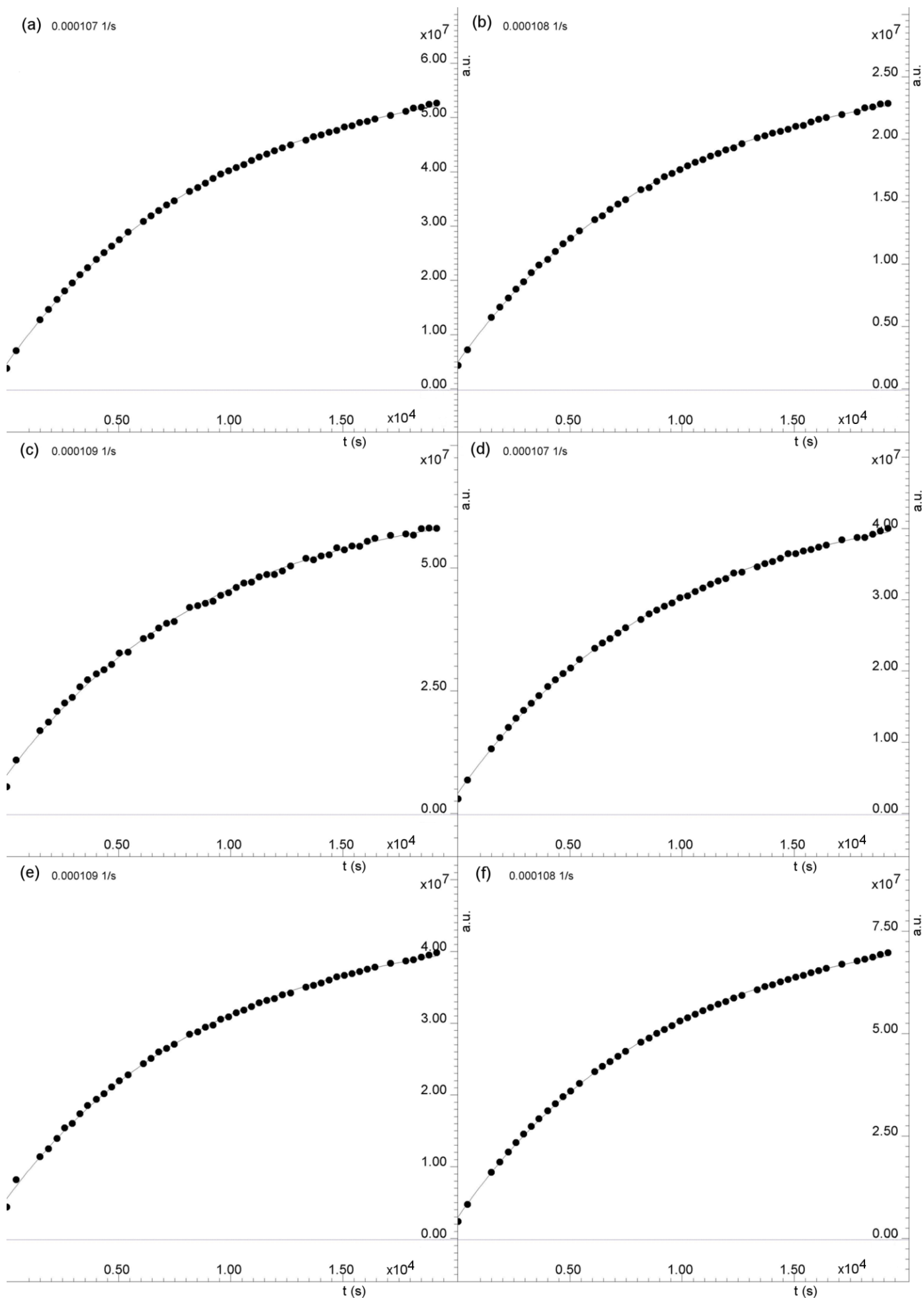


**Figure S46.** Reaction between  $[(\eta^6\text{-}p\text{-MeC}_6\text{H}_4\text{Pr}^i)\text{Ru}(\mu^2\text{-Cl})\text{Cl}]_2$  and *p*-nitrothiophenol towards **2** in  $\text{CD}_2\text{Cl}_2$  at  $0^\circ\text{C}$  followed by  $^1\text{H}$  NMR. (a) resonance at 7.89 ppm; (b) 7.51 ppm; (c) 3.81 ppm; (d) 2.29 ppm; (e) 1.83 ppm; (f) 1.68 ppm.

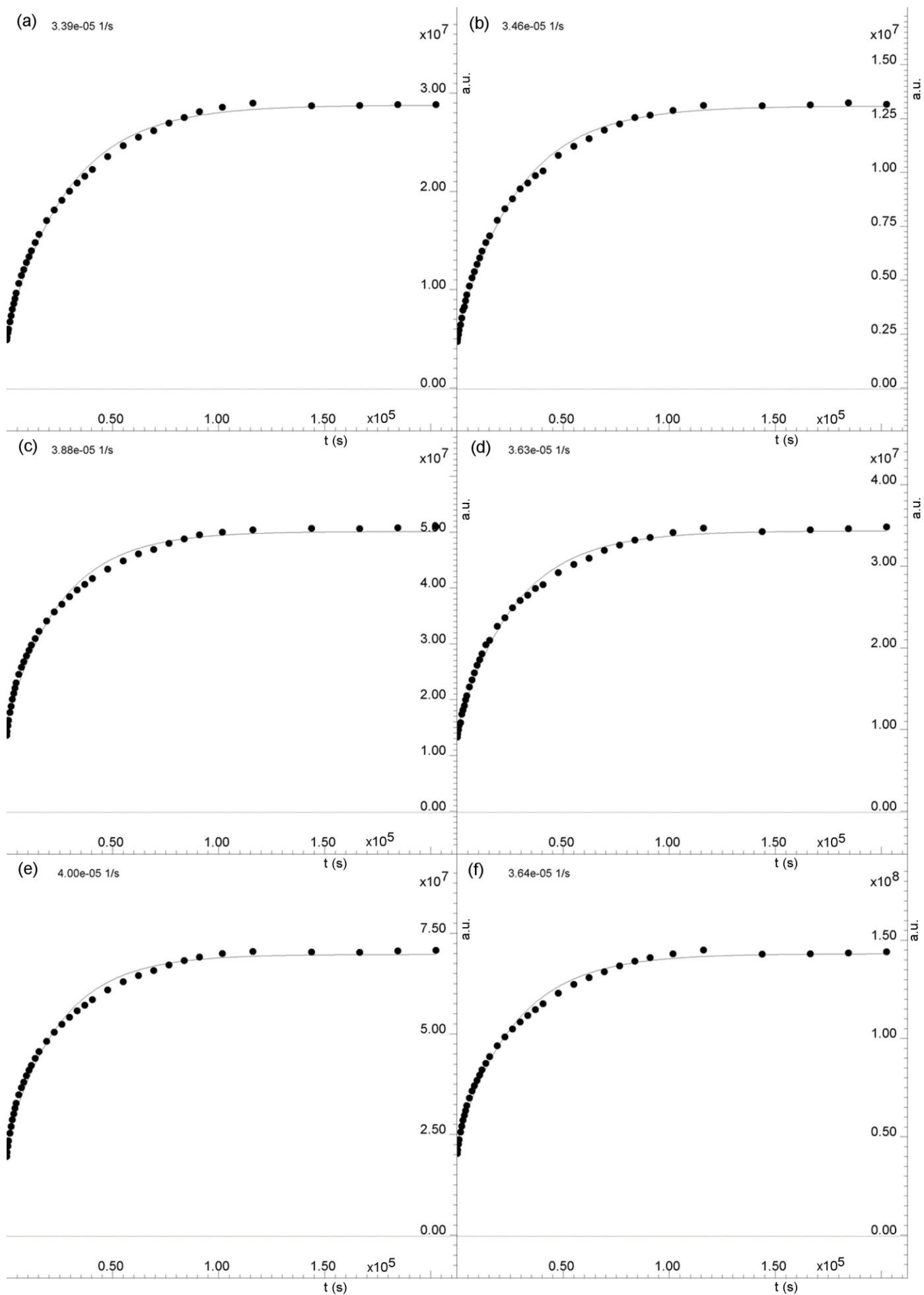


**Figure S47.** Reaction between  $[(\eta^6\text{-}p\text{-MeC}_6\text{H}_4\text{Pr}^i)\text{Ru}(\mu_2\text{-Cl})\text{Cl}]_2$  and *p*-methoxythiophenol towards **2** in  $\text{CD}_2\text{Cl}_2$  at 25 °C followed by  $^1\text{H}$  NMR. (a) resonance at 7.89 ppm; (b) 7.52 ppm; (c) 6.86 ppm; (d) 5.13 ppm; (e) 3.79 ppm; (f) 1.01 ppm.

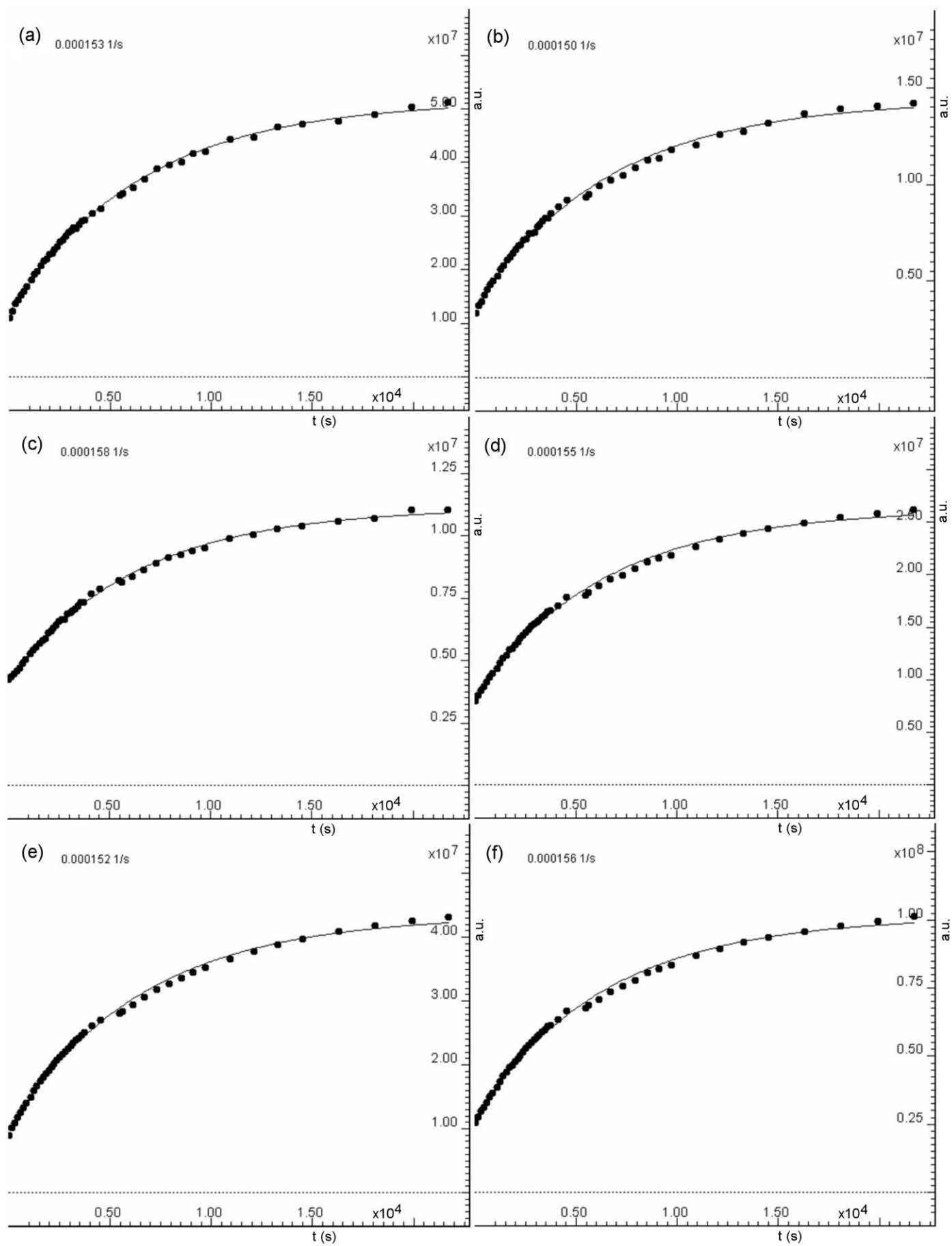


**Figure S48.** Reaction between  $[(\eta^6\text{-p-MeC}_6\text{H}_4\text{Pr}^i)\text{Ru}(\mu_2\text{-Cl})\text{Cl}]_2$  and *p*-nitrothiophenol towards **3** in  $\text{CD}_2\text{Cl}_2$  at  $0^\circ\text{C}$  followed by  $^1\text{H}$  NMR. (a) resonance at 8.23 ppm; (b) 7.85 ppm; (c) 5.37 ppm; (d) 1.88 ppm; (e) 1.71 ppm; (f) 0.98 ppm.

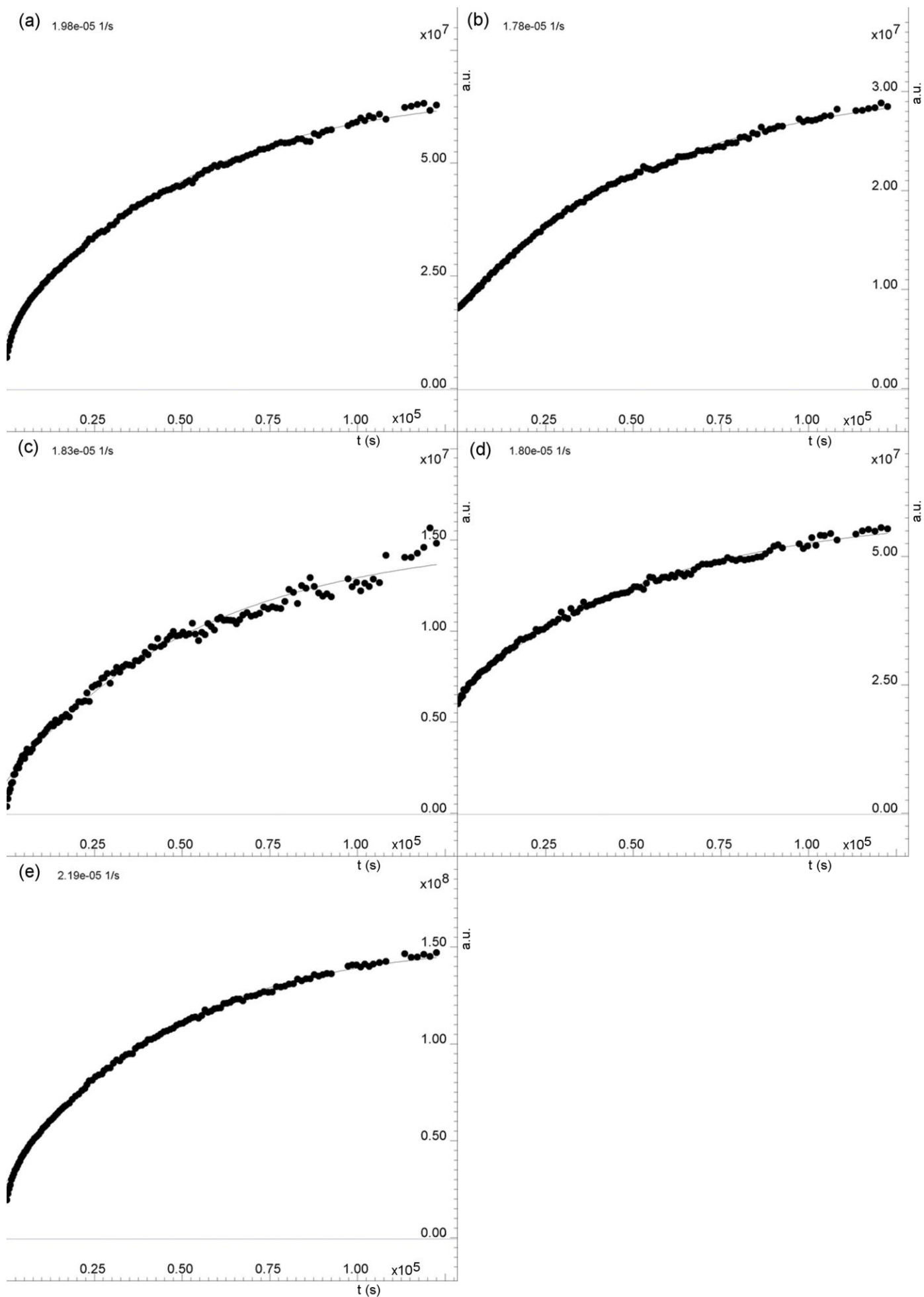


**Figure S49.** Reaction between  $[(\eta^6\text{-}p\text{-MeC}_6\text{H}_4\text{Pr}^i)\text{Ru}(\mu_2\text{-Cl})\text{Cl}]_2$  and *p*-nitrothiophenol towards **3** in  $\text{CD}_2\text{Cl}_2$  at  $25^\circ\text{C}$  followed by  $^1\text{H}$  NMR. (a) resonance at 8.22 ppm; (b) 8.18 ppm; (c) 7.88 ppm; (d) 5.29 ppm; (e) 1.01 ppm.

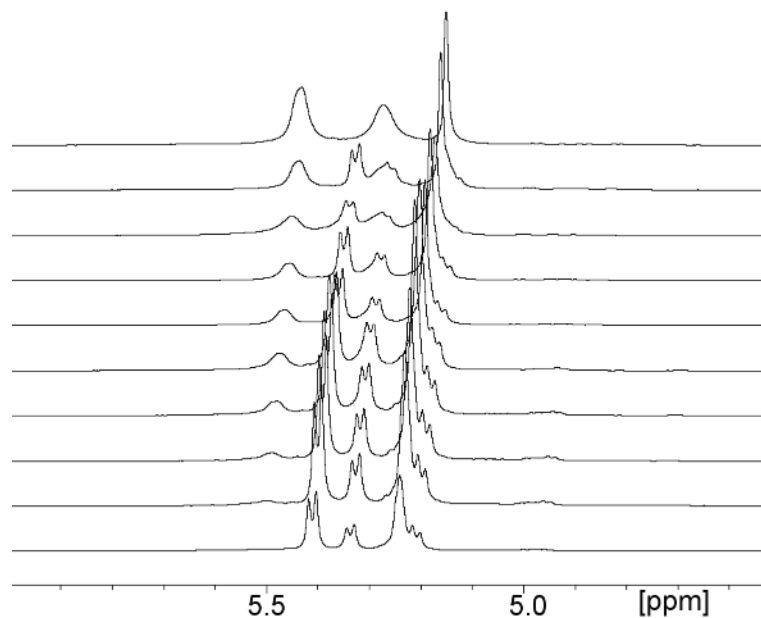


**Figure S50.** Kinetics of formation of **4** and intermediates. 400.1 MHz <sup>1</sup>H NMR in CD<sub>2</sub>Cl<sub>2</sub> recorded at  $t =$ : (from bottom to top): 0h, 2h, 5h, 11h, 15h, 30h, 35h, 50h, 70h, 409h. Aromatic region.

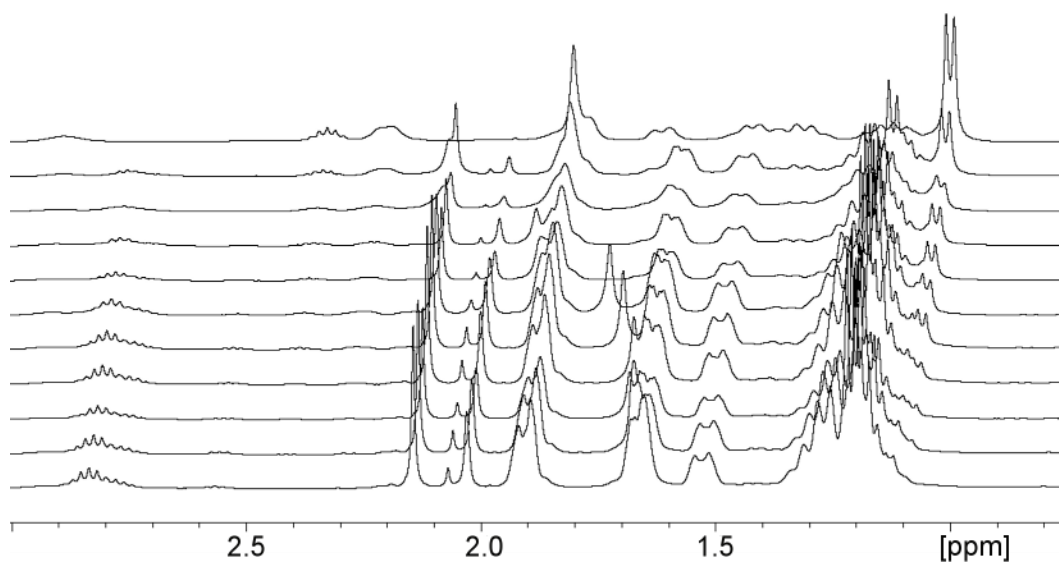


**Figure S51.** Kinetics of formation of **4** and intermediates. 400.1 MHz <sup>1</sup>H NMR in CD<sub>2</sub>Cl<sub>2</sub> recorded at  $t =$ : (from bottom to top): 0h, 2h, 5h, 11h, 15h, 30h, 35h, 50h, 70h, 409h. Aliphatic region.

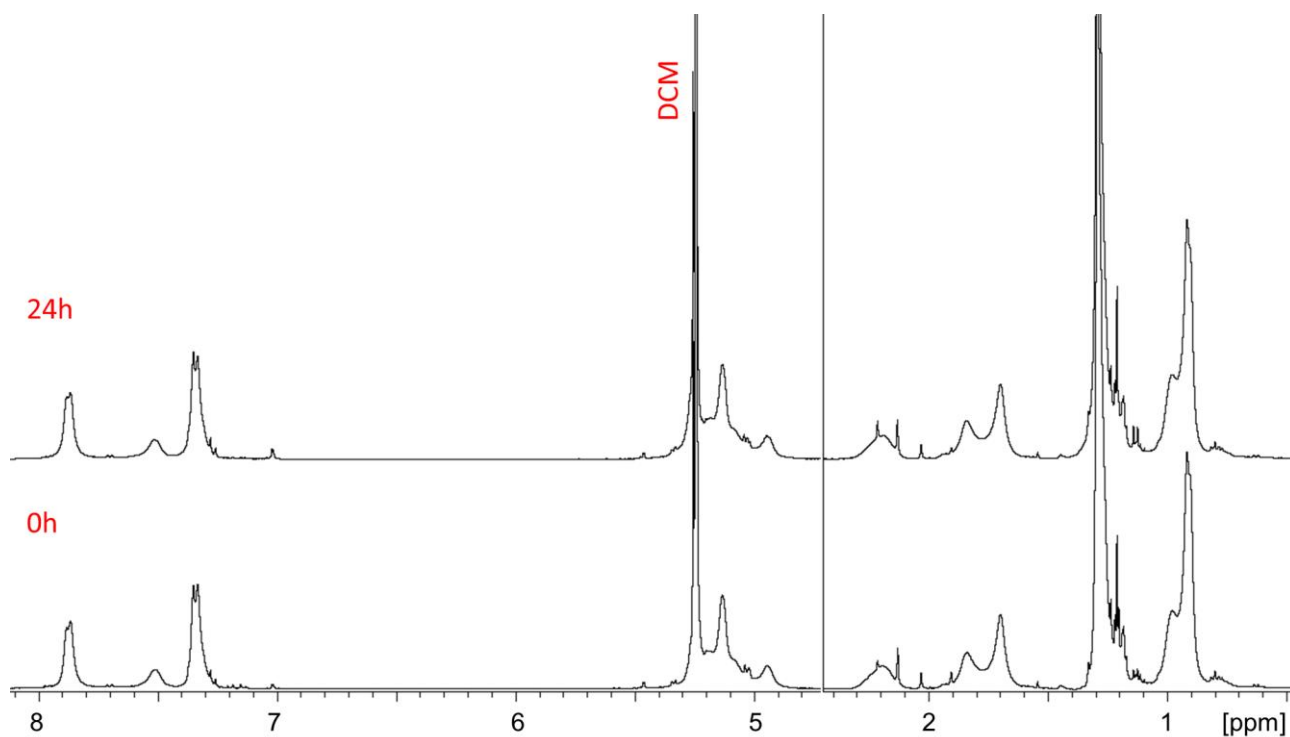


**Figure S52.** Stability test, 400.1 MHz <sup>1</sup>H NMR of crude 7 in CD<sub>2</sub>Cl<sub>2</sub> at 25°C. (Region 2.45-4.70 ppm containing no 7 signals excluded.)

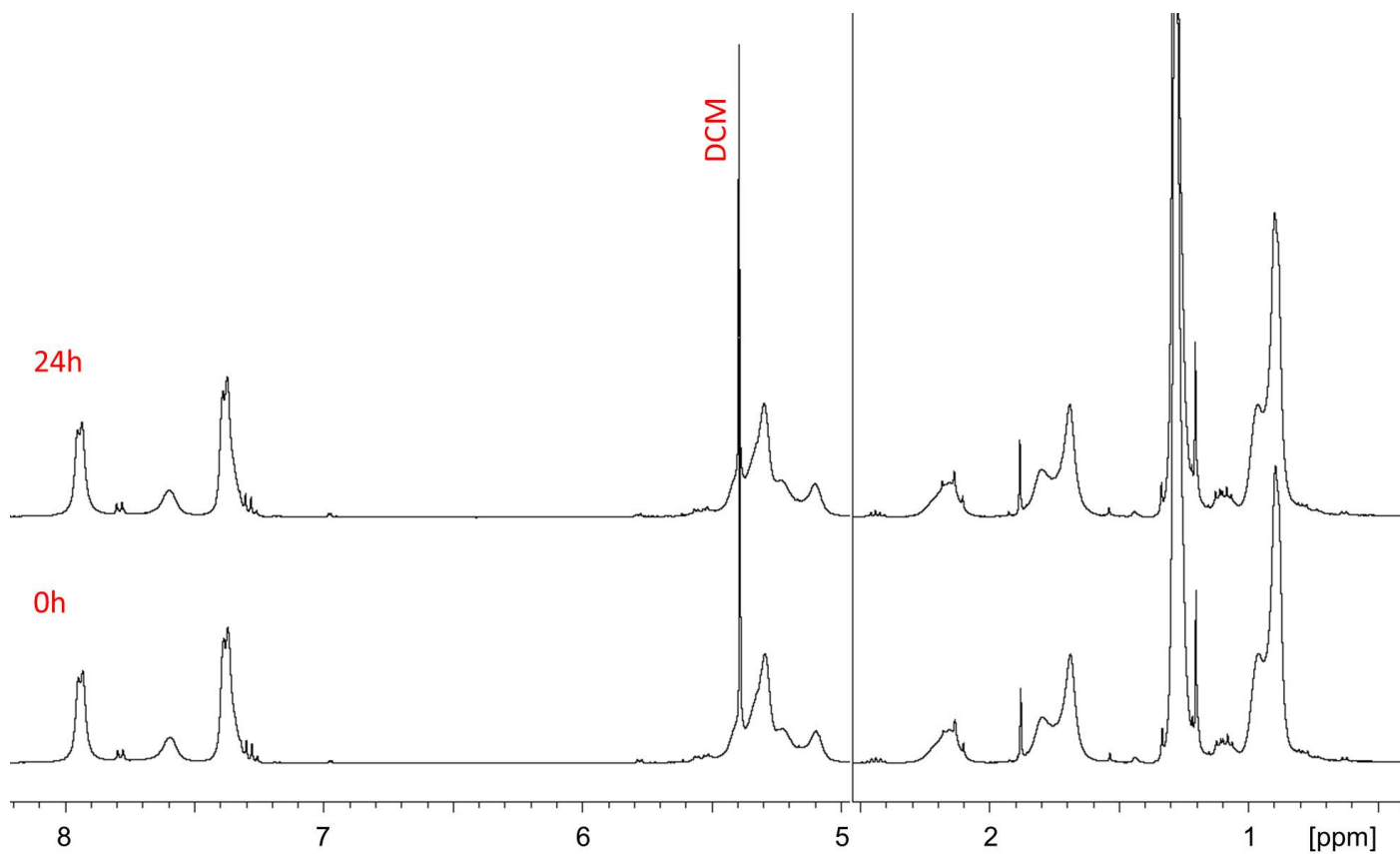


**Figure S53.** Stability test, 400.1 MHz <sup>1</sup>H NMR of crude 7 in MeOD at 25°C. (Region 2.53-4.95 ppm containing no 7 signals excluded.)

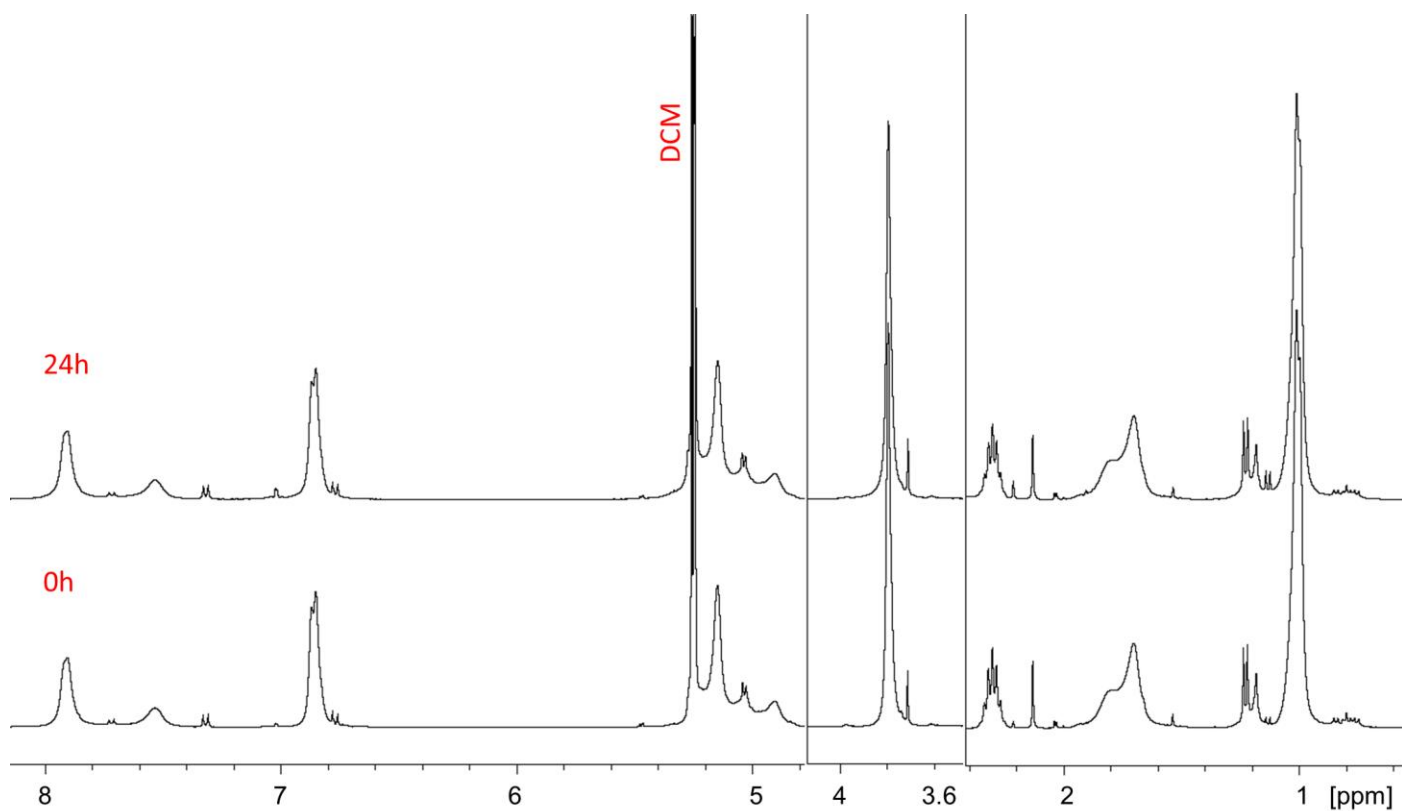


**Figure S54.** Stability test, 400.1 MHz  $^1\text{H}$  NMR of crude **8** in  $\text{CD}_2\text{Cl}_2$  at  $25^\circ\text{C}$ . (Regions 2.41-3.45 ppm and 4.60-4.78 ppm containing no **8** signals excluded.)

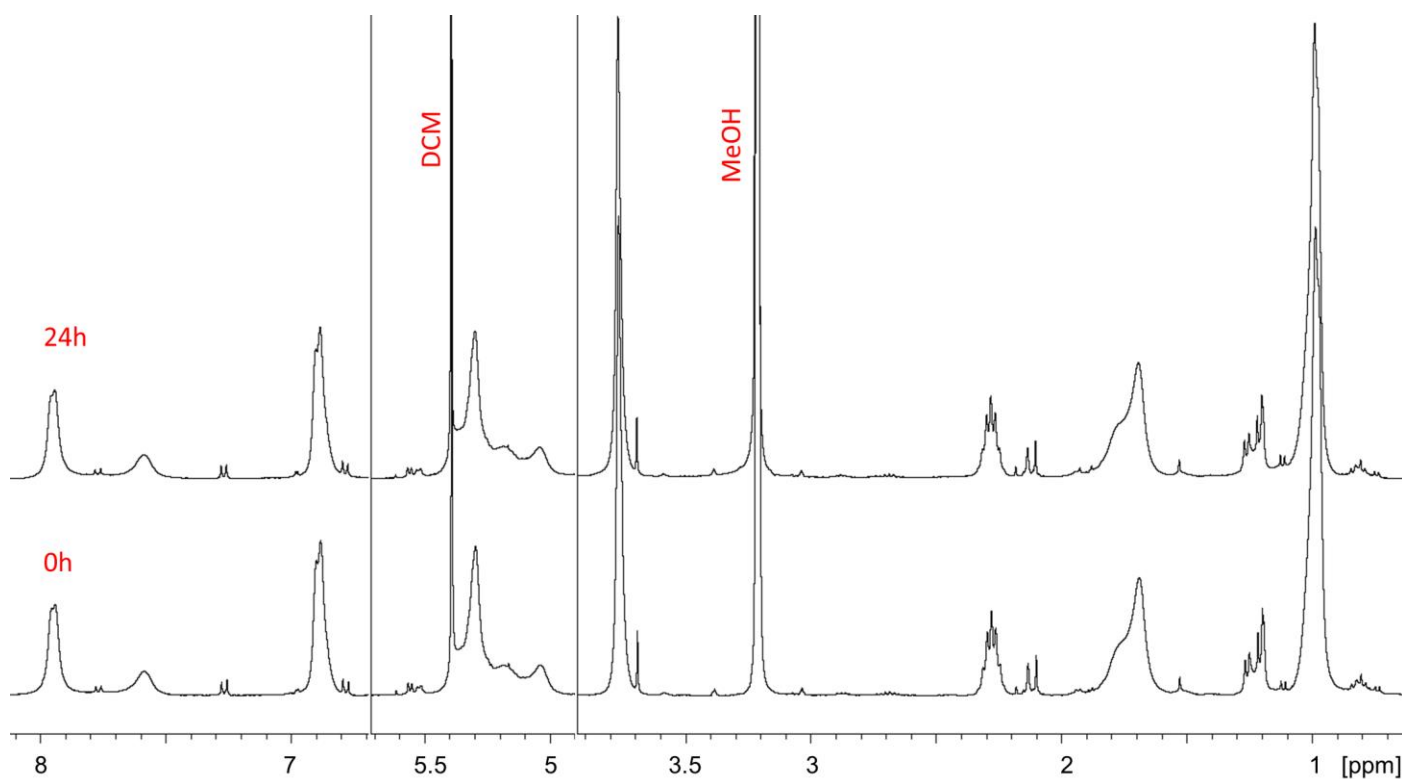


**Figure S55.** Stability test, 400.1 MHz  $^1\text{H}$  NMR of crude **8** in MeOD at  $25^\circ\text{C}$ . (Regions 3.93-4.90 ppm and 5.71-6.69 ppm containing no **8** signals excluded.)

## References

- (1) Claire S Allardyce, Paul J Dyson, David J Ellis, Paul A Salter, Rosario Scopelliti, Synthesis and characterisation of some water soluble ruthenium(II)-arene complexes and an investigation of their antibiotic and antiviral properties, *Journal of Organometallic Chemistry*, **2003**, 668, 35-42